Upscaling Fill-and-Spill Hydrologic Processes

by

Mahkameh Taheri

A thesis
presented to the University of Waterloo
in fulfillment of the
thesis requirement for the degree of
Doctor of Philosophy
in
Civil Engineering (Water)

Waterloo, Ontario, Canada, 2023

Examining Committee Membership

The following served on the Examining Committee for this thesis. The decision of the Examining Committee is by majority vote.

External Examiner:
Amin Elshorbagy
Professor
Department of Civil, Geological, and Environmental Engineering
Global Institute for Water Security
University of Saskatchewan

Supervisor:
James R. Craig
Associate Professor
Department of Civil and Environmental Engineering
University of Waterloo

Internal Members:
Bryan Tolson
Professor
Department of Civil and Environmental Engineering
University of Waterloo

John Quilty
Assistant Professor
Department of Civil and Environmental Engineering
University of Waterloo

Internal-External Members:
Kumaraswamy Ponnambalam
Professor
Department of Systems Design Engineering
University of Waterloo

Author's Declaration

This thesis consists of material all of which I authored or co-authored: see Statement of Contributions included in the thesis. This is a true copy of the thesis, including any required final revisions, as accepted by my examiners.

I understand that my thesis may be made electronically available to the public.

Statement of Contributions

Mahkameh Taheri was the sole author for Chapters 1, 2, 4, 6, and Appendices A and B which were written under the supervision of Dr. James R. Craig. Exceptions to sole authorship of material are as follows:

Chapter 3 is the main paper of this thesis which is under-review in the Water Resources Research journal. Mahkameh Taheri developed the analytical and Monte Carlo solution of the fill-and-spill hydrological process for different cascade depths. The algorithm was written in C++ and implemented in Raven by her. She tested the model performance in streamflow simulation of several prairie watersheds. She also prepared the manuscript. Dr. Craig provided the key idea of investigating the effect of wetland heterogeneity using probability distribution function. Moreover, he provided guidance through supervising the mathematical formulations and editing the manuscript. Dr. Mark Ranjram contributed in editing the manuscript and specifically, creating Figures 3.8 and 3.9.

Citation: Taheri, M., Ranjram, M., and Craig, J. (2023). An upscaled model of fill-and-spill hydrological response. Under review in Water Resources Research journal.

Chapter 5 is prepared for publication. Mahkameh Taheri created and calibrated the hydrologic model for the Scotty Creek basin. Shaghayegh Akbarpour developed the land cover classification and prediction model and provided the useful land cover transitions data. Additionally, Mahkameh Taheri and Shaghayegh Akbarpour contributed to the generation of climate data. Dr. Craig provided key insights during manuscript preparation.

Abstract

Low-gradient landscapes found in parts of the Taiga Plains and the North American Prairies can be dominated by many depressional wetlands with variable storage capacity. Runoff from these regions is influenced by the local storage capacity of individual wetlands and water exchange between the wetlands. Fill-and-spill conceptual models have been proposed to consider the connectivity-controlled process in wetland dominated catchments. Although fill-and-spill phenomenon has been locally observed, few studies examine the response of a landscape to thousands of cascading wetlands, as is seen in a number of Canadian landscapes. Being able to characterize, understand, and parameterize this response in hydrological models may enable successful simulation of the contribution area and runoff response in wetland-dominated regions. Current probabilistic fill-and-spill models consider individual features rather than the cumulative connections between adjacent wetlands in a cascade. The lack of understanding of the regional effects of wetland distributional characteristics on landscape hydrology, combined with insufficiently resolved elevation data, particularly in flat terrains, are two concerns that signify the need for an improved probabilistic runoff model. We propose an upscaled wetland fill-and-spill (UWFS) algorithm to investigate the response of large-scale wetland systems in low gradient areas to rainfall or snowmelt events. The research addressed in this thesis consists of the following:

1. An explicit probabilistic-analytic model is developed and tested for cascades of wetlands, providing an upscaling approach to understand and characterize system responses. To do this, first, a probabilistic analytic model is developed based on the fill-and-spill conceptualization, which considers each wetland in the basin as a member of an ensemble. The mathematical solution requires information about the initial deficit distribution and distribution of wetland local contributing areas which may be estimated via a combination of spatial analysis and field observation. Then, by using the derived distribution approach, the response of a landscape with a single wetland cascade is upscaled to the response of a landscape with thousands of wetlands. This event model is extended to evaluate the continuous response of a heterogeneous wetland complex to rainfall and snowmelt events by evolving the deficit distribution based on evaporation and precipitation.

2. A Monte Carlo based approach is proposed here that samples from initial deficit and concentrating factor distributions and finds the generated runoff from water balance equation applied to wetland cascade networks. This model along with the analytical model enables us to explore the impacts of network depth, branching, and gatekeeping on fill-and-spill runoff responses from complex wetland networks. The accuracy of

the probabilistic analytical solution is also assessed by comparing the results with those from the Monte Carlo approach.

3. The proposed probabilistic analytical runoff model has been implemented into an existing two-dimensional semi-distributed hydrologic model, Raven, to test the ability of the upscaling method in lumped runoff simulation of wetland-dominated basins influenced by fill-and-spill hydrology. The model has been tested at 10 subbasins inside the Qu'Appelle River Basin in Prairie and the simulation results has been compared to an existing Prairie model named HYdrological model for Prairie Region (HYPR).

4. The proposed UWFS algorithm has been applied to a discontinuous permafrost region, Scotty Creek basin in the Northwest Territories, to simulate runoff generation from secondary runoff areas (the wetlands not directly connected to the fen network). The streamflow responses to different landcover transitions and meteorological forcings from different climate change scenarios are applied to quantify the effects of lateral permafrost thaw on the hydrological response of the study basin.

The UWFS algorithm is applied to improve our understanding of the effects of distribution characteristics, network branching, wetland deficit conditions, and cascade depth upon the contributing area and effective runoff from heterogeneous wetland-dominated basins. We can use the proposed model to understand potential long-term hydrological impacts of climate change located in regions where climate warming changes the role of wetlands from storage features to water conveyors.

Acknowledgements

I would like to begin by expressing my sincere gratitude and appreciation to my advisor, Dr. James R. Craig. I consider myself incredibly fortunate to have had the trust and belief of Dr. Craig from the very beginning, as well as his insightful ideas, patience, and understanding throughout the research journey. I feel proud to have had the opportunity to work with such an outstanding and genius advisor.

Furthermore, I would like to express my appreciation to my colleagues and friends at the Hydrology Research Group in the Civil and Environmental Engineering department at the University of Waterloo, particularly Shaghayegh, Mark, and Rezgar for their collaborative support during the past years.

I would also like to thank Mehrangiz, Shamsi, Mastaneh, Masoud, Reza, Yalda, and Marjan for their support and encouragement throughout these years. I would like to express my deepest appreciation to Mahnameh and Mehrad for being my role models and sharing their wealth of experience with me throughout my academic journey. I am also grateful to Myla for bringing joy and happiness to my life during this challenging time.

I would also like to express my heartfelt appreciation to my father, Hassan, who has always believed in me. Your encouragement has been crucial in shaping me into the civil engineer I am today. I aspire to follow in your footsteps and become an accomplished engineer like you, who instilled in me the values of meticulous attention to detail and analytical thinking. You are the greatest engineer in my world. I would also like to express my deep gratitude to my mother, Mahboubeh, who has been my biggest source of motivation and inspiration. You have been invaluable in helping me navigate through the highs and lows of this journey. Your constant presence, even from thousands of kilometers away through phone calls, have been a ray of hope during the toughest of times. I am forever indebted to both my parents for shaping me into the person I am today, and for everything I have achieved up until this point.

Last but not least, I would like to thank my loving husband, Milad, for his love and motivation through the past years. Although the first few months of this journey were challenging without his presence, I am grateful to have had him by my side for the rest of it. I appreciate his calmness, patience, and unconditional support, specially when I was feeling overwhelmed. I cannot thank him enough for all that he has done for me and being the driving force behind my decision to initiate and complete this journey.

To the brave women of Iran

To the memory of the graduate students who were on board flight PS752

Table of Contents

List of Figures

List of Tables

List of Abbreviations

CRHM the Cold Regions Hydrological Model 68

DDS Dynamically Dimensioned Search 34

DEMs Digital Elevation Models 1

GIW Geographically Isolated Wetland 9, 53

HBV Hydrologiska Byrns Vattenbalansavdelning 14, 23, 31, 34, 68, 71

HEW Hydrologic Equivalent Wetland 53

HRU Hydrologic Response Unit 9, 10, 53, 70

HYPR HYdrological model for Prairie Region 23, 34–36, 42, 45, 51, 53, 86

KGE Kling–Gupta Efficiency 35, 45, 71, 74

LiDAR Light Detection and Ranging 9

NWT Northwest Territories 2, 4, 67, 69, 87

PBIAS Percent Bias 35, 45

PBU-PDM Puddle-based Unit PDM 23

PCM Pothole Cascade Model 11, 22

PDLD Probability Distributed Landscape Depressions 14, 53

PDM Probability Distributed Rainfall-Runoff Model 2, 12–15, 22–25, 30, 31, 33, 49, 51, 53

PDMROF Probability Distribution Model based RunOFf generation 14, 23, 30, 31, 34, 45, 49, 53

PPR Prairie Pothole Region 1, 4, 86

PRIMA Prairie Region Inundation Mapping 11

QRB Qu'Appelle River Basin 34, 36, 42, 43, 86

RDRS Regional Deterministic Reanalysis System 36

SCS-CN Soil Conservation Service curve number 12, 14, 23

SPILL Simple Pothole Terrain Analysis Algorithm 22

SWAT Soil Water Assessment Tool 8, 9, 14, 22, 53, 68

TOPMODEL TOPography-based hydrological MODEL 12–14

TSLCM Time Series Land Cover Model 70, 72, 73, 76, 79, 83

TWINN Taiga PlainsWetland Identification Neural Network 70, 71, 73, 76, 83

UWFS Upscaled Wetland Fill-and-Spill Model 3, 24, 25, 30–36, 42, 45, 46, 49, 51, 52, 54, 55, 59, 60, 65, 66, 71, 76, 79, 83, 86–88

VIC Variable Infiltration Capacity 12, 23, 30, 33, 49

WDPM Wetland DEM Ponding Model 10, 11, 15, 22

List of Symbols

$\mathbf{A_u}$ Local contributing area of the wetland 25

$\mathbf{A_w}$ area of the wetland 26

$\mathbf{D}$ the wetland deficit depth 26

$\mathbf{H}(\mathbf{x})$ Heaviside function 28

$\mathbf{N}$ Cascade depth number 29

$\mathbf{O}^*$ Potential outflow 25

$\mathbf{O}$ Actual outflow 25

$\mathbf{P}'$ Rainfall over the wetland area 26

$\mathbf{P_f}$ The percentage of the wetlands with zero deficit prior to the runoff event 28

$\mathbf{R}$ Rainfall excess from local contributing area 26

β Local contributing area ratio 26

$\mathbf{b}$ The shape parameters of the β distributions 28

$\mathbf{c}^*$ Critical storage capacity of PDM 30

$\mathbf{c_{max}}$ Maximum storage capacity of PDM 30

$\mathbf{c}$ Storage capacity of PDM 30

$\delta(\mathbf{x})$ Delta Function 28

$\mu_{\mathbf{obs}}$ The mean observed streamflow 35

$\mu_{\mathbf{sim}}$ The mean simulated streamflow 35

r The correlation between simulated and observed streamflow 35

$\sigma_{\mathbf{obs}}$ The variance of observed streamflow 35

$\sigma_{\mathbf{sim}}$ The variance of simulated streamflow 35

s Shape factor of storage capacity distribution of PDM 30

Chapter 1

Introduction

In low gradient landscapes, such as the Prairie Pothole Region (PPR) of central Canada or the Boreal and Taiga plains, the landscape is covered by depression storage features (often wetlands) which control runoff generation. In the simplest conceptual model for the functioning of these regions, each depression is filled by the lateral and vertical addition of water, and when the water level reaches a certain level, water spills, and runoff is produced. In the hydrology literature, this process is called "fill-and-spill", and has received significant attention in the research literature (Tromp-van Meerveld and McDonnell, 2006; Shaw et al., 2012; Spence and Woo, 2006). A number of studies have investigated the local-scale storage effects on catchment-scale runoff, including through the development of numerical models (Watson et al., 2008; Shook et al., 2013; Evenson et al., 2016; Muhammad et al., 2019). However, the problem with most existing models is that each depression must be individually defined within a detailed physically-based model. They may also require complex processing of high resolution Digital Elevation Models (DEMs) to determine outflow and storage characteristics. The shallow subsurface water movement in Taiga Plains plays a critical role in filling depressions (Connon et al., 2014), and accurately quantifying the water pathways is a major limitation as it cannot be achieved through LiDAR data. In contrast, the dynamic connection of wetlands is neglected in lumped models, which integrate the storage capacity of a catchment over a hydrologic unit rather than considering the cascades between different wetlands. Probabilistic approaches are a potential solution that may avoid the need to characterize individual wetlands while not oversimplifying the response of these complex systems.

Some discontinuous permafrost regions in Canada's north are dominated by wetlands such as bogs and fens. Those regions are experiencing twice as much warming as the rest of the world as a result of anthropogenic climate change, which is speeding up the thawing

of permafrost (IPCC, 2014). A proper representation of wetland fill-and-spill processes in hydrological models can help to improve our understanding of the effects of permafrost thaw induced by climate change. A large portion of Canada's northern regions, including the southern portion of the Northwest Territories, is covered by discontinuous permafrost, which is a landscape that is partially covered by ground that has been frozen for two or more years in a row (NRC, 1995). Permafrost thaw alters water balance components in basins, disrupts or expands connectivity between hydrological features, and consequently changes total discharge from a basin. Although there are several studies on fill-and-spill processes and connectivity variations between wetlands and other hydrological features in discontinuous permafrost regions (Connon et al., 2015, 2014; Haynes et al., 2018; Mack et al., 2021), there are few studies which utilize hydrological models to simulate streamflow in those regions (Stone et al., 2019) and investigate lateral permafrost thaw influences at the regional scale. A hydrological modeling approach coupled with a landcover transition model is needed to provide insight into potential long-term hydrological impacts of climate change and permafrost thaw for future decision making in discontinuous permafrost regions.

1.1 Thesis Objectives and Structures

This thesis studies the fill-and-spill process and influence of the heterogeneity of thousands of wetlands throughout a basin using a probabilistic approach. The approach is a generalization of the Probability Distributed Rainfall-Runoff Model (PDM) of Moore (1985). In addition, we apply discrete network models of wetlands to examine the upscaling behavior of fill-and-spill systems, and test the approaches developed herein in an existing distributed hydrological model (i.e., Raven developed by Craig et al. (2020)) to enable successful simulation of the contributing area and runoff responses in wetland-dominated regions.

The objectives of this thesis are

1. To develop and test a probabilistic-analytic event model for cascades of wetlands, providing an upscaling approach to understand and characterize system responses;
2. To use the analytical event based model and numerical network models to explore the impacts of network depth, branching, and gatekeepers on fill-and-spill network responses;
3. To extend the event based model to a continuous model and examine the capability of the algorithm in accurate simulation of prairie basins by comparing the simulation results with an existing prairie lumped model.

4. To investigate the impacts of permafrost thaw induced by climate change on a hydrological response of a wetland-dominated basin in the Northwest Territories (NWT).

In order to present the methods and findings of this research, the thesis is organized as follows: Chapter 2 provides a comprehensive review of the literature on upscaling methods of hydrological processes, fill-and-spill hydrological models, and representation of wetland complexes. Chapter 3 introduces the methodology of the Upscaled Wetland Fill-and-Spill Model (UWFS) and the application of this algorithm in wetland dominated subbasins in prairie. Chapter 4 investigates the effects of UWFS assumptions and how different properties of wetlands can be captured by a single parameter. Chapter 5 demonstrates a coupling approach that utilizes information from a land cover change model in a hydrologic model to examine the effects of climate change on streamflow generation in discontinuous permafrost regions. Chapter 6 concludes with a summary of the contributions made. The detailed analytical solutions of the UWFS algorithm is presented in Appendix A.1 to A.4. Appendix B.1 includes supplementary materials related to Chapter 3.

Chapter 2

Background and Literature Review

Depressional wetlands are dominant features in low gradient landscapes such as the PPR of southern Alberta and Saskatchewan or the Taiga plains of the NWT. These terrains are historically challenging to simulate in hydrological models. In order to accurately simulate the historical hydrological responses to climatic inputs and predict the responses to future climate change impacts, it is important to understand the role of wetlands, the dominant hydrological process in those regions, and the current state-of-the-art in modelling approaches for these landscapes.

For this purpose, this chapter first discusses the connectivity and hydrology of wetlands. After that follows a review of the fill-and-spill phenomenon, the hydrological process that serves as the focus of this study, and the modelling techniques employed in the literature. Then, permafrost hydrology and climate change in cold regions are covered. Knowledge gaps and takeaway messages are presented at the chapter's conclusion.

2.1 Wetland Hydrological Connectivity

Depressional wetlands are also known as sloughs, bogs, depressions, ponds, or potholes (van der Kamp and Hayashi, 1998), and in this thesis they are referred to as wetlands. They have a significant impact on a catchment's water balance because they gain water from local runoff, overflow from upstream wetlands, and precipitation/snowmelt, store water as storage features, and lose water via groundwater recharge or evaporation (Bullock and Acreman, 2003). Wetlands carry out the three main hydrological functions of storing, contributing, and transmitting water (Spence and Woo, 2006) based on the weather condition. Wetlands' high storage capacity during dry conditions can disrupt water movement

and block interconnection between wetlands. During wet conditions, the depressions may fill, and once they reach a certain threshold, they may spill and can then be hydrologically connected to each other or basin's outlet (Hayashi et al., 2016; Shaw et al., 2012). Water exchange between wetlands has a significant impact on the water budget and hydrological processes within the catchment, including overall runoff. For example, during dry conditions in 2011, 4.4% of the St. Denis Basin in Saskatchewan, Canada contributed to runoff, compared to 11.9% during the same year's spring snowmelt event (Shook et al., 2013).

Hydrological studies have recently paid significant attention to hydrological connectivity. According to the definition given in Bracken and Croke (2007), hydrological connectivity refers to a concept of runoff generation that happens wherever there is a possibility for water to move between various zones and locations. This connectivity can be achieved through surface, shallow subsurface, and deep groundwater fluxes or combinations of such flows (Golden et al., 2017), and can be of "permanent, intermittent, ephemeral or episodic" duration (Leibowitz et al., 2016). The role of wetlands in catchment runoff is determined by the degree of hydrological connectivity and controlled by wetland proximity, location, and storage capacity (Spence, 2010). Wetland connectivity, along with other properties of a watershed and weather conditions such as topography, landcover, precipitation frequency, duration, and magnitude (Rains et al., 2016), can control the quantity of runoff and the extent of the contributing area in a basin.

Field studies in the Taiga Plains (e.g., Connon et al. (2014, 2015)), Canadian shield (e.g., Spence and Woo (2003)), and Canadian Prairies (e.g., Shaw et al. (2012)) have repeatedly demonstrated the importance of connectivity on runoff generation. Connon et al. (2014) investigated the effects of permafrost thaw on runoff and streamflow variations in the lower Liard River valley within the Northwest Territories, Canada. Results of their study show that land-cover change, i.e., transformation from plateaus to wetlands (or flat bogs) caused by permafrost thaw, has increased the resulting runoff, runoff ratio, and contributing area because of the increasing hydrological connectivity through surface and subsurface pathways. Investigation of runoff generation in the bog cascades at Scotty Creek research basin by Connon et al. (2015) shows that neglecting wetland connectivity in those areas leads to 5-15% underestimation in the streamflow magnitude. The field observations in that study also revealed that remotely sensed imagery cannot accurately characterize the hydrological connectivity in the basin. This is because the previously assumed isolated bogs were found to be connected, highlighting the limitations of using remote sensing for this purpose.

In the Canadian Prairies, runoff generation is influenced by water input from precipitation, wind-driven snowmelt, and the spilling of upstream wetlands (Fang and Pomeroy, 2007). Surface spilling is the main cause of total landscape outflow in those basins due to

the low infiltration rate of wetlands into subsurface glacial till (van der Kamp and Hayashi, 1998). In some Canadian Shield landscapes, inputs from upland bedrock, which is driven by hydrological linkage, into the soil-filled valleys are higher than the input from vertical sources, i.e., snowmelt and precipitation (Spence and Woo, 2003). This shows the significance of taking hydrological connectivity into account to enhance the performance of hydrological models. According to the results of a surface water survey conducted for the spring freshet runoff event in 2006 (Shaw et al., 2012), only 39% of the St. Denis basin in Saskatchewan contributes runoff to the outlet and this can be impacted by dynamic basin conditions like man-made structures and antecedent conditions of the basin that can change the hydrological connectivity.

Several investigations into the connectivity of wetlands in low relief landscapes have been conducted using both field-based and modelling techniques. Wetlands are often treated as isolated in the isolation-connectivity continuum framework because they can be connected or isolated at different points in time (Leibowitz, 2003). A threshold concept that suggests wetlands are disconnected prior to the satisfaction of a storage threshold can be used to represent wetlands in such frameworks. Wetlands move from being isolated to being connected after achieving a specific storage threshold. Models that simulate connectivity in a watershed, whether via surface or subsurface pathways, were categorised by Golden et al. (2017) into three general categories: spatially lumped, semi-distributed, and fully distributed, as shown in Figure 2.1.

A brief explanation of each category is provided here. The lumped models (e.g., Liu and Schwartz (2011)) represent implicit connectivity of a watershed's entire area. The semi-distributed models linked to "quasi-explicit" connectivity take similar connection patterns into account for parts of the watershed (e.g., Mekonnen et al. (2016) and Beven and Kirkby (1979) rely upon some form of probabilistic treatment of the landscape). For each wetland in fully distributed models, connectivity is explicitly calculated (e.g., Shook and Pomeroy (2011); Shaw et al. (2013a); Shook et al. (2013); Ameli and Creed (2017); Amado et al. (2018); Ahmed et al. (2020a); Ahmed et al. (2021)). Underestimating the significance of wetlands on the structure and function of watersheds and water supplies can result from a lack of understanding of wetlands' hydrologic connectivity (Ameli and Creed, 2017). This thesis aims to address a critical gap between understanding of the significance of connectivity and the capacity to represent it on a landscape predominated by hundreds or thousands of wetlands.

The distribution of surface storage affects wetland connectivity and consequently the area that contributes runoff to the outlet of a basin. Shaw et al. (2013a) has shown this relationship for four types of landscapes with different spatial storage distribution patterns located inside the Prairie Pothole Region as depicted in Figure 2.2. Curve A,

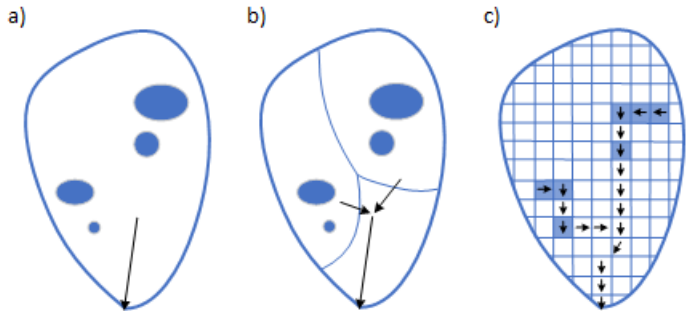

Figure 2.1: Representation of connectivity by a) lumped (implicit), b) semi-distributed (quasi-explicit), c) fully-distributed (explicit) models (adapted from Golden et al. (2017))

C, and B in Figure 2.2 depicts the contributing area/ storage relation for systems where storage is concentrated in the upper portion, lower portion, or evenly in the entire basin, respectively. The situation where both stream channels and wetlands are present within the catchment is depicted by Curve D. Wetlands with a lot of storage capacity (labelled G in Figure 2.2) appear to be inactive before a certain amount of precipitation. These wetlands were referred to as "gatekeepers" by Phillips et al. (2011) because they can only gather and store precipitation during normal events, only releasing water during extreme events. Gatekeepers can contribute to runoff and become active based on their storage threshold (i.e., the volume of water needed to fill a storage capacity before the flow cascades downslope) (Spence, 2007), the intensity and the duration of storm, and the upstream runoff (Phillips et al., 2011). Curve C in Figure 2.2 shows that decreases in storage capacity are not immediately reflected in increases in the percentage of contributing area. The location and relative size of the gatekeeper can significantly affect the relationship between the depressional storage and the connected fraction of a basin (Shook et al., 2021a). In fact, a larger percent of the storage capacity must be filled to generate runoff from gatekeeper "G" leading to the outflow. In this extreme case, other wetlands may be full and will connect together after the threshold has been reached, making the resulting contributing area significant. The importance of size and spatial distribution of depressions may be controlled by the number of depressions in a basin. Shook et al. (2021a) shows that the spatial distribution of depressions loses significance as the number of depressions rises, which is followed by a decline in the areal fraction of gatekeepers (i.e., the area of the gatekeeper relative to the total area of depressions).

The wetland stage relative to the threshold can control the magnitude and timing of the hydrologic connectivity. McLaughlin et al. (2019) developed an empirical tool (i.e., the Connectivity and Flow from Stage model (CFS)) to find the hydrologic connectivity

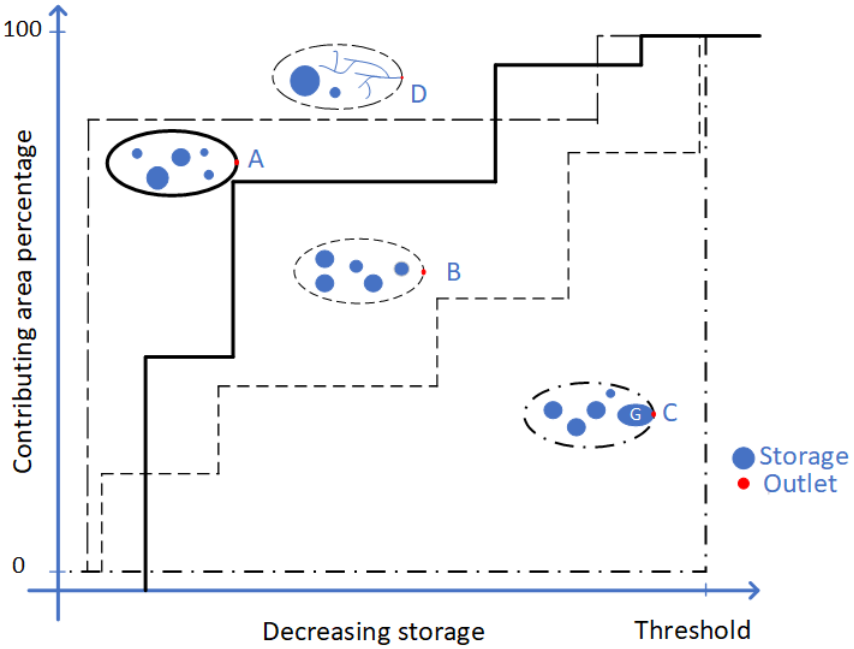

Figure 2.2: A schematic overview of the relationship between spatial distribution of basin storage and contributing area (adapted from Shaw et al. (2013a))

threshold. This model is based on a daily water budget, which is used to calculate a metric called netflow based on daily precipitation, evaporation, and wetland stage variations. Negative netflow represents initiation of surface hydrologic connectivity and the associated wetland stage is assumed to be the threshold height. The model's reliance on bathymetric data, however, limits its usability in regions with ungauged basins (McLaughlin et al., 2019). Furthermore, this model does not take into account the cascading effects of wetlands on connectivity.

To demonstrate the developments and knowledge gaps in wetland connectivity and runoff simulation, existing hydrological models of fill-and-spill are examined for their strengths and weaknesses in Section 2.2.

2.2 Fill-and-spill Phenomena and Existing Models

Wetlands are either explicitly or implicitly represented in hydrological models. In order to comprehend the scientific context and the challenges of wetland-dominated landscape

simulations, this section reviews both kinds of wetland representations in hydrological models.

2.2.1 Explicit Representation of Wetlands

Many studies on wetland hydrologic simulation have been carried out using different versions of the Soil Water Assessment Tool (SWAT) (Arnold et al., 1998). This model previously had used three different methods to represent wetlands (Mekonnen et al., 2016). One strategy is to ignore depressions because they all contribute to the outlet within the catchment. Another strategy is to view depressions as isolated geographical features disconnected from the rest of the basin. A third strategy is to combine all of the depressions in each sub-basin into a single, large depression (Almendinger et al., 2014). The third method divides each basin into number of sub-basins, which are further divided into several Hydrologic Response Unit (HRU). The curve number (CN) method is used to calculate surface runoff in each HRU. The resulting runoff is then directly discharged into a single depression, which serves as an effective representation of all of the depressions' combined storage in the sub-basin. The accumulated water draining from each sub-basin's depression then spills into the main channel of the basin. This lumped model has the drawback of simulating just one wetland, with a single overflow threshold, ignoring the heterogeneity of landscape depression storage. Moreover, this version of SWAT did not take into account the storage and retention capacities of wetland HRUs. To account for the hydrological functions of wetlands, Wang et al. (2008) incorporated the Hydrologic Equivalent Wetland (HEW) concept into SWAT. Each HEW is defined by parameters that represent the spatial distribution of wetlands, a retention function, the storage capacity of wetlands, channel length, and Manning's n value. Its area is equal to the sum of the wetlands area in each subbasin. However, in these lumped models, the threshold of each individual wetland and its effects on runoff generation are simply ignored.

In order to improve the representation of wetland inter-connectivity through the fill-and-spill process, Evenson et al. (2016) redefined HRU boundaries in SWAT as shown in Figure 2.3. In this method, every Geographically Isolated Wetland (GIW) is an HRU with a catchment area, as indicated by the dashed line in the Figure 2.3, and all HRUs that are part of a GIW's catchment area drain to that GIW. Each "GIW-HRU" then drains to the downstream one, and finally to the outlet. As a result of this boundary refinement, the number of HRUs for a small study area increases about 50 times comparing to the initial version. This makes the simulation computationally expensive and increased the run times from hours to weeks (Muhammad et al., 2019). This method is also hard to apply in large basins without fine resolution elevation data. Evenson et al. (2018) later developed

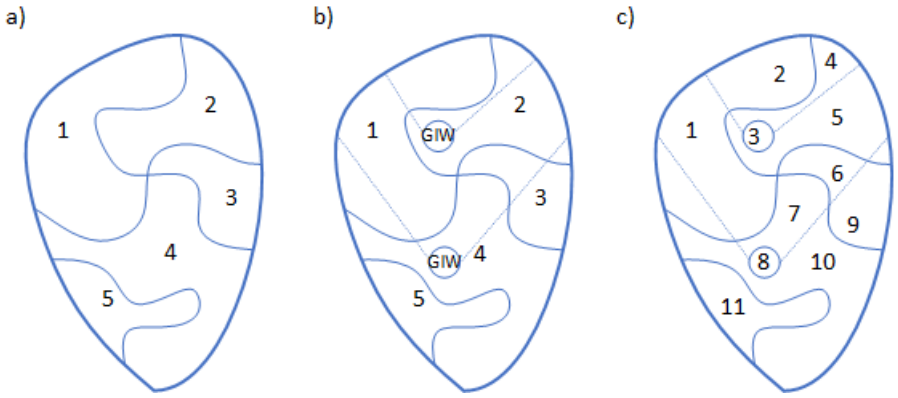

Figure 2.3: a) Standard HRU boundaries, b) GIW placement in the watershed with contributing area, c) HRU refinement in a way that each wetland is identified as a new HRU itself and all unique parts of drainage area are respected (adapted from Evenson et al. (2016))

SWAT for Depression Storage and Flows (SWAT-DSF), which treats depressions and the contributing area as a single HRU rather than two separate ones. They incorporated high resolution Light Detection and Ranging (LiDAR) data for delineation of depression HRUs. They also removed small depressions with perimeter to area ratio less than 0.3 and catchments with insufficient runoff. Muhammad et al. (2020) also proposed a modified form of wetland representation to reduce the computational costs of this "fully-discretized" version of wetland modelling in SWAT. They compared wetland storage capacity with a predetermined threshold that reduces computational cost. Wetlands that have storage capacities above the threshold are referred to as "GIW-HRU" and the remaining wetlands are removed from the model and their combined storage capacity is added to the capacity of the remaining wetlands in the subbasin. If there are no more wetlands in the subbasin with storage capacities greater than the threshold, the total volume of low storage wetlands is distributed equally among the remaining wetlands in the catchment. This approach reduces the number of HRUs and, consequently, the run time. Although these more complex models more accurately depicted the dynamics of wetland water storage, the explicit representation of wetlands and the need for high resolution data are problematic in low-gradient landscapes with many wetland features.

Wetlands can be explicitly represented in fully distributed models. For instance, Shook and Pomeroy (2011) created the Wetland DEM Ponding Model (WDPM), a fully distributed model of prairie wetlands based on high resolution LiDAR data. Within this distributed model, a variety of hydrological processes, including evaporation, runoff, and

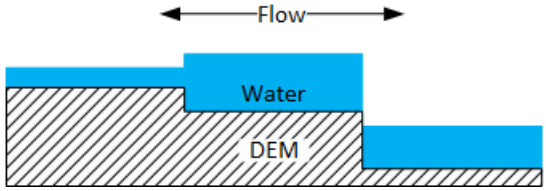

Figure 2.4: Schematic diagram of water flow from a DEM cell using WDPM (adapted from Shook et al. (2021b))

drainage, can be modelled. The three modules that make up WDPM are based on the Shapiro and Westervelt (1992) iterative algorithm. First, a uniform depth of water is added as rainfall and water can be distributed to a lower cell or to a higher cell with insufficient water as shown in Figure 2.4 depending on the elevation of the water surface at adjacent cell to make the flat surface. Second, without considering any specific evaporation fluxes, a uniform depth of water is subtracted from each cell to represent the evaporation process. Finally, the excess water flows to depressions and the outlet of the basin by draining downhill.

There are several limitations in using the WDPM (Shook et al., 2013). First, the model's dependency on high resolution LiDAR data restricts its applicability and increases its computational complexity. Second, the water depth in depressions is limited to the land elevation at that point which confines the depression elevation variation. Third, wetland lateral extent is limited to the LiDAR resolution and it fails to account for the presence of subsurface flow pathways. The methodology of WDPM is similar to the Scalable Pothole terraIn anaLysis aLgorithm (SPILL) model by Shaw et al. (2013a) who developed a "simple pothole terrain analysis algorithm", which applies a certain depth of water to each wetland considering its contributing area. Using the watershed function in ArcGIS, this model delineates the resulting contributing area. In this model precipitation is uniformly redistributed within a basin and the interactions between various wetlands and between inputs from other wetlands in a cascading network are neglected. This leads to inaccurate estimates of the inputs to each wetland and, as a result, inaccurate estimates of the magnitude and timing of streamflows, which affect how much water is stored and released by wetlands. Although, the methodologies of WDPM and SPILL model are similar, the SPILL model does not simulate the removal of water. Similar models developed later include the Prairie Region Inundation Mapping (PRIMA) model by Ahmed et al. (2020a), later implemented in MESH (MESH-PRIMA by Ahmed et al. (2021)), and the Pothole Cascade Model (PCM) by Shook and Pomeroy (2011), which take into account the addition and removal of water. The removal of water per iteration is possible in PRIMA and

makes this model to be more efficient than WDPM.

PCM treats wetlands as distinct reservoirs and randomly chooses the wetland dimensions from the frequency distribution of wetlands' characteristics, such as areas and volumes, in each basin rather than relying on a high resolution elevation data like WDPM. The collective wetland behaviour can then be simulated with the aid of parameterization. However, since wetlands dimensions have been recognised based on the maximum area and volumes of water, the drawback of using PCM is that it cannot subdivide wetlands when water level drops below internal sill elevations. Thus, the size and number of empty or partially full wetlands are simulating incorrectly, which affects the accuracy of runoff calculations (Shook et al., 2013). Furthermore, wetland contributing areas in flat landscapes are hard to estimate from digital elevation data, and can prevent PCM from determining the correct distribution frequency of the volume and area of wetlands. Also, wetlands are receiving water from shallow subsurface flow which cannot be accurately delineated since even LiDAR data are not sufficient to characterise subsurface water pathways.

2.2.2 Implicit Representation of Wetlands

Saturation/infiltration excess models, such as the Soil Conservation Service curve number (SCS-CN) method, have been commonly used to simulate runoff generation (Wang, 2018). Runoff production by SCS-CN event-based empirical model is based on a rainfall-runoff curve, a function of the cumulative storm rainfall and antecedent wetness condition, and has been used since 1970s, widely because of its simplicity. However, the lack of sufficient description of the runoff physics and the influence of spatial variability of antecedent moisture affects the accuracy of the runoff simulation (Bartlett et al., 2016a). Several semidistributed rainfall-runoff models account for a watershed's heterogeneity by considering distributions of watershed properties including storage. Xinanjiang (Zhao, 1980), TOPography-based hydrological MODEL (TOPMODEL) (Beven and Kirkby, 1979)), and the PDM (Moore, 1985) models are saturation excess runoff models that use a distribution function to account for the spatial variability of watershed properties, particularly water storage capacity. These models were developed between the mid 1970s to 1980s and have been repeatedly modified and improved until now. For instance, TOPMODEL is a semi-distributed rainfall-runoff model which considers each point of the landscape as a soil reservoir (Beven and Kirkby, 1979). In this model, a topographic index distribution is used to describe the spatial variability of the reservoir's storage capacity in a landscape. The area draining through a point from an upslope divided by the local slope angle is the topographic index. The key premise of the method is that it is not necessary to model every point in a catchment because points with similar index values should respond similarly

to equivalent rainfall. Although TOPMODEL has been used by several studies (Goudarzi et al., 2023; Zulkafli et al., 2021; Beven et al., 2021), the assumptions of the model regarding runoff mechanisms limit its successful use to certain types of basins, and excludes utility in wetland systems.

The Xinanjiang model is another implicit probabilistic runoff model that considers a Pareto probability distribution of soil water storage capacity. This model then uses the Muskingum method to route the runoff generated at each sub-basin to the outlet of the catchment (Zhao, 1980). There exist several improved versions of the Xinanjiang model (Sahoo, 2005), that add new parameters to increase the model ability in simulating complex hydrological process in a basin. One is the study by Jayawardena and Zhou (2000) that considers a double parabolic distribution to account for the complexity of soil moisture variability in landscapes. Another example is the Variable Infiltration Capacity (VIC) that considers the distribution of infiltration capacity to represent variable soil moisture storage (Wood et al., 1992). To separate subsurface flow from surface flow, Liang et al. (1994) added a new soil layer to the structure of the TOPMODEL model, called VIC-2L, which responds to the rainfall only once the main layer is saturated. The ARNO model of Todini (1996) is another semi-distributed model which uses the basics of the soil moisture balance concept of the Xinanjiang, but adds features to incorporate drainage and percolation losses.

Moore (1985) proposed a rainfall-runoff model called PDM, further discussed in Moore (2007), which considers each point at a catchment to act like a single tank with a storage capacity of c', as shown in Figure 2.5-a. Each point is characterized with a storage capacity. The spatial variation of storage capacity is represented by a distribution function to calculate runoff. Each storage level can be exceeded due to rainfall or depleted by evaporation, continuously until the input exceeds a critical storage capacity threshold, c^*, and generates runoff as depicted in Figure 2.5-b. Moore (2007) showed that total water storage within a basin, $S(t)$, can be related to a critical capacity, $C^*(t)$, through:

$$S(t) = \int_0^{C^*(t)} cf(c)dc + C^*(t) * \int_{C^*(t)}^{\infty} f(c)dc = \int_0^{C^*(t)} (1 - F(c))dc. \tag{2.1}$$

where c is the storage capacity/depth of the soil column at each point, $f(c)$ represents the frequency of occurrence of a storage's depth, and $F(c)$ is the cumulative distribution function of storage capacity. The PDM provides a starting point for probabilistic description of the storage dynamics in heterogeneous catchments. However, the connectivity between different storage features is not replicated by PDM. Rather, water is redistributed such that the storage is always uniform, equal to $C^*(t)$ in all non-full storage situations. The

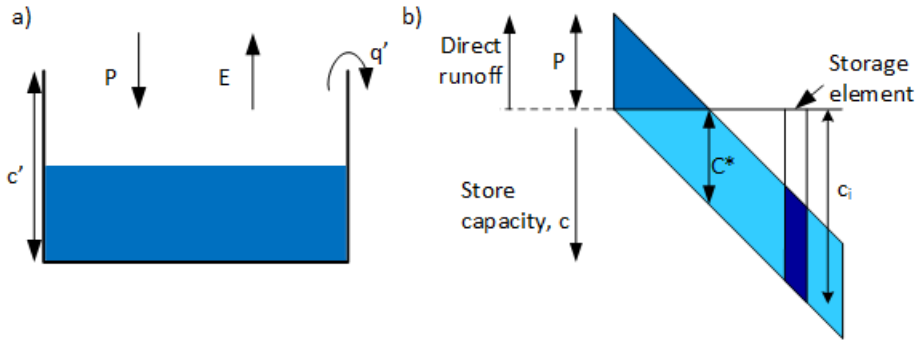

Figure 2.5: Graphical illustration of a) runoff production by a single store, b) storage elements of different depth and direct runoff production from a population of stores (adapted from Moore (2007))

invocation of this type of simplifying approximation is common in analytic-probabilistic methods such as PDM and the methods derived in this thesis.

Bartlett et al. (2016b) suggest a generalized expression of runoff curve which relates average runoff to antecedent potential retention to unify the SCS-CN, TOPMODEL, TOPMODEL, and PDM based models, although each of these models assumes a different probability distribution of storage capacity. Bartlett et al. (2016a) also suggest a framework that uses joint distributions of soil moisture deficit, water storage capacity, and rainfall to modify the runoff simulation by SCS-CN model. The new probabilistic method accounts for watershed heterogeneity and improves the saturation excess representation by separation of runoff production into classes of "pre-threshold" and "threshold" runoff. While the Bartlett et al. (2016a,b) model was able to unify those approaches for treating heterogeneous landscape storage, the interaction between adjacent stores is still not represented – each store is assumed to function independently. These methods therefore cannot represent the impact of cascading flow between stores or the impact of different types of storage networks.

To implicitly represent the effective response of a heterogeneous watershed with thousands of wetlands, multiple efforts have applied the ideas developed in PDM (Moore, 1985, 2007). For instance, Mekonnen et al. (2014) developed the Probability Distribution Model based RunOFf generation (PDMROF) algorithm in a streamflow routing model (WATFLOOD) to represent the spatial variability of wetlands storage capacity (rather than soil storage) in a basin, using the Pareto distribution function. This algorithm also provided a relationship between direct runoff and available storage in a basin by considering depressions with different storage capacities on a "tile". "Tile", defined as a hydrological unit

accounts for sub-grid scale heterogeneity. The equation used in PDM is identical to that of PDM, except that in PDM, water storage is assumed to be wetland storage, rather than soil storage. Ahmed et al. (2020b) incorporated the PDM algorithm in Hydrologiska Byrns Vattenbalansavdelning (HBV)-light model and introduced a new conceptual HYdrological model for Prairie Region called HYPR. This algorithm is one of the Prairie algorithms embeded in Raven, the hydrological model (Craig et al., 2020), and will be more discussed in chapter 3. A shortcoming of the PDM is that it considers all the water draining from a wetland flows to the outlet, directly, without consideration of runoff movement in a cascading network. It also neglects local runoff contributing area, implicitly treating entire landscape as wetlands. Another model based on the PDM model has been developed by Mekonnen et al. (2016). This model incorporates the Probability Distributed Landscape Depressions (PDLD) approach into the SWAT. SWAT-PDLD considers the water balance equation in every single depression, and by aggregation of runoff from each depression calculates the total outflow from the basin. The exponential distribution of depression storage enables SWAT to consider spatial heterogeneity of numerous wetlands within the basin. PDMROF, PDLD, and PDM (Mekonnen et al., 2014, 2016; Moore, 1985, 2007) are among the few models that represent fill-and-spill in a probabilistic framework. However, these models represent overflow from individual storage units rather than interaction between different depressions. All depressions in these models receive the same amount of water, resulting in an equal filling of each depression. The PDM approach redistributes basin-average storage between various-sized wetlands during evaporation periods. This means that even when the depressions are at or below their storage capacity, water is unrealistically redistributed among depressions. Also, it means that the model is unable to replicate the hysteresis in the filling and emptying of various-sized depressions and between storage and contributing fraction (Clark and Shook, 2022; Shook and Pomeroy, 2011) because there is a simple 1:1 relationship which relates a basin contributing area to average storage. Hysteresis matters since it defines the dependency of model simulation output (in this case, runoff) on the "history of cause" (in this case relationship between contributing area and storage, now and past) (Gharari and Razavi, 2018). Clark and Shook (2022) formulated a spatially integrated model, called meta-depression model as a modified form of PDM which includes hysteretic behavior between storage and contributing area. They demonstrated that the new meta-depression model is comparable with an ensemble-depression model similar to WDPM which explicitly simulate depression storage dynamic. They use the same formulas as Moore except instead of using probability distribution of depressions they defined a meta depression with the area and volume equal to spatial average area and volume of depressions in the basin.

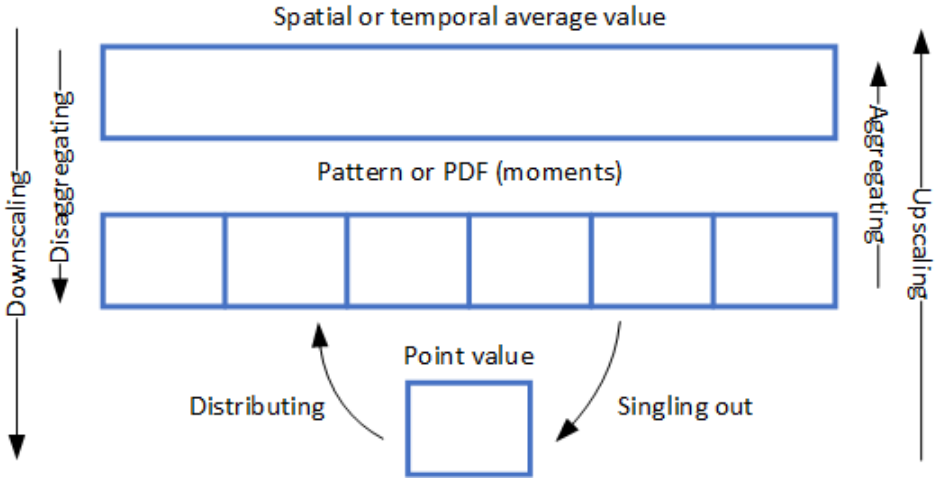

Figure 2.6: Length and time scale of hydrological processes (adapted from Blöschl and Sivapalan (1995))

2.3 Upscaling Hydrological Process

Hydrological processes function at different length scales from several meters to a million square kilometers (Blöschl and Sivapalan, 1995). Blöschl and Sivapalan (1995) defined upscaling as a process by which small-scale (sub-grid) information is transferred to increasingly large (grid) scales. It is not always possible to simulate all processes at the fine scale, typically because of data and computational limitations. The linkage between scales is depicted in Figure 2.6, which classifies upscaling as having two steps: first, small scale variables are distributed over the catchment and then, the spatial distribution of variables are aggregated in one large scale value. As is consistent with Figure 2.6, the purpose of the current study is to transfer the hydrological response of the small scale, with one cascade sequence of wetlands (one small scale value) to a larger scale that has thousands of wetlands (many small scale values) and aggregate this response to find the total outflow from the basin given some snowmelt or rainfall event.

2.3.1 Upscaling Methods

Upscaling methods in hydrology may be classified in three groups based on how they account for sub-grid variability, i.e., the heterogeneity within a unit: effective parameterization; stochastic method, and bulk description (Blöschl and Sivapalan, 1995). Effec-

tive parameterization essentially ignores sub-grid heterogeneity by substitution of a single macro-scale parameter in the micro-scale equations. Stochastic approaches (e.g., Beven and Kirkby (1979), Zhao (1980), Moore (1985), or Craig et al. (2010)) often rely upon probabilistic representation of landscape heterogeneity using probability distribution functions. The upscaled value of interest is generated by aggregation of distributed values using ensemble or volume averaging methods. In volume averaging methods, integration is accomplished over physical volumes of the media rather than in ensemble space (Wood, 2009). In the third approach, an aggregated bulk description replaces sub-grid variability using a single lumped equation. For instance, in Darcy's Law, hydraulic conductivity instead of detailed geometric information about a soil's pore network, represents sub-grid variability (Blöschl and Sivapalan, 1995).

2.3.2 Derived Distribution Approach

In the probabilistic treatment of upscaling, small scale variability is characterized by a probability distribution function (PDF) which represents the spatial variability of small scale parameter values and/or state values over a computational unit. Here, the derived distribution approach which propagates probability distributions through known functions, is used to aggregate this variability and generate an upscaled response. For instance, if $y = g(x)$ defines the relationship between two random variables, X and Y, the derived distribution approach helps to calculate the CDF of outputs/dependent variables (y) based on the known variability of inputs (x). For a monotonic function $g(x)$, we can relate the input (x) and output (y) CDFs as follows (Benjamin and Cornell, 2014):

$$F_Y(y) = P[Y \leq y] = P[X \leq g^{-1}(y)] = F_X(g^{-1}(y)) \tag{2.2}$$

where F_Y represents the cumulative distribution function of random variable Y, and P stands for the probability. The function, $g(x)$, relates dependent parameter y to the independent parameter x, and $g^{-1}(y)$ is its inverse. Here, the PDF of the dependent variable can be calculated from differentiation of the CDF. Using the following equation (Benjamin and Cornell, 2014), we can find the PDF of the dependent variable directly from the PDF of the independent one:

$$f_Y(y) = \frac{d}{dy}F_Y(y) = \frac{d}{dy}[F_X(g^{-1}(y))] = \frac{d}{dy}[\int_{-\infty}^{g^{-1}(y)} f_X(x)dx] = \frac{dg^{-1}(y)}{dy} f_X(g^{-1}(y)) \tag{2.3}$$

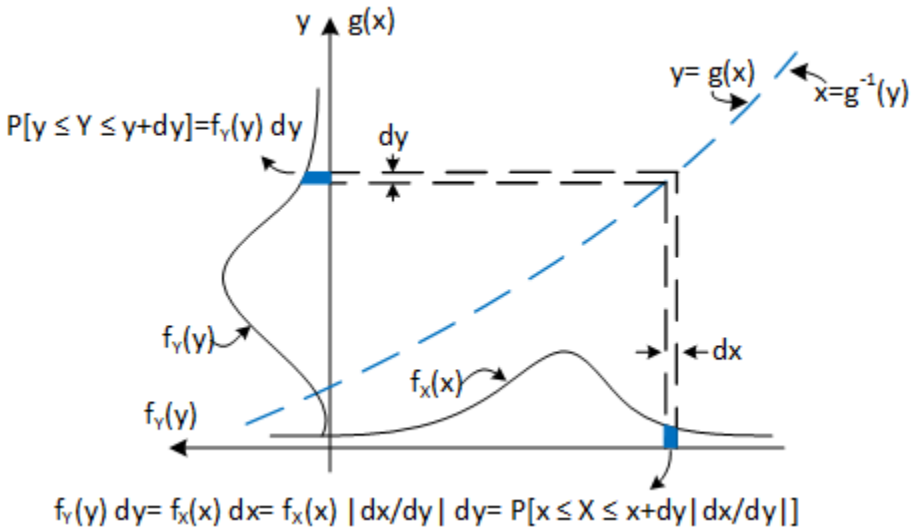

Figure 2.7: Graphical representation of the derived distribution approach while $f_Y(y) = |dx/dy| f_X(x)$ and the shaded areas are equal (adapted from Benjamin and Cornell (2014))

where f_Y represents the probability distribution function of random variable Y. A graphical representation of the derived distribution approach is depicted in Figure 2.7, which shows a single one-dimensional monotonic input-output relationship.

For any function z, as a function of two random variables, x and y, the probability distribution function of a dependent variable z can be calculated based on the x, the y and the function g. For instance, the respective distribution relationships for scaling, sum, and ratio operations upon random variables are as follows (Papoulis, 1965):

$$f_z(z) = \frac{1}{|a|} f_x\left(\frac{z}{a}\right) \text{ where } z = ax \tag{2.4}$$

$$f_z(z) = \int_{-\infty}^{\infty} f_x(x) f_y(z-x) dx \text{ where } z = x + y \tag{2.5}$$

$$f_z(z) = \int_{-\infty}^{\infty} |y| f_x(zy) f_y(y) dy \text{ where } z = x/y \tag{2.6}$$

Based on this approach, Craig (2018) derived the following distribution function for $z = \max(x, a)$

$$f_z(z) = \delta(z-a)\int_{-\infty}^{a} f_x(x)dx + H(z-a)f_x(z) \tag{2.7}$$

where $H(x)$ is the Heaviside step function, which returns one for positive arguments and returns zero for negative one, and $\delta(x)$ is the Dirac delta function, which returns zero everywhere except at $x = 0$ and its integral over the entire domain is one (Arfken and Weber, 1999). Output distributions of more complicated functions can be generated via repeated application of these basic rules, provided that the input distributions are not correlated. This approach may be thought of as a closed-form analytical version of Monte Carlo methods, which requires repeated sampling of the input distribution and model to generate a discrete output distribution.

2.4 Wetland Hydrology in the Taiga Plains

Rapid permafrost thaw is occurring in the subarctic, especially at thaw sensitive discontinuous permafrost regions. Thawing occurs as a result of large-scale drivers, like warming air temperature and intensifying wildfire activity, and low-scale drivers, like lateral thaw through advection and conduction from water bodies and permafrost-free wetlands adjacent to permafrost (Devoie et al., 2021). Permafrost thaw might increase streamflow in discontinuous permafrost region because of thawing of ice-rich peat plateaus, groundwater discharge increase caused by reactivation of groundwater flow paths, and (most importantly) increased hydrological connectivity due to thaw-induced landcover changes (Wright et al., 2022). There has been widespread thawing and degradation of permafrost in southern regions of Canada's permafrost region, where permafrost is discontinuous, narrow, and relatively warm, with an increase in the thickness of the supra-permafrost layer, which includes both the active layer (i.e., the region of soil on top of the permafrost that freezes and thaws annually) and the talik (the region of soil which is permanently thawed) (Connon et al., 2018). The mean annual temperatures in discontinuous permafrost region is mainly above zero (about +2°C), making it hard for reformation of permafrost in those regions (Shur and Jorgenson, 2007; Bonnaventure and Lamoureux, 2013; Quinton et al., 2019). The permafrost in this climate regime remains from previous colder climate periods and without the insulation provided by peat deposits, it would thaw (Devoie, 2021).

Between 1950 and 2009, the areal permafrost extent in the North Slave region, one of five administrative regions in Canada's Northwest Territories, decreased by approximately 28% (Zhang et al., 2014). Morse et al. (2016) note that due to significant latent heat effects and the insulating qualities of organic ground cover, permafrost in the fine-grained sediment

beneath forests is currently being protected from thawing. However, these landscapes are becoming more and more vulnerable to climate change, and a warmer climate can be expected to significantly reduce the extent of permafrost such that a small extent of permafrost region might remain by 2090 (Zhang et al., 2014). Permafrost thaw in the Taiga Plain has been accelerated by climate change, and landscapes that were previously dominated by forests and permafrost are now more frequently wetland-dominated and free of permafrost (Wright et al., 2022; Gibson et al., 2021; Quinton et al., 2011).

To date, several studies have investigated the effects of permafrost thaw on the generated runoff from a basin using observational research. Previously, it was thought that the most important reason for increased streamflow was the reactivation of groundwater pathways caused by permafrost thaw (St. Jacques and Sauchyn, 2009). Connon et al. (2014) studied the increase in annual runoff between 1995 and 2012 in four river basins in the lower Liard River valley, Northwest Territories, Canada, where permafrost-free wetlands have expanded because of the thawing of the permafrost. By using historical aerial photographs and high-resolution satellite imagery, they discovered the most likely factor in increasing annual runoff rate is the conversion of storing landcover features to producing ones, as well as increase in hydrological connectivity between runoff producing landcovers. In this study, they defined secondary and primary contributing areas as parts of a basin that drains to bog and fen, respectively (This terminology will be used in chapter 5 of this thesis).

Taiga shield and taiga plains hydrology are dominated by the "fill-and-spill" processes discussed in Section 2.2. Forested peat plateaus underlain by permafrost and interspersed with permafrost-free wetlands, including channel fens and flat bogs, form the landscape in much of the Taiga plains (Connon et al., 2015). Channel fens transfer water to the basin outlet via wide, hydraulically rough channels and flat bogs retain moisture inputs as storage features, draining to other bogs and fens once full. During spring freshet, large volumes of snowmelt over frozen active layer produces large surface runoff (Wright et al., 2009). It was also observed by Connon et al. (2015) that secondary runoff from bog cascades is comparable to the basin average during melt events when the bog is frozen and infiltration is restricted. Bogs are dynamic transmission features and a key element of the water balance in discontinuous regimes, as demonstrated by a study of two adjacent bog cascades by Connon et al. (2015). Ignoring this storage dependency of runoff leads to an underestimation of streamflow magnitude and an incorrect estimation of the contributing area.

Most studies of the effects of permafrost thaw on runoff generation in headwater basins are based on comparing streamflow observations over time and few of them use hydrological models (Stone et al., 2019). How these basins will hydrologically respond to climate change

is still poorly understood. Stone et al. (2019) simulated the discharge of a channel fen sub-basin in the headwaters of Scotty Creek, Northwest Territories, dominated by peat plateau-bog complexes from 2009 to 2015, using the Cold Regions Hydrological Modelling Platform (CRHM; Pomeroy et al. (2007, 2022)) which is a physically based model capable of simulating key hydrological processes predominant in cold region hydrology (Annand et al., 2022; Spence et al., 2022). According to the findings of this study, for every 10% reduction in permafrost area, the total annual discharge increased by 2.5%. They related this reduced discharge to increase in the surface storage due to the peatland thaw, landscape evapotranspiration, and underground flow path routing. Field observations in the studied basin were used to collect the water balance components, which is impractical in larger basins. Also, instead of using the actual historical landcover transitions, they defined transition scenarios to estimate the permafrost thaw effects on the hydrological response.

There is a need for additional techniques and conceptual models to distinguish between runoff generation processes in primary and secondary contributing areas while taking intermittent wetland interconnections into account, in order to better understand and manage northern water resources. Also, because of the non-stationary landcover due to climate change, use of coupled landcover-hydrological models is desired to comprehend how landcover transitions affect the hydrologic response. Chapter 5 of the thesis will suggest a coupling approach in which the information from a landcover classification and prediction model is used in the hydrological model to investigate the effect of land cover transition induced by permafrost thaw on the generated streamflow magnitude and timing.

Chapter 3

An Upscaled Model of Fill-and-Spill Hydrological Response

The hydrology of wetland-dominated landscapes is often controlled by a fill-and-spill mechanism, whereby surface depressions retain water and release it once a deficit is filled. The response of these systems to precipitation/snowmelt events is influenced by the local storage deficit and connectivity between storage features. To estimate runoff generated from a heterogeneous wetland complex, a closed-form analytical upscaled probabilistic model is developed. The mathematical solution requires information on the distribution of initial deficits and wetland local contributing areas, which may be estimated via a combination of spatial analysis and field observation. The model is used to explore the influence of spatial heterogeneity of wetland properties including deficit depth, local contributing area, and cascade depth (the number of wetlands in-series within a cascade) on runoff response. It is also used to clarify "gatekeeper" storage features role at large scales and for systems with shallow wetland cascade depths. The proposed solution is shown to be a generalization of the well-known Probability Distributed Model and Xinanjiang runoff models, augmented to include information about local contributing areas and wetlands connectivity. The closed form probabilistic mathematical solution is verified by comparing results with Monte Carlo simulations. The proposed runoff model has been implemented in Raven, a hydrologic model, to test the method performance in lumped runoff simulation of wetland-dominated basins influenced by fill-and-spill hydrology. This study can contribute to our understanding of wetland characteristics distribution on landscape hydrology, and compensate for insufficiently resolved elevation data in flat terrains where threshold criteria are hard to estimate.

3.1 Introduction

The term 'fill-and-spill' has been used to describe runoff generation for situations where a portion of the landscape first stores incoming water and then releases it once a storage threshold has been reached. First, recognized as an important rainfall-runoff process by Spence and Woo (2003), it has been found to be a key driver of the hydrologic response in wetland systems (Connon et al., 2014), lake systems (Spence and Woo, 2006), and pothole regions of Canadian prairies (Shaw et al., 2012). In cold regions such as prairies, topographic depressions (here referred to as 'wetlands' for simplicity) also receive water from precipitation, snowmelt and redistribution of snow by wind, and runoff from upstream wetlands and local contributing areas (Fang and Pomeroy, 2008; Shook et al., 2013). They lose water by evaporation, infiltration, discharge to ground water, evapotranspiration, and overflow after exceeding a threshold storage (Hayashi et al., 2003; Shook et al., 2013). This threshold behavior has also been observed in the Boreal Canadian Shield and Taiga plains in the Northwest Territories where wetlands are surrounded by raised land underlain by frozen permafrost Connon et al. (2015). In prairies, wetlands tend to be bowl-like topographic depressions with larger contributing areas, whereas in the discontinuous permafrost region they are steep-sided and separated by berms of permafrost. The fill-and-spill process has likewise been observed in shallow stormflow from hillslopes (Tromp-van Meerveld and McDonnell, 2006), runoff over frozen ground (Coles and McDonnell, 2018), and between lakes in Arctic regions (Bowling and Lettenmaier, 2010; Spence and Woo, 2003). A literature review of field investigations of such fill-and-spill phenomenon may be found in Spence (2010).

Modelling the fill-and-spill phenomenon on a unit-by-unit basis is relatively straightforward, and is the foundation of a number of lumped conceptual models (e.g., the Tank model of SugaWara (1979)). In these models, individual storage compartments (i.e., soil or wetland stores) are represented explicitly, and are allowed to fill and overflow once a storage threshold is exceeded. Other examples include the fully distributed WDPM, a hydraulic model that distributes a simulated water depth over land (Shook and Pomeroy, 2011; Shook et al., 2013), and conceptual reservoir network models such as the parameterized PCM (Shook and Pomeroy, 2011; Shook et al., 2013, 2021a), Simple Pothole Terrain Analysis Algorithm (SPILL) (Shaw et al., 2013b), and modified versions of the SWAT used to assess the effects of geographically isolated wetlands (Wang et al., 2008; Evenson et al., 2015, 2016; Lee et al., 2018; Muhammad et al., 2020). Ease of implementation is a reason why distributed modelling is often applied to simulate threshold-controlled systems. Challenges arise, however, in wetland complexes with thousands of storage features. Not only are these thresholds for individual storage features often poorly known, but these are

heterogeneous systems with spatial variability in contributing area, runoff fluxes, storage, and storage capacity. This complicates our ability to effectively estimate the basin-scale response and if we choose not to explicitly represent individual wetlands, leads to an up-scaling problem.

A variety of probabilistic models have been used to investigate the response of a landscape characterized by a distribution of storage areas to a runoff event. The PDM of Moore (1985) envisioned soil storage on a landscape as a continuum of interacting or non-interacting stores with different storage capacity; smaller stores were more likely to be full and spill water, larger stores would store water until their capacity was satisfied. Once a probability distribution of storage capacity is specified, the rainfall/snowmelt magnitude and system mean storage are sufficient to mathematically estimate landscape-scale runoff using a closed-form expression. In the non-interacting form of PDM, there can be a nonuniform distribution of water through the stores. In the interacting form (most often used), the PDM assumes that unfilled stores have uniform water content, that stores are independently receiving water from precipitation with no contribution from or to upstream/downstream stores, and that all portions of the landscape are covered with storage features. The PDM has been applied successfully to the Canadian prairies, by re-conceptualizing the algorithm in terms of wetland stores rather than the original soil stores, without changing the mathematics. Examples include the PDMROF algorithm in MESH land surface model (Mekonnen et al., 2014) to replicate streamflow and changing contributing area (Mengistu and Spence, 2016) and a modified version of HBV model called HYdrological model for Prairie Region (HYPR) (Ahmed et al., 2020b). In these models, the presence of local contributing areas to wetlands is neglected (i.e., the entire landscape is implicitly covered in wetlands), and cascades of wetlands, where wetlands can fill-and-spill in series, are not represented. Another example of using the PDM for wetland simulation is the Puddle-based Unit PDM (PBU-PDM) implementation in SWAT (Zeng et al., 2020). They aggregated all the depressions located in a subbasin into one large depression and applied the PDM to find the generated runoff from the aggregated landscape. A shortcoming of such a model is that the fill-and-spill process is considered implicitly in groups of depressions while explicit connectivity between storage features (wetlands) and contributing areas are ignored.

A similar strategy, with different assumptions about the storage capacity distribution, leads to the Xinanjiang runoff model (Zhao, 1980; Sahoo, 2005). In the Xinanjiang model, a Pareto distribution characterizes the point-scale spatial heterogeneity in storage capacity. The equivalent forms of the PDM and the Xinanjiang model were first recognized in Moore (1985). Working with the VIC model, an evolution of the Xinanjiang model, Bartlett et al. (2016a) derived analytical expressions that translate the semi-distributed frameworks of

the PDM and Xinanjiang approaches into event-based rainfall-runoff relationships, and demonstrated that the SCS-CN method, PDM, and VIC model are effectively equivalent.

We here develop an upscaled model of fill-and-spill runoff from cascading storage features, henceforth referred to as wetlands, for effective simulation of runoff in prairies, Taiga plains, and Boreal regions of Canada - landscapes composed of thousands of cascading wetlands which drain into channels (Connon et al., 2014, 2015). The model is unique in that: (1) storage features are not necessarily disconnected from upstream storages; the impact of cascading wetlands is explicitly treated and assessed; (2) the landscape is divided into storage features and permeable local contributing areas to those storage features; (3) the approach simulates the storage deficit relative to the overtopping threshold rather than storage volume; and (4) the approach explicitly (and probabilistically) represents heterogeneity in local contributing area, infiltration capacity of local contributing area, and local storage deficit. The use of a derived distribution approach enables the development of closed-form expressions for landscape runoff and local contributing areas as a function of system deficit distribution, precipitation/snowmelt magnitude, and landscape characteristics. The closed-form analytical solution is first derived and then incorporated into a semi-distributed hydrological model to simulate runoff in wetland dominated basins.

The following steps are taken to present the new fill-and-spill method for simulating the hydrological responses of wetland-dominated landscapes. Here, we:

1. Introduce a new method, the UWFS method, which handles the probabilistic treatment of fill-and-spill phenomenon in systems represented by wetland cascades

2. Derive the closed-form analytical solution for the special case of specified truncated exponential distributions of wetland storage deficit and wetland local contributing area ratio

3. Demonstrate that the approach is a generalization of the PDM (Moore, 1985), and Xinanjiang (Zhao, 1980) models

4. Compare the analytical event model against Monte Carlo solutions of thousands of wetlands

5. Demonstrate the sensitivity of landscape runoff response to the deficit distribution, wetland cascade depth, and local contributing area ratio

6. Assess the performance of the proposed method by incorporating it into a continuous-time hydrologic model, where deficit distribution is allowed to evolve in time, and simulating the upscaled daily runoff response and mean storage dynamics in systems

of hundreds to thousands of wetlands in prairie basins at the spatial scale of on the order of 1000 km^2 without simulating individual wetlands.

3.2 Methods

The UWFS method is presented here in four parts. First, general expressions are established for event runoff from a landscape in which individual wetlands drain to a surface stream network. Second, the full UWFS method is extended to account for the impact of (1) the number of wetlands in a cascade series (termed the "wetland cascade depth") and (2) the effective outflow from a wetland-dominated landscape comprised of thousands of cascading storage features. Third, the PDM and Xinanjiang methods are demonstrated to represent a specific simplified case of the UWFS method. Finally, the event-based model is extended for continuous applications and deployed to simulate runoff response in a set of prairie basins.

3.2.1 Conceptual Model and Approach

The foundation of the probabilistic treatment of fill-and-spill in this work is the categorization of the landscape into wetland cascades: groupings of wetlands that are serially ordered with one downstream connection to a surface water network (i.e., streams or fen channels). Initially, only cascades with a network branching ratio equal to one are considered (i.e., wetlands are structured in series and each has a maximum of one upstream input). If the distribution of initial storage across all wetland cascades is specified, an analytical upscaling procedure can be used to determine the bulk response of a basin to continuous series of rainfall or snowmelt events. A conceptual illustration of a wetland cascade is provided in Figure 3.1a. For each wetland in a cascade, a simple event model (or single-time step) represents the fill-and-spill response, as depicted in the conceptual model in Figure 3.1b. In this conceptualization, the total water available to the most upstream wetland in a cascade is the sum of the water directly falling onto the wetland and the runoff from the surrounding local contributing area. Wetlands are effectively treated as prismatic storage units that receive water until a threshold is reached, after which any additional water flows downstream. The assumption of prismatic storage unit is not wholly necessary for the derivations, but simplifies presentation of the basic model and deficit volume-depth relationship. The total outflow from the most upstream wetland in a cascade can be derived based on the amount of water input minus the storage deficit that would prevent the downstream movement of water as follows,

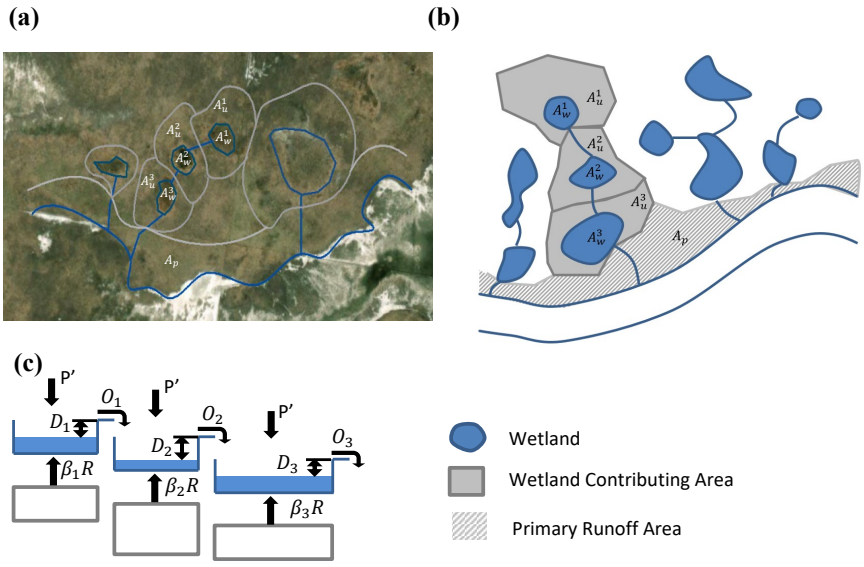

Figure 3.1: (a) Plan view of a wetland cascade network focusing on one wetland cascade with the depth of three wetlands (Sources: Google Earth), (b) schematic of the wetland cascade network, and (c) simplified model representation. D represents deficit depth of each wetland, βR represents the runoff from each wetland's local contributing area, normalized by wetland area, and O represent outflow from a wetland.

$$O_1^* = \frac{A_u^1}{A_w^1} \cdot R + P' - D_1 = \beta_1 . R + P' - D_1 \tag{3.1}$$

$$O_1 = \max(O_1^*, 0) \tag{3.2}$$

where $\mathbf{O^*}_1$ [mm] and $\mathbf{O}_1$ [mm] represent the potential and actual volumetric outflow normalized by the wetland area to reduce calculation dimension and prevent the need for wetland area values, respectively ("potential" in that Equation 3.1 can resolve in a negative value, which cannot be defined as outflow); $\mathbf{A_u}^1$ $[L^2]$ is the local contributing area of the first wetland, which does not include the wetland area; $\mathbf{A_w}^1$ $[L^2]$ is the area of the wetland itself; and β_1 [-] is the relative size of the local contributing area ($\beta_1 = A_u^1/A_w^1$), herein defined as the "local contributing area ratio"; $\mathbf{R}$ [mm] is the rainfall excess from

the local contributing area (i.e., the fraction of precipitation or snowmelt remaining after other processes such as evapotranspiration are applied and that can contribute to runoff, which can be found from any desired runoff generation algorithm); $\mathbf{P'}$ is rainfall over the wetland area and it is equal to zero during snowmelt events; and $\mathbf{D}_1$ [mm] is the wetland storage deficit. Note that if the local contributing area greatly exceeds the wetland area, the deficit term becomes negligible and the wetlands play no role in moderating the outflow. Conversely, for large deficits and low runoff ratio (such as when a storm happens after a dry period) wetlands play a dominant role in controlling basin runoff response. Based upon integral relations describing the sum of two random variables, (Papoulis and Pillai, 2002):

$$f_A(A) = \int_{-\infty}^{\infty} f_B(x) f_C(x - A) dx \quad \text{where } A = B - C \tag{3.3}$$

where A, B, and C are random variables and $f_A(A)$, $f_B(B)$, and $f_C(C)$ are their distributions, Equation 3.1 may be written for an infinite number of wetlands subjected to a fixed runoff, R, initial deficit, D, and local contributing area ratio, β, sampled from frequency distributions, f_D and $f_{\beta R}$, as,

$$f_{O^*}(O^*) = \int_{-\infty}^{\infty} f_{\beta R + P'}(x) f_D(x + P' - O^*) dx \tag{3.4}$$

where $f_{\beta R+P'}$ and f_D are the probability distributions of the local inflow and deficit, respectively. The probability distributions of local contributing area ratio, β, and deficit, D, represent spatial variability in the size of the contributing areas for individual wetlands and variability in the water level of each wetland relative to its spilling threshold, respectively. Note that Equation 3.1 describes the most upstream wetland in a cascade, which is distinct from all other wetlands in that it has no upstream input. The water balance equation or potential outflow from the nth wetland within a cascade of depth $N > 1$ is,

$$O_n^* = \beta_n R + P' - D_n + \left(\frac{A_w^{n-1}}{A_w^n} O_{n-1} \right) = \gamma_n + O_{n-1} \tag{3.5}$$

where γ_n is the sum of the water added through precipitation/snowmelt minus the storage deficit ($\gamma_n = \beta_n R + P' - D_n$). Note that in this work, all wetlands in a single cascade are assumed to have comparable areas to make the problem mathematically tractable. The impacts of this assumption on generated runoff from wetlands in wetland cascade depth greater than one is later investigated in Section 3.4.5. The distribution of potential outflow from any wetland in the cascade is therefore (using the same relations used to generate Equation 3.4):

$$f_{O_n^*}(O_n^*) = \int_{-\infty}^{\infty} f_{\gamma_n}(O_n^* - x) f_{O_{n-1}}(x) dx \tag{3.6}$$

Using the derived distribution relationships for the maximum of two random variables as,

$$f_A(A) = \delta(A) \int_{-\infty}^{0} f_B(x) dx + H(A) f_B(A) \quad \text{where } A = \max(B, 0) \tag{3.7}$$

The actual outflow from a wetland cascade is derived as the maximum of the potential outflow and zero (Equation 3.2) as

$$f_{O_n}(O_n) = \delta(O_n) \int_{-\infty}^{0} f_{O_n^*}(x) dx + H(O_n) f_{O_n^*}(O_n) \tag{3.8}$$

where $\mathbf{H(x)}$ is the Heaviside step function, which returns one for positive arguments and returns zero for negative one, and $\delta\mathbf{(x)}$ is the Dirac delta function, which returns zero everywhere except at $x = 0$ and its integral over the entire domain is one (Arfken and Weber, 1999). These integrals may be handled via numerical or analytical integration and are an alternative to Monte Carlo simulation of wetland outflow via sampling of the input distribution. This equivalency is discussed in section 3.4.1.

3.2.2 Analytical Solution for Wetland Cascade Depth of One

A closed-form analytical solution for the total outflow from a landscape of wetland cascades can be derived by assigning practical and mathematically tractable probability distributions to the distributions of the local contributing area ratio, β_1 which is equal to A_u^1/A_w^1, and deficit, D. Here, these distributions are characterized by truncated exponential distributions as follows,

$$f_D(D) = H(D - D_{min}) d e^{-d(D - D_{min})}(1 - P_f) + \delta(D) P_f \tag{3.9}$$

$$f_\beta(\beta) = H(\beta - \beta_{min}) b e^{-b(\beta - \beta_{min})} \tag{3.10}$$

$$f_{\beta R + P'}(\beta R + P') = H(\beta R + P' - \beta_{min} R) \frac{b}{R} e^{-\frac{b}{R}(\beta R + P' - \beta_{min} R)} \tag{3.11}$$

where $f_D(D)$, $f_\beta(\beta)$, and $f_{\beta R+P'}(\beta R + P')$ are the distribution functions of deficit, D, local contributing area ratio, β, and the available water to wetlands (i.e., local inflow), $\beta R + P'$,

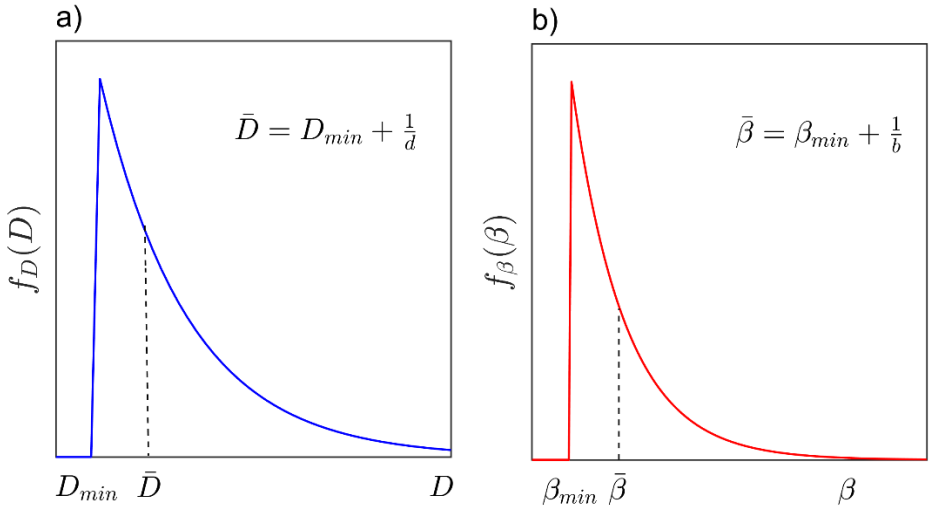

Figure 3.2: Distribution functions of wetlands' a) initial deficit and b) local contributing area ratio. Dashed lines show the average of deficit ($\bar{D}$) and local contributing area ratio ($\bar{\beta}$).

respectively; $D = (\overline{D} - D_{min})^{-1}$ and $\mathbf{b}$= $(\overline{\beta} - \beta_{min})^{-1}$ are the shape parameters of the exponential distributions, $\mathbf{P_f}$ is the percentage of the wetlands with zero deficit prior to the runoff event, D_{min} and β_{min} are the minimum deficit and local contributing area ratio, and $\overline{D}$ and $\overline{\beta}$ are the average deficit and local contributing area ratio, respectively. A β_{min} greater than zero implies that all wetlands must have non-zero contributing area. These distributions are depicted in Figure 3.2.

Following Equations 3.4 and 3.8, an analytical solution for a landscape of wetland cascades, each composed of an identical number of wetlands, can be derived. For example, the analytical solution for the mean outflow from a landscape of wetland cascades with a wetland cascade depth of one ($\mathbf{N}$= 1) is (by evaluating integral in Equation A.2 using Equations 3.9 and 3.10),

$$\bar{O_1} = \int_0^\infty O f_O(O) dO = \frac{1}{(\bar{\beta}+1)} \begin{cases} \frac{ad}{a+d}(1-P_f)\left[\frac{dP^*-1+e^{-dP^*}}{d^2} + \frac{aP^*+1}{a^2}\right] + & \\ P_f(P^* + \frac{1}{a}) & \text{for } P^* > 0 \\ \frac{ad}{a+d}\left[\frac{e^{aP^*}}{a^2}\right] & \text{for } P^* \leq 0 \end{cases} \tag{3.12}$$

where $a = b/R$ and $P^* = \beta_{min}R + P' - D_{min}$. Also, since the outflow rate is for the outflow in mm normalized by the wetland area, to convert the outflow to a mean basin-wide runoff the term $1/(\bar{\beta}+1)$, equivalent to $A_w/(A_u + A_w)$, is needed. The detailed derivations for a wetland cascade depth, N, of one, two, three, and four are provided in Appendix A.1 to A.4.

To test the validity of the proposed model, the analytical solution presented in Equation 3.12 is compared to a Monte Carlo model. A Monte Carlo sampling of the two distributions (initial deficit and local contributing area ratio defined in Equations 3.9 and 3.10, respectively) is performed. Outflows for each wetland are calculated directly using Equations 3.1 and 3.5 and the total outflow form a system of 10000 wetlands are compared to those obtained analytically.

3.2.3 Equivalency to PDM and Xinanjiang Model

The proposed model is a generalization of the existing PDM of Moore (1985) and the VIC model (Wood et al., 1992), both of which follow the basic approach of the Xinanjiang model (Zhao, 1980). The PDM is underpinned by a Pareto distribution function of the soil storage capacity ($\mathbf{c}$) over a basin (Moore, 1985),

$$f_c(c) = \frac{s}{c_{max}}\left[1 - \frac{c}{c_{max}}\right]^{s-1} \qquad 0 \leq c \leq c_{max} \tag{3.13}$$

where $\mathbf{s}$ is the shape factor parameter, and $\mathbf{c_{max}}$ [mm] is the maximum storage capacity within the basin. After a precipitation event of magnitude P, all soil columns with a storage capacity less than the critical storage capacity, $\mathbf{c}^*$, are considered to be full. Here, we considered the approach in the PDMROF model of Mekonnen et al. (2014), in which the storage capacity of wetlands is used rather than soil columns. Because the VIC/Xinanjiang and PDMROF/PDM approaches are equivalent (Bartlett et al., 2016b), the UWFS method is here only directly compared to the results of the PDMROF method. Although the PDMROF model characterizes the total contributing area of the basin, it is unable to characterize the local contributing area of each wetland store, which in PDMROF is assumed to be equal to the storage area. To establish equivalency of UWFS with PDMROF (based on a distributed store capacity of wetlands), the wetland is forced to have no local contributing area by setting β to zero. Thus, the potential outflow, O^*, of Equation 3.1 is simplified to,

$$O^* = P' - D \tag{3.14}$$

The PDMROF model is expressed in terms of the distribution of storage capacity, c. Here, we first re-express the formulation in terms of deficit distribution, which is related to the critical storage capacity (the storage beneath which all storage compartments have a deficit). The relationship between $f_c(c)$ and $f_D(D)$ is,

$$f_D(D) = H(D)f_c(c - c^*) + \delta(D)\int_0^{c^*} f_c(c)dc \tag{3.15}$$

By substituting Equation 3.15 and a fixed single value of βR in Equation 3.4, the distribution function of potential outflow from all wetlands across the landscape in response to a rainfall magnitude, P', can be characterized as,

$$f_{O^*}(O^*) = H(O^* - P')f_c(O^* - (c^* + P')) + \delta(O^* - P')\int_0^{c^*} f_c(c)dc \tag{3.16}$$

The average runoff from the UWFS method can be calculated by subsequently inserting Equation 3.16 into Equation 3.8 then calculating the expected value of the resultant outflow distribution $f_O(O)$,

$$\begin{aligned}\bar{O} &= \int_{\max(P'+c^*-c_{max},0)}^{P'} O f_O(O)dO \\ &= P' - \frac{c_{max}}{s+1}\cdot\begin{cases}(1-\frac{c^*}{c_{max}})^{s+1} & \text{for } P' > c_{max} - c^* \\ [(1-\frac{c^*}{c_{max}})^{s+1} - (1-(1-\frac{c^*+P'}{c_{max}})^{s+1})] & \text{for } P' < c_{max} - c^*\end{cases}\end{aligned} \tag{3.17}$$

which is equivalent to the relationship between rainfall and runoff proposed in the PDM of Moore (1985),

$$V(t+\Delta t) = \pi_i \Delta t - \frac{c_{max}}{s+1}\cdot\begin{cases}[(1-\frac{c^*(t)}{c_{max}})^{s+1} & \text{for } \pi_i\Delta t > c_{max} - c^*(t) \\ (1-\frac{c^*(t)}{c_{max}})^{s+1} - (1-\frac{c^*(t+\Delta t)}{c_{max}})^{s+1}] & \text{for } \pi_i\Delta t < c_{max} - c^*(t)\end{cases} \tag{3.18}$$

where V is the direct runoff, and $\pi_i\Delta t$ is the net rainfall over the time interval of $(t, t+\Delta t)$ which is equivalent to P' in UWFS method. Figure 3.3 shows the runoff calculated from Equation 3.17 by UWFS method versus runoff calculated from Equation 3.18 by PDM. The perfect match between those two shows the ability of the UWFS formulation to replicate the results of PDM when β is set to zero and a Pareto distribution is used. Although the UWFS model is able to replicate the PDMROF simulation results, it additionally includes the impact of local contributing areas and cascading wetlands.

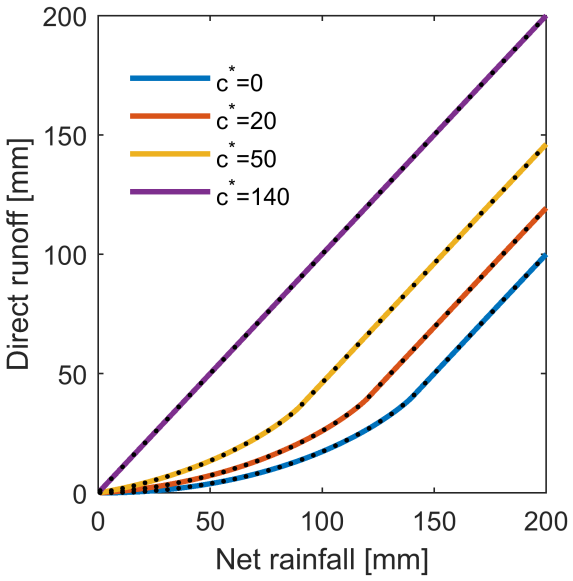

Figure 3.3: Direct Runoff, $\bar{O}$, generated by PDM (points) and simplified UWFS method (lines) in response to the net rainfall or rainfall excess for $s = 0.4$, $c_{max} = 140$, and varying critical storage capacities (c^*) (Modified from Moore (2007))

3.2.4 UWFS Algorithm Implementation in a Hydrologic Model and Performance Evaluation

In previous sections, the event-based form of the UWFS algorithm was presented. The continuous-time UWFS model is a modified version of HBV-light model (Seibert, 2005) which simulates streamflow in the following steps: first, degree day method is used to represent melt and refreezing of the snow-packs. Then, the abstraction process (i.e., redirecting the rainfall and rainfall excess including snowmelt and runoff from local contributing area to surface wetlands) is computed using the UWFS algorithm presented in section 3.2.1. Here, to extend the UWFS method into a continuous runoff model, the evolving deficit distribution across the landscape is tracked and modified via evapotranspiration between runoff events. The magnitude of runoff in wetland complexes is highly dependent on the storage dynamics rather than the travel time; therefore, the advection due to the travel time is neglected. To revise the deficit distribution, the values of D_{min} and P_f, which characterize the distribution, are updated at each time step. If runoff is released from the whole basin, the new minimum deficit depth, $D_{min}(t + \Delta t)$, is set to zero and the new

percentage of full storage units, $P_f(t+\Delta t)$ may be calculated as

$$P_f(t+\Delta t) = \begin{cases} 1 - \frac{a}{a+d} e^{-dP^*}(1 - P_f(t)) & \text{for } P^* > 0 \\ 1 - (\frac{a}{a+d}(1 - P_f(t)) + (\frac{d}{a+d}(1 - P_f(t)) + P_f(t))(1 - e^{aP^*})) & \text{for } P^* \leq 0 \end{cases} \tag{3.19}$$

which takes a value between zero and one. Alternatively, if no runoff is released from the wetland complex the $P_f(t+\Delta t)$ is set to zero and the deficit distribution is shifted rightward after accounting for the added runoff from the local contributing area to the wetlands,

$$D_{min}(t+\Delta t) = \max(D_{min}(t) - min(\bar{\beta}R + P', D_{min}(t)) + ET, 0) \tag{3.20}$$

where $\bar{\beta} = \beta_{min} + 1/b$, the mean local contributing area ratio and ET stands for evapotranspiration calculated using the method of Oudin et al. (2005). The average deficit, D_{avg} as one of the parameters required to characterize the exponential distribution is calculated as

$$D_{avg} = \frac{Dep_{max} - Depression}{Dep_{frac}} \tag{3.21}$$

where Dep_{max} and Dep_{frac} represent the maximum of depression depth and maximum area that is covered my depressions, respectively.

Figure 3.4 shows the shifted deficit distribution after an evapotranspiration and precipitation event. The approach outlined here is designed to preserve the global mass balance of the wetland complex. To have a tractable description of the resultant deficit distribution, the local mass balance is adjusted by a redistribution of water between wetlands, as done in comparable statistical models such as the PDM and VIC. Otherwise, in order to exactly adjust deficit depths for each event, the distribution would quickly become intractable, and would have to be defined as a summation of multiple Dirac functions and truncated exponential distributions. This probabilistic approach is required in order to respect spatial variable deficit depths without explicitly representing thousands of wetlands or converting all wetlands into a single effective wetland. The initial deficit distribution is shown in Figure 3.4-a, where $P_f\%$ of the wetlands are full. After evapotranspiration the entire deficit distribution and the Dirac representing the truncated part is shifted to the right as shown in Figure 3.4-b. Then, the distribution is updated, as the average deficit becomes equal to initial average deficit plus evapotranspiration, as shown in Figure 3.4-c. It can also be noted that the magnitude of these changes to the distribution are quite small over a single time step, since the daily evapotranspiration magnitude is small. The deficit distribution changes in response to precipitation is depicted in Figure 3.4-d to f. Where available water, $\beta R + P'$, is applied to the deficit depths and the distribution is shifted to

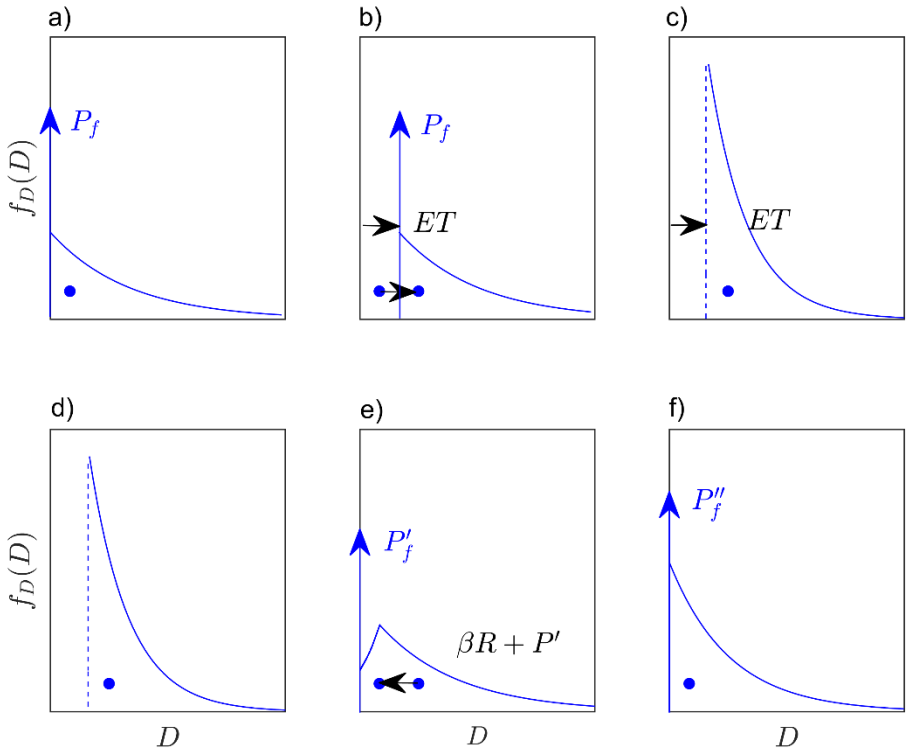

Figure 3.4: Deficit distribution change after evapotranspiration (top-row) and precipitation (bottom-row). Black arrows show the distribution shift due to evapotranspiration and precipitation. P_f, P'_f, and P''_f are the initial, after precipitation, and modified percentage of full wetlands in a basin, respectively.

the left. A new Dirac, P'_f, represents the full deficit after precipitation in Figure 3.4-e. The distribution is updated as depicted in Figure 3.4-f to a new exponential distribution with a new Dirac, P''_f. The final distribution may be narrower or broader since the distribution is adjusted differently in response to precipitation and evapotranspiration. The excess runoff not stored in wetlands infiltrates and the infiltration rate is calculated using the partition coefficient method (Craig, 2020).

The UWFS algorithms were implemented in the Raven hydrologic modeling framework (Craig et al., 2020) along with the other hydrological processes mentioned above. Raven is a flexible hydrologic modelling framework that has over 100 hydrological process algorithms and new hydrological processes are readily implemented in the source code. The UWFS model used here is a modification of the HBV model, where the runoff calculation is handled via Equation 3.17 and the deficit is updated via Equation 3.20. The UWFS

Raven implementation is therefore analogous to the HYPR model of Ahmed et al. (2020b) except the PDMROF algorithm is replaced with the UWFS algorithm. Raven can also emulate the HYPR model, which facilitates direct comparison between simulated runoff using the HYPR and the UWFS algorithms.

Ten hydrological models were built for ten prairie sub-basins inside the Qu'Appelle River Basin (QRB) as discussed in Section 3.3. A set of parameters affecting the model performance and their ranges are listed in Table 3.1, and used in the manual and automated calibration. The Dynamically Dimensioned Search (DDS) algorithm (Tolson and Shoemaker, 2007) in OSTRICH (Matott, 2017) with 2,000 iterations and ten replicates is used to calibrate parameters to improve the performance of the model in streamflow simulation. The capability of the model in simulation of runoff response during the model calibration and validation periods is assessed using the Kling–Gupta Efficiency (KGE) (Gupta et al., 2009) metric which is calculated as,

$$KGE = \sqrt{(r-1)^2 + (\frac{\mu_{sim}}{\mu_{obs}} - 1)^2 + (\frac{\sigma_{sim}}{\sigma_{obs}} - 1)^2} \tag{3.22}$$

where **r** is the correlation between simulated and observed streamflow, $\mu_{\mathbf{sim}}/\mu_{\mathbf{obs}}$ is the ratio of the mean simulated to mean observed streamflows, and $\sigma_{\mathbf{sim}}/\sigma_{\mathbf{obs}}$ is the ratio of the simulated to observed streamflow variance. The Percent Bias (PBIAS) is another metric used here to evaluate the performance of runoff simulation during calibration and validation period. This metric is calculated as,

$$PBIAS = \frac{\Sigma_{i=1}^{n} X_i^{obs} - X_i^{sim}}{\Sigma_{i=1}^{n} X_i^{obs}} \tag{3.23}$$

where X_i^{obs} and X_i^{sim} are the observed and simulated streamflow, respectively. The acceptable range for PBIAS in streamflow simulation is typically less than ±25% (Moriasi et al., 2007), though larger PBIAS values are common for models of prairie basins (Ahmed et al., 2020b), which are notoriously challenging to simulate.

3.3 Study Area

To test the ability of the UWFS algorithm in simulation of wetland-dominated low-gradient landscapes, ten prairie sub-basins inside the QRB in Saskatchewan, Canada were selected as the study area, shown in Figure 3.5. The Prairie Pothole Region of Canada is one of the challenging wetland-dominated landscapes to simulate using hydrological models (Mekonnen et al., 2015, 2016). The required meteorological forcing data for hydrologic simulation

Table 3.1: UWFS parameters range for calibration

Parameter name	Description	Units	Min	Max	Model configuration
RAIN_CORR	Rain bias correction factor	[-]	0.8	1.2	
SNOW_CORR	Snow bias correction factor	[-]	0.8	1.2	
DD_MELT_TEMP	Degree day melt coefficient	°C	-3	3	
FIELD_CAPACITY	Field capacity saturation of the soil	[0..1]	0	1	
BASEFLOW_COEFF	Linear baseflow storage/routing coefficient	1/d	0.01	1	
DEP_{max}	Maximum amount of water that stored in depressions	mm	50	500	UWFS, HYPR
DEP_{frac}	Percent of landscape covered by depressions when full	[0..1]	0.1	0.8	
DEPRESSION	Initial amount of water that stored in depressions	mm	0	300	Initial parameters
RAINSNOW_DELTA	Range of rain-snow transition zone	°C	0	4	
HBV_BETA	HBV soil evaporation exponent	[-]	0	7	
PONDED_EXP	Exponent used in HYPR model	[-]	1	5	HYPR
PDMROF_B	Shape factor for Pareto distribution in pothole storage module	[-]	0.1	30	
PARTITION_COEFF	Runoff fraction	[0..1]	0.5	1	
RAINSNOW_TEMP	Rain/snow halfway transition temperature	°C	-1	1	
FOREST_COVERAGE	Fraction of land covered by vegetation canopy	[0..1]	0	1	
OW_PET_CORR	Fraction of PET to apply to open water evaporation	[-]	0.8	1.2	UWFS
β_{min}	Minimum local contributing area ratio	[-]	0	4	
b	Shape factor of local contributing area ratio distribution	[-]	0.01	10	
D_{min}	Minimum amount of deficit in each depression	mm	0	50	Initial parameters

by UWFS and HYPR in the Raven model includes precipitation and temperature. The model uses the Regional Deterministic Reanalysis System (RDRS) second version (Gasset et al., 2021) as retrieved from CaSPAr website (Mai et al., 2020) as meteorological forcing inputs. The data are available at an hourly temporal scale and at 10 km spatial resolution from 2000 to 2017. The streamflow data at the gauge located at the outlet of each sub-basin is sourced from the Water Survey of Canada (WSC, 2022a). The stations names and areas are reported in Table 3.2.

Table 3.2: QRB sub-basin properties

Sub-basin name	MooseJaw	Cutarm	Ekapo	JumpingDeer	KronauMarsh
WSC gauge number	05JE006	05JM015	05JM010	05JK004	05JF012
Total drainage area [km^2]	9230	766	1100	1680	2980
Sub-basin name	Lanigan	Lewis	Pheasant	Ridge	Saline
WSC gauge number	05JJ003	05JH005	05JL005	05JG013	05JJ009
Total drainage area [km^2]	2280	572	1150	460	950

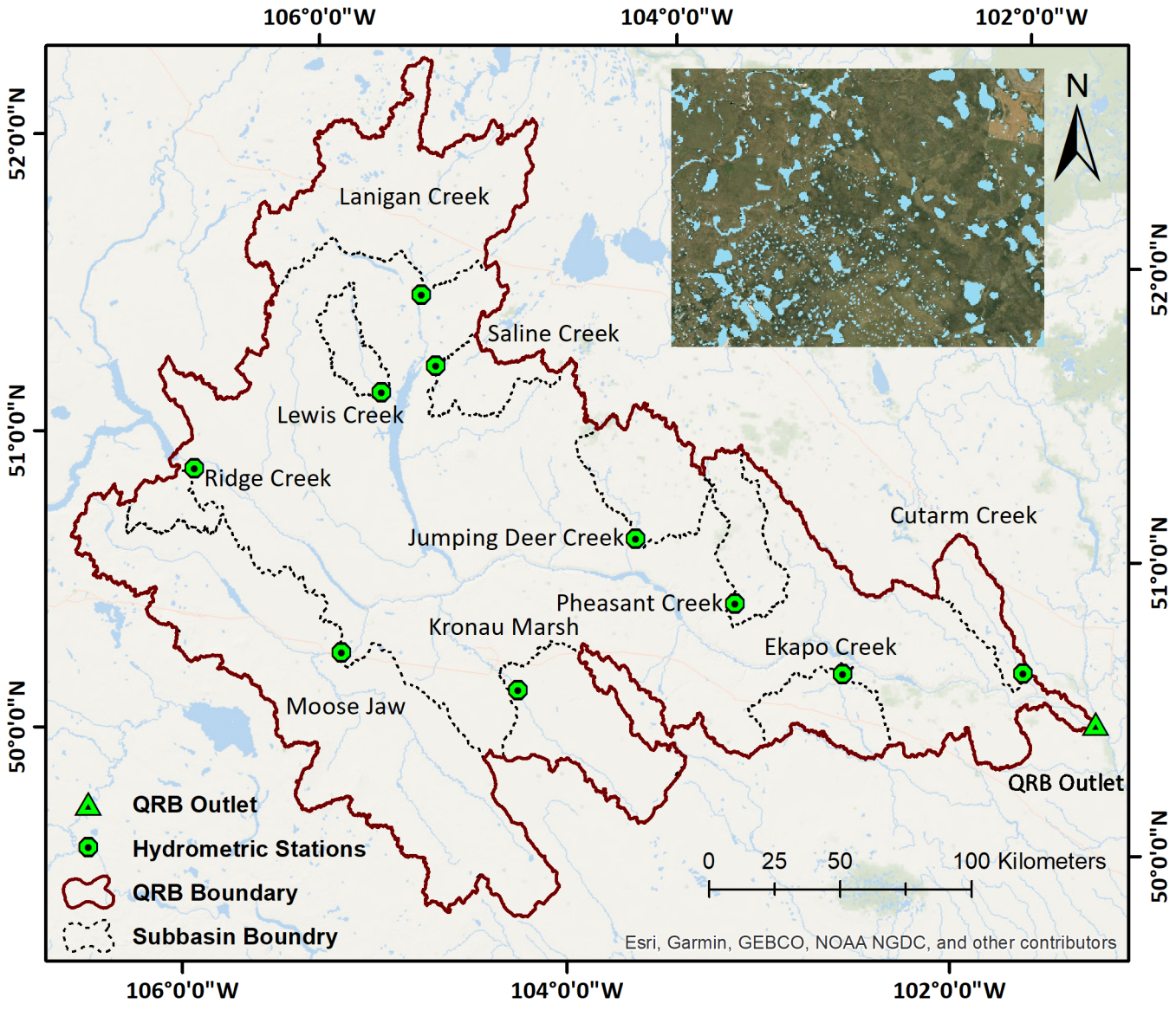

Figure 3.5: Location of the ten study subbasins, and their hydrometric stations inside the Qu'Appelle River Basin in Saskatchewan, Canada. The inset map is a typical land cover in this basin.

3.4 Results and Discussion

The evaluation of the UWFS method is herein demonstrated in relation to four objectives. First, the method is benchmarked against Monte Carlo simulations to verify its mathematical correctness. Second, the outflow response of a landscape comprised of wetland cascades of varying depth as well as varying initial deficit distributions is examined. Third, a sensitivity analysis is completed to scrutinize the dependence of landscape outflow to wetland initial deficit (i.e., wetness of the basin) and local contributing area ratio (i.e., wetland geometry). Lastly, the capability of the proposed method in simulation of the runoff response from the ten sub-basins in the QRB is assessed by comparison of simulated and observed streamflow.

3.4.1 Benchmarking Against Monte Carlo Solutions

Figure 3.6 illustrates the normalized outflow (i.e., outflow for unit precipitation) from a landscape in response to a range of precipitation events as derived by the analytical solution and the Monte Carlo model using 10000 random samples from input deficit and local contributing area ratio distributions. This figure also demonstrates the changing outflow behavior as the depth of each wetland cascade evolves from a wetland cascade depth of one to four. The close match between the two models, the average RMSE value of 0.2% in all four cases of wetland cascade depth, demonstrates the validity of the analytical solution. In general, this exercise also demonstrates that the Monte Carlo approach, while more computationally expensive, is an effective alternative to the derivation of new analytical solutions at wetland cascade depths greater than four, for which the derivation of an analytical solution is mathematically challenging.

3.4.2 Effect of Wetland Cascade Depth and Initial Deficit on Normalized Outflow

Figure 3.7 depicts the simulated range of outflow responses of a wetland landscape and how it changes as a function of the wetland cascade depth, N, and the antecedent water deficit, D. The landscape is subjected to a range of precipitation events of different magnitudes at four minimum deficit values, representing wetter ($D_{min} = 0$ mm, $P_f = 30\%$), wet ($D_{min} = 0$ mm, $P_f = 0$), average ($D_{min} = 50$ mm, $P_f = 0$), and dry ($D_{min} = 100$ mm, $P_f = 0$) conditions. Qualitatively, these regimes represent how quickly the landscape tends to spill in response to an input precipitation event (e.g., in the wet and very wet

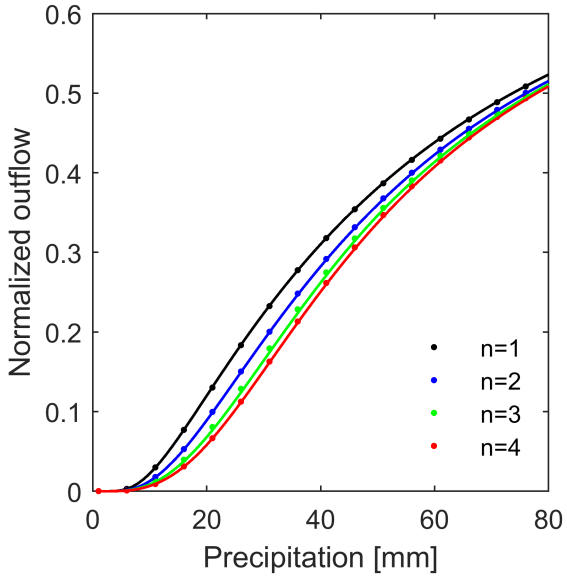

Figure 3.6: UWFS (lines) and Monte Carlo (points) simulation of normalized outflow in response to precipitation in a landscape with a wetland cascade depth (n) of one, two, three, and four. In all cases $\beta_{min} = 0$, $\bar{\beta} = 2$, $b = 0.5$, $R = 0.8P$, $P' = P$, $D_{min} = 50$ mm, and $D_{avg} = 100$ mm.

conditions, any added precipitation causes an immediate outflow). The effect of the initial deficit on the outflow from the landscape is illustrated in Figure 3.7. It can be inferred that, for the same wetland cascade depth, as the initial condition is wetter the normalized outflow is higher. This fact is consistent with the observations from Ahmed et al. (2020a) in which the probability of streamflow exceedance is shown to be higher where potholes are full compared to empty potholes. This figure also illustrates the lag in outflow response that occurs under dryer conditions, where the initial deficit must be overcome before any outflow is produced and the effect of the initial deficit condition in minimizing the disparity between the outflow produced from wetland cascades composed of different wetland cascade depths. For example, at lower runoff magnitudes and under wet conditions, a wetland with a wetland cascade depth of one will produce as much as 10% more outflow than a cascade composed of four wetlands in series; conversely, under dry conditions, the difference is only around 5%. This reflects the known control of "gatekeeper" wetlands (Phillips et al., 2011) (which can only exist in a cascade of depth greater than one). In the case of wetland cascade depth of one, a large deficit acts as a gatekeeper for its own contributing area.

However, for the wetland cascade depth larger than one, the gatekeeper disconnects the downstream wetlands from upstream landscape until they themselves are over-topped and outflow is generated. Previous studies show that large gatekeepers (i.e., 30% of the total basin area) located close to the outlet of a basin have dramatic impacts on the generated streamflow; however, for basins with thousands of wetlands and no large gatekeepers, the spatial arrangement of wetlands is less important (Shook et al., 2021a). At larger precipitation magnitudes, the influence of wetland cascade depth becomes negligible, as input volumes are large enough to overcome the deficits in all members of a wetland cascade, therein overriding the gatekeeper effect. This, notably, also depends on the assumption that the population of wetlands is so large that it can be represented by a continuous probability distribution; for small watersheds with low number of wetlands (e.g., 20 wetlands), the role of gatekeepers can be more salient.

It is worthy here to note the observed convergence of the curves with increasing wetland cascade depth, N, in Figure 3.7 is also a sign of the presence of gatekeepers. Inactive gatekeepers disrupt wetland connectivity in cascades, disconnect upstream wetlands from the outlet, and limit the number of wetlands that are connected to the outlet and generate outflow. For this reason, the normalized outflow does not change significantly with the increasing wetland cascade depth. This suggests that if the local contributing area and deficit can be presumed to be independent of the wetland location in the cascade sequence, there is little practical need to extend the model to large values of N. It also implies that N=3 is a reasonable surrogate for deeper cascade networks. In examining the 'wet' curves of Figure 3.7, it is clear that for the $N = 1$ case, when the P_f is 30%, which means 30% of full wetlands are overflowing, immediate runoff generates from the landscape upon receiving any rainfall. However, the deeper networks decrease the generated runoff, since the 30% of full wetlands may be further up the network and the downstream wetlands need to be filled to generate outflow.

3.4.3 Sensitivity Analysis

To further explore the controls of the initial deficit and local contributing area ratio distributions on landscape outflow, a sensitivity analysis is conducted on a wetland system comprised of individual wetlands draining to a main channel (N=1). Here, R, the excess rainfall in Equation 3.1, is considered to be equal to $0.8P$ where b and β_{min}, the parameters of local contributing area ratio distribution in Equation 3.10, are perturbed. To capture a feasible range of distributional characteristics, four different deficit distributions (representing different initial landscape wetness conditions) and three local contributing area ratio distributions are considered. The sensitivity analysis demonstrates that a tendency

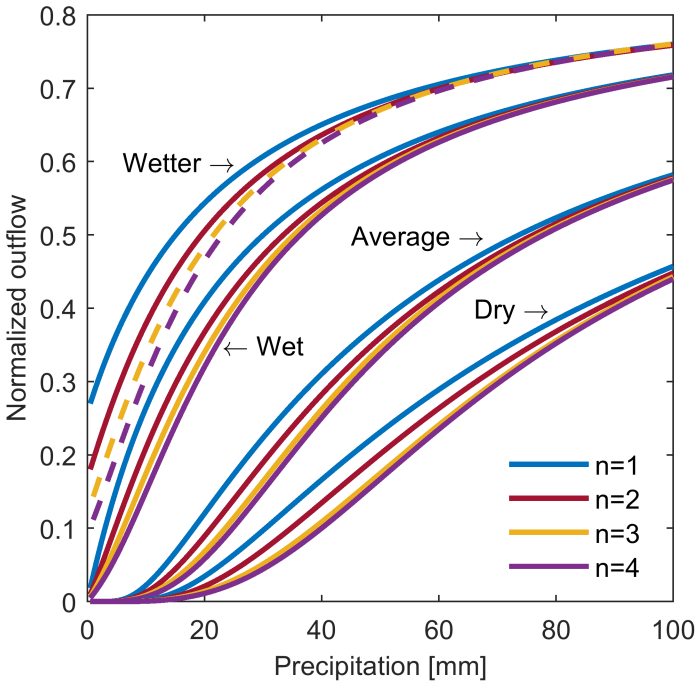

Figure 3.7: Normalized outflow (outflow for unit precipitation) for a given precipitation magnitude under wetter ($P_f = 30\%$, $D_{min} = 0$ mm), wet ($P_f = 0\%$, $D_{min} = 0$ mm), average ($P_f = 0\%$, $D_{min} = 50$ mm), and dry ($P_f = 0\%$, $D_{min} = 100$ mm) conditions in a landscape with one, two, three, and four wetland cascade depths (n). In all cases $\beta_{min} = 0$, $\bar{\beta} = 2$, $R = 0.8P$, $P' = P$, and $b = 0.5$. Dashed lines for the wetter condition are the results of the Monte Carlo simulation.

towards larger local contributing area ratio, interpreted as a higher ratio of non-wetland to wetland area, increases the landscape outflow, which we see manifested as a leftward shift in the curves in Figure 3.8. As the local contributing area ratio, β, increases the role of wetlands becomes negligible, as any amount of precipitation immediately cause all wetlands to overflow. Conversely, as the landscape tends towards dryer initial conditions, landscape outflow decreases, which we see manifested as a vertical downward shift in the curves in Figure 3.8. During the dry periods, there is very little observed outflow from wetlands, and they are effectively isolated from the surface water flow network. The sensitivity analysis also indicates that the landscape approaches an asymptotic outflow limit $O = R$ as precipitation magnitude increases. This limit reflects the limited effect of the

"fill" component of the fill-and-spill process as the precipitation magnitude is large enough to immediately induce outflow, regardless of the initial deficit or local contributing area ratio.

The degree of clustering of the wetland complex is controlled by the parameter b in the local contributing area ratio distribution function, Equation 3.10, a large b corresponds to uniformly sized local contributing areas, whereas a small b corresponds to a large variation in the local contributing areas across the landscape as shown in the bottom row of Figure 3.9. Figure 3.9 shows that when wetlands are more evenly distributed through the landscape, the normalized outflow is generally lower during dryer initial conditions. However, for the wetter condition the curves are very similar indicating relative insensitivity of the outflow to the distribution (i.e., how regular or clustered the wetlands are), as long as the mean local contributing area ratio is the same. It also suggests that a proper estimate of the average local contributing area ratio with high population of wetlands would be sufficient for the simulation in these cases. In accordance with Figure 3.8, Figure 3.9 shows that as precipitation magnitudes increase, the influence of the initial deficit distribution is minimized, such that the difference between the wet and dry conditions is reduced. However, the outflow from dry initial conditions is distinct from wet initial conditions under average precipitation magnitudes, as dry conditions result in a lag time before outflow is produced. It can be concluded that the maximum landscape outflow occurs when the landscape is wet and the local contributing area ratio is large (i.e., when dealing with a clustered distribution of wetlands, or a configuration of smaller wetlands with larger local contributing areas). The first observation is well documented (Shaw et al., 2012; Spence and Woo, 2006). However, the role of local contributing area has received less focus. Conversely, more densely packed wetlands systems with higher infiltration capacity will tend towards storing water.

The sensitivity analysis undertaken here assists in our understanding of the role of the spatial distributions of wetlands characteristics on the total generated runoff. As the spacing between wetlands increases, the local contributing area increases and more water flows to each wetland. This allows the storage deficit to be overcome more rapidly, resulting in an increase in maximum outflow and a reduction in lag times for dry initial conditions. Unsurprisingly, this solution indicates that the upscaled fill-and-spill response from thousands of cascading wetlands differs quite dramatically from the response of a single wetland. Thus, care must be taken with models that aggregate the bulk response of a wetland complex by representation as a single equivalent wetland (e.g. Liu et al. (2008); Yang et al. (2010)); the emergent upscaled response could not be emulated using a single wetland, regardless of whether effective parameterization or calibration is used. This finding is consistent with other studies (e.g., Clark and Shook (2022); Mekonnen

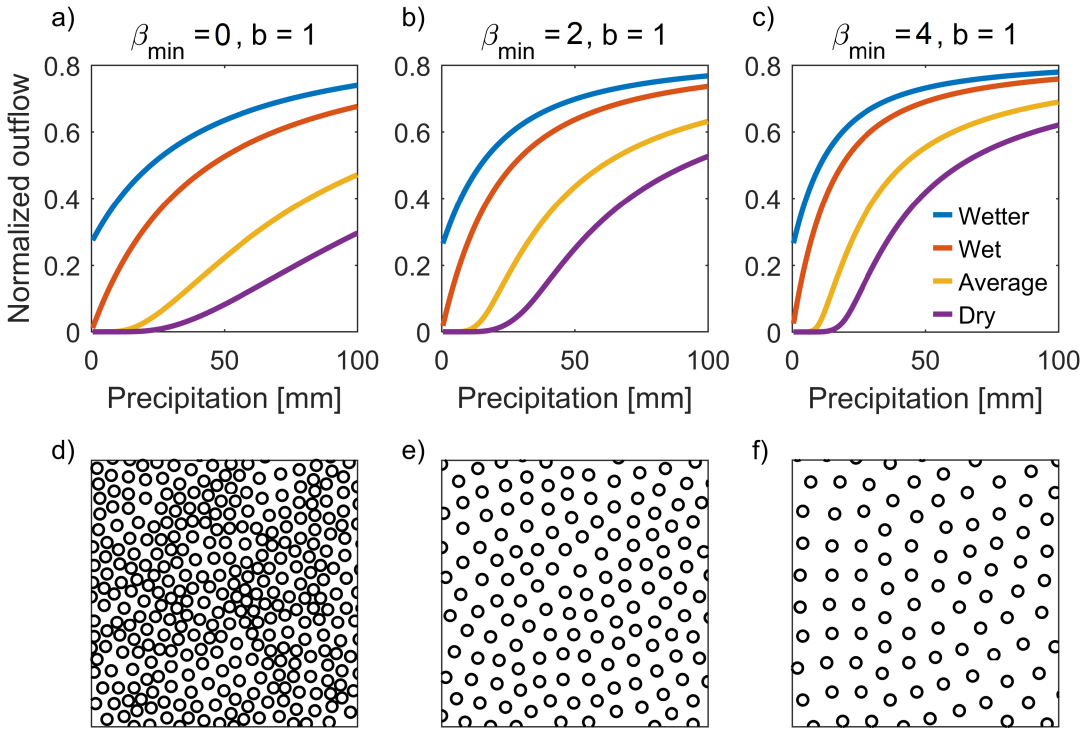

Figure 3.8: Top row (a to c): Sensitivity of the model to the variation of β_{min} for wetter, $D_{min} = 0$ mm and $P_f = 30\%$, wet, $D_{min} = 0$ mm and $P_f = 0$, average, $D_{min} = 50$ mm, and dry, $D_{min} = 100$ mm, conditions. In all cases b is kept constant and equal to 1, $R = 0.8P$, and $P' = P$. Bottom row (d to f): a representative spatial distribution of wetlands for different local contributing area ratios

et al. (2016); Pomeroy et al. (2014); Shook and Pomeroy (2011); Evenson et al. (2016)) which emphasize that for modelling complex fill-and-spill dynamics in wetlands, a single "equivalent wetland" is insufficient. The capability of the UWFS model to consider the effects of local contributing area of wetlands and wetland cascading depth increases the ability of hydrological models to account for dynamics of fill-and-spill process in wetland complexes.

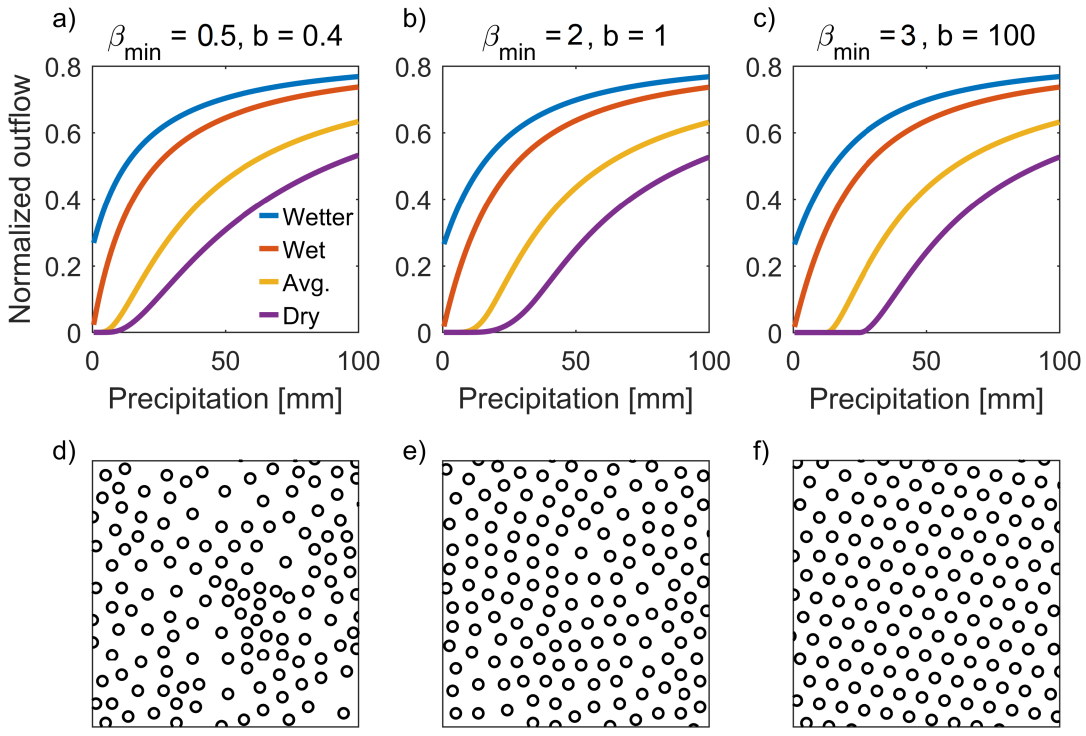

Figure 3.9: Top row (a to c): Sensitivity of the model to the variation of b in the local contributing area ratio distribution for wetter, $D_{min} = 0$ mm and $P_f = 30\%$, wet, $D_{min} =$ 0mm and $P_f = 0$, average, $D_{min} = 50$ mm, and dry, $D_{min} = 100$ mm, conditions. In all cases β_{avg} ($\overline{\beta} = \beta_{min} + 1/b$) is kept constant and equal to 4, $R = 0.8P$, and $P' = P$. Bottom row (d to f): a representative spatial distribution of wetlands for different clustering conditions

3.4.4 Raven-UWFS and HYPR Streamflow Simulations

Figures 3.10 and 3.11 depict the daily simulated and observed hydrographs for two sub-basins in the QRB simulated using Raven-UWFS and HYPR models (Ahmed et al., 2020b), where the HYPR model has also been implemented in Raven. The total study duration is from 2001-10-01 to 2017-12-31 and it is divided into two parts for the purpose of calibration (2001-10-01 to 2011-10-01) and validation (2011-10-02 to 2017-12-31). The initial parameter values are selected randomly and inspired from Ahmed et al. (2020b) within the specified range indicated in Table 3.1. No run-up period was used, rather the initial deficit distribution was one of the calibration targets. The vertical dashed line in Figure 3.10 and 3.11 separates the calibration and validation period. The simulated and observed hydrographs for the rest of the sub-basins in the QRB can be found in the Supplementary

Material.

By visual inspection of the hydrographs in Figure 3.10 and 3.11, it can be inferred that both UWFS and HYPR algorithms are reasonably successful in simulating streamflow in the QRB during the calibration period, with the exception of the Ridge sub-basin. Figure 3.12, which reports the calibration and validation metrics for the studied sub-basins indicates that both models suffer in validation for most sub-basins (common in prairie hydrological modeling literature). The KGE values for Ridge sub-basin during the validation period is not presented in Figure 3.12, because both models failed in simulating streamflow from this sub-basin during validation period. Poor model performance in Ridge sub-basin might be originated from the presence of a high embankment upstream of the gauge which regulates the streamflow as discussed by Ahmed et al. (2020b).

Figure 3.12 shows that UWFS outperformed HYPR in terms of calibration KGE values for Cutarm, Saline, and Pheasant creek sub-basins, while HYPR performed better for Lanigan creek and Moose Jaw sub-basins. During validation, UWFS had higher KGE scores than HYPR for four sub-basins, with similar performance for three others. UWFS reliably simulated streamflow at Cutarm creek with calibration KGE of 0.85 and validation KGE of 0.8. Detailed analysis of the simulated hydrograph in Figure 3.10 and 3.11 indicates that the UWFS model has potential in accurately capturing the timing, duration, and magnitude of high streamflow. Specifically, the high streamflow in May 2011 was well-captured by the UWFS model for the Cutarm sub-basin, while HYPR underestimated it.

Table 3.3 also includes the values of KGE and percent bias for each model during calibration and validation period for the ten study sub-basins. Percent bias values are near zero for most sub-basins during the calibration period, which confirms acceptable performance of the UWFS and HYPR models. However, large percent bias values for a few sub-basins show deteriorated performance of the models which is confirmed by poor KGE metrics. During the validation period, both models show satisfactory performance, except in the Ridge sub-basin. Large number of zero streamflow magnitudes observed at the sub-basins over the historical record could be a reason for the deteriorated performance. The calibration or validation results will be significantly impacted if the model cannot accurately simulate the major observed events. Another factor could be human interference, such as occurs when wetlands are connected via drainage ditches, which alters the basin's natural responses to precipitation/snowmelt events but also violate the assumptions of the UWFS model. In that case, model parameters are calibrated to manipulated streamflow values which deteriorate the model simulation accuracy during validation period.

Overall, the results presented here indicate that the UWFS is comparably successful to

the HYPR model in predicting streamflow in prairie regions: neither model is uniformly better across the multiple basins in terms of validation performance. However, unlike the HYPR model, the UWFS model may be informed by map-based estimates of distribution parameters. In addition, it may be considered more physically appropriate for simulating runoff in prairie regions as it includes the effects of lateral flow from the local contributing areas.

Table 3.3: Performance metrics of UWFS and HYPR simulations for calibration and validation duration

	UWFS (KGE)		HYPR (KGE)			UWFS (PBIAS%)		HYPR (PBIAS%)	
Sub-basin	Calibration	Validation	Calibration	Validation	Best model	Calibration	Validation	Calibration	Validation
Cutarm	0.85	0.8	0.8	0.44	U	-0.90	-5.23	2.14	-26.98
Ekapo	0.87	0.88	0.86	0.8	U	0.01	-6.18	-0.25	4.98
Saline	0.84	0.67	0.81	0.47	U	-1.30	-18.23	-0.33	10.84
MooseJaw	0.79	0.6	0.81	0.59	=	-0.33	-4.77	0.40	-8.28
Pheasant	0.84	0.85	0.8	0.41	U	-2.09	5.09	2.24	-34.52
KronauMarsh	0.79	0.36	0.8	0.35	=	-3.27	4.25	3.55	-3.30
Lewis	0.75	0.36	0.75	0.44	H	3.13	-31.35	4.60	-29.85
Lanigan	0.73	0.56	0.84	0.52	=	-0.38	2.98	0.14	26.90
JumpingDeer	0.82	0.28	0.83	0.67	H	3.25	-54.41	1.47	8.07
Ridge	0.48	-2.4	0.5	-0.761	-	6.85	249.40	2.33	98.62

Unlike the PDMROF algorithm embedded in HYPR, the UWFS model is able to represent hysteretic in wetting and drying during the simulation period, a key element of prairie storage/drainage characteristics (Shook and Pomeroy, 2011). Figure B.10 shows the hysteresis relationship between contributing area ratio found from Equation A.4 versus deficit depth simulated by the UWFS model. Direct comparison between the hysteresis observed using the UWFS model and those of studies such as Shook and Pomeroy (2011) is not possible because the UWFS model tracks wetland deficit instead of explicitly representing the absolute value of basin storage.

3.4.5 Model Limitations

Although the UWFS method provides some insights into the influence of landscape characteristics on wetland system runoff response, this model has yet to incorporate some wetland network characteristics that may additionally influence this response. The key assumptions are that the wetlands are relatively uniform in size, that deficit in single cascading wetlands are independent of upstream, that wetland cascade depth is limited (N<5), that there is no branching of networks, that the wetland response is fast enough to ignore transient effects, that exponential distribution is appropriate for deficit and local contributing area ratio,

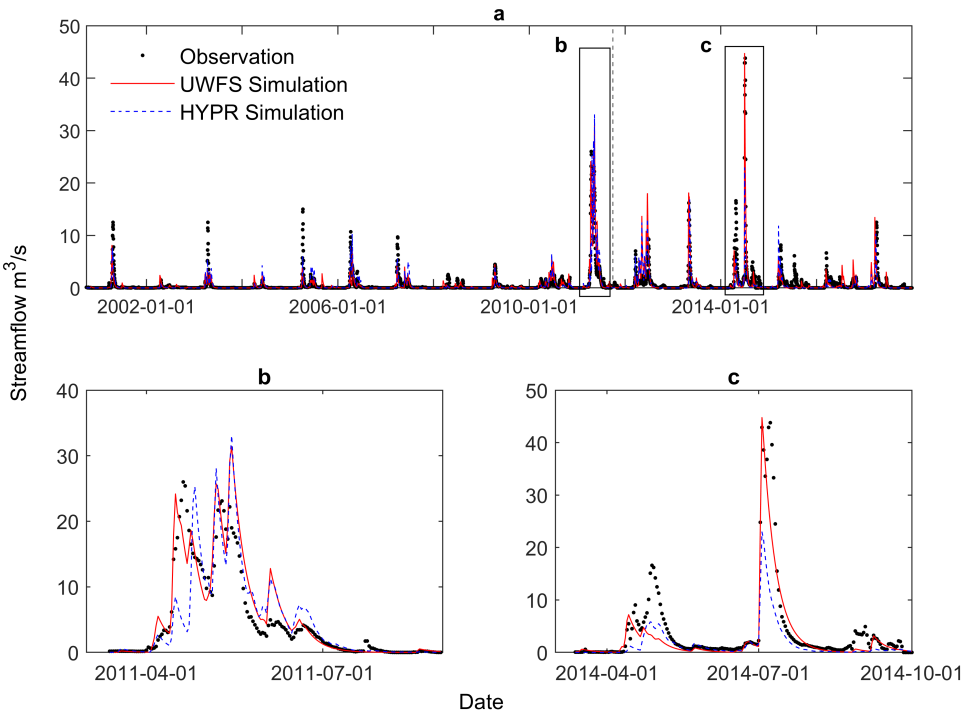

Figure 3.10: Observed and simulated hydrograph generated with UWFS and HYPR models in Raven for the Cutarm creek sub-basin for a) the total duration of the study period from 2000 to 2017, b) for an event in the Calibration period, c) for an event in the validation period. The vertical dashed line separates calibration and validation period.

and the flow is all surface flow without considering the subsurface flow. However, the proposed methodology is intended to be an improvement upon existing approaches for treating lumped wetland systems with internal variability not a perfect assumption-free rendering of reality. The impact of uniform size wetlands is considered in the following paragraph and the assumption of an exponential distribution of local contributing area ratio is validated in this section. The impact of other assumptions require future investigation. The specific functional form of the probability distributions, here treated as exponential for analytical tractability, is only moderately influential, which is consistent with results of the sensitivity analysis. Instead, the mean local contributing area ratio has a dominant effect on the generated runoff, while the impact of degree of clustering is minor, except in dry conditions.

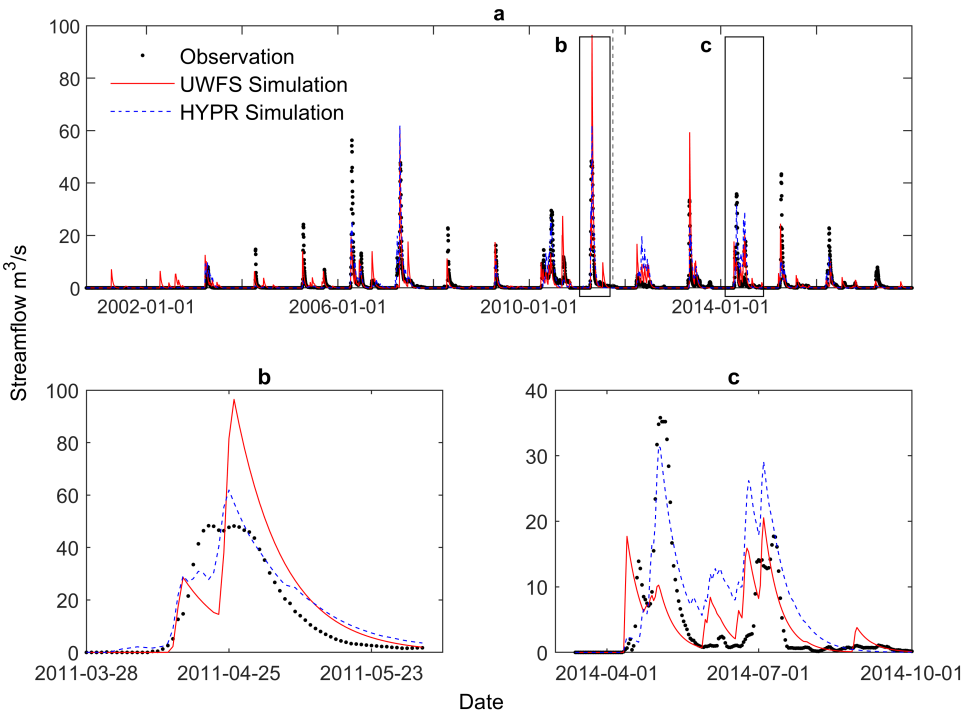

Figure 3.11: Observed and simulated hydrograph generated with the UWFS and HYPR models in Raven for Lanigan sub-basin for a) the total duration of the study period from 2000 to 2017, b) for an event in the Calibration period, c) for an event in the validation period. The vertical dashed line separates calibration and validation period.

To evaluate the impacts of the assumption of uniform size wetlands, the normalized outflow from a basin with wetlands of uniform size has been compared to the normalized outflow from three different sets of non-uniform distributions of wetland area, using a Monte Carlo approach. Considering non-uniform wetland area, potential outflow from the n^{th} wetland in the wetland cascade depth of N from Equation 3.5 is changed to

$$O_n^* = \beta_n R - D_n + \left(\frac{A_w^{n-1}}{A_w^n} O_{n-1}\right) = \gamma_n + m.O_{n-1} \tag{3.24}$$

where m is the area ratio of the upstream wetland to the downstream wetland ($m = \frac{A_w^{n-1}}{A_w^n}$). To solve Equation 3.24 and find the average runoff, a Monte Carlo approach is developed by sampling from the area ratio distribution in addition to sampling from the deficit and

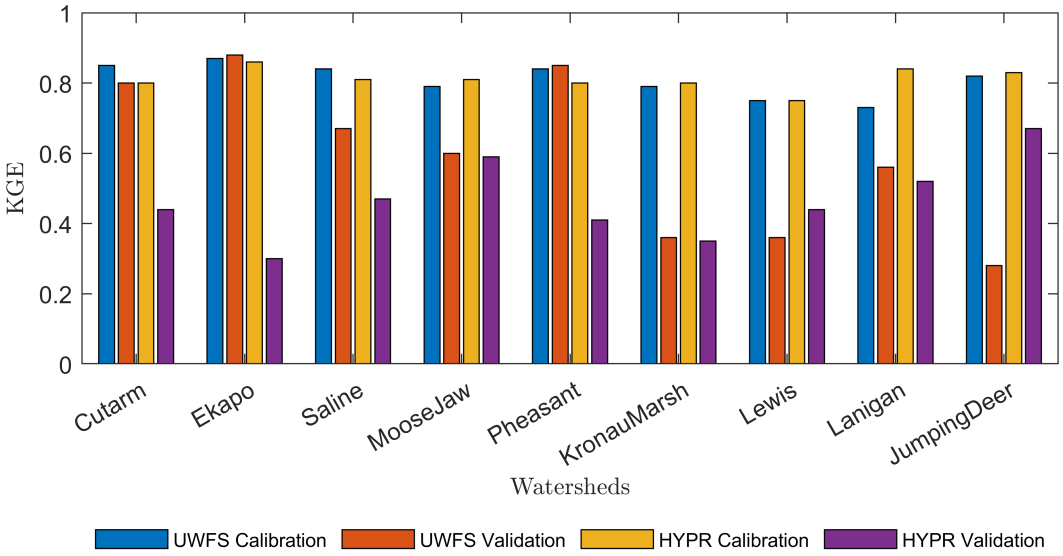

Figure 3.12: Comparison of KGE values for calibration and validation period at nine sub-basins in QRB, located in Saskatchewan, Canada

local contributing area ratio exponential distributions as discussed in section 3.4.1. In the Monte Carlo approach, the wetland area ratio is approximated by a log normal distribution with an average value of one and different standard deviations: one, five, and 10. The generated normalized runoff from the four aforementioned distributions of wetland area ratio is presented in Figure B.9 in Appendix B.1. The slight deviation between the resultant curves shows the minimal impact of the assumption of uniform size wetlands on runoff generation, provided the mean is one (i.e., larger or smaller wetlands do not preferentially occur downstream or upstream).

The assumptions of branching wetland cascading networks may later be evaluated in extensions to the UWFS model. Regardless, the current model does extend the existing PDM/Xinanjiang distributed runoff paradigm by recognizing the influence of local contributing areas and cascading of the fill-and-spill process. Therefore the method is readily used to extend the applicability of models built based on these methods (e.g., VIC or the PDMROF model of Mekonnen et al. (2014)).

Deployment of the UWFS method for effective understanding of the hydrological response of a wetland dominated landscape requires an accurate estimation of the parameters. In this study, we calibrate the exponential distributions of initial deficit and local

contributing area ratio. While measurement of the deficit distribution is likely to remain elusive because of the lack of information, this work may be extended in the future by considering the actual distributional characteristics of local contributing area ratio. Because the model only requires four parameters - two of which (β_{min} and b) are directly determinable via geospatial analysis, the model is well suited for calibration. To examine the fitness of an exponential distribution to local contributing area ratio, the wetland areas for the Saline sub-basin were extracted using Geospatial Data Extraction tools (NRC, 2022). Each wetland contributing area was estimated using a shape Voronoi diagram - any now-wetland area closer to the wetland of interest than to the other wetlands was treated as that wetland's contributing area. The ratio of wetland local contributing area to wetland area was then calculated. An exponential distribution was fitted to the observed local contributing area ratio distribution by minimizing the weighted error,

$$\epsilon = \Sigma_{i=1}^{NB}(h(i).|h(i) - be^{-b\beta_i}|) \tag{3.25}$$

where NB and h show the number of bins in the histogram and the observed histogram, respectively. The fitted exponential distribution to the local contributing area ratio values with an error value of 0.008 is shown in Figure 3.13. This approach can be used to find the distribution function of local contributing area ratio of any watershed.

3.5 Conclusions

Accurate estimation of basin-scale hydrological responses in wetland-dominated landscapes is challenging due to the heterogeneity in wetlands properties. This study set out to develop an upscaled fill-and-spill model to provide basin-scale understanding of the impact of wetland properties on hydrologic responses from a wetland-dominated landscape. The low-parameter wetland model proposed in this study is the first closed form upscaled runoff model to explicitly consider lateral flow from the local contributing area of wetlands. The spatial variability in wetland properties, including wetland deficit depth and local contributing area ratio, is difficult to identify in low-gradient landscapes where those properties cannot be easily measured due to a lack of high-resolution data. The probabilistic treatment of wetland properties is in part motivated by the need to compensate for the lack of high-resolution data and avoid high computational costs of representing individual wetlands properties. In addition, it is hard to estimate the available storage volume in wetlands due to the lack of accurate high resolution data. To overcome this issue, the components of water balance have been defined in units of depth to reduce the degrees of freedom in the model storage. The utility of the model, a generalization of the well-known

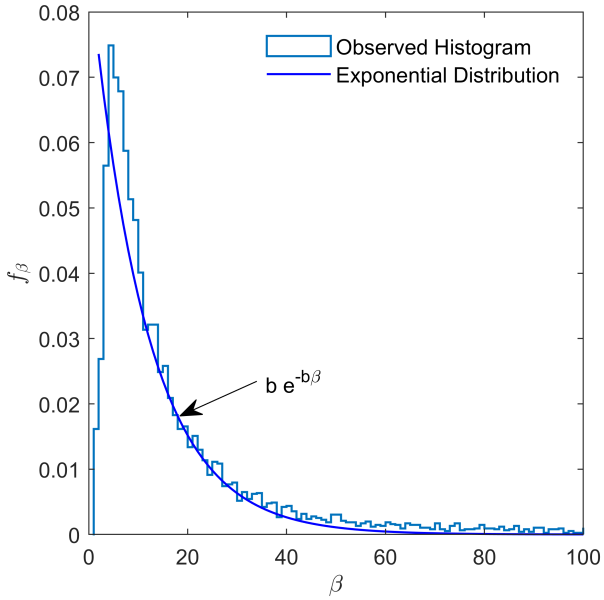

Figure 3.13: Representation of the fitted exponential distribution to the histogram of local contributing area ratio values for the Saline sub-basin in Saskatchewan, Canada

PDM and Xinanjiang runoff models, is assessed through an equivalency to previous conceptualizations of fill-and-spill landscapes, as well as a numerical Monte Carlo exercise. The sensitivity of landscape outflow to changes in wetland connectivity, landform geometry, and antecedent storage deficit has been assessed. The relatively simple low parameter model explicitly supports the impact of cascading wetlands on streamflow generation, spatially variable infiltration capacity, and precipitation/snowmelt magnitude. Sensitivity analysis shows that the wetland local contributing area has a significant impact on runoff generation from basin, even during high flows when wetlands are connected. The UWFS algorithm has been implemented in the semi distributed hydrological model, Raven, to evaluate the performance of the model in hydological simulation of wetland-dominated low-gradient landscapes. The streamflow simulation by the UWFS method has been compared with the simulation results generated using the HYPR model, an alternative wetland runoff model used for simulating streamflows in prairie basins. Although, there are challenges in comparing two model structures with multiple calibrated parameters, the results of this comparison are favorable, and demonstrate the utility of the UWFS model. The ability of UWFS algorithm to represent wetland properties and network structures overcome

the challenges of parameterizing thousands of wetlands and may improve the accuracy of streamflow simulation by current hydrological models in heterogeneous basins.

Chapter 4

Analyzing Assumptions of Wetland Representation in the UWFS Algorithm

Wetlands are one of the important features in hydrological modeling of low-gradient landscapes. In order to simulate how a basin will respond to precipitation/snowmelt events, it is essential to account for the hydrological connectivity within wetland networks and between wetlands and other hydrological features of a basin. Different branching or cascading network structures can be used to define the connectivity of wetlands. Wetlands' deficit, contributing area, and geometry are crucial characteristics that need to be considered in hydrological modeling of wetlands. The complexity and computational costs may rise if wetland properties are explicitly represented in hydrological models. In this chapter, the ability of the UWFS algorithm, an upscaled fill and spill model, to accurately capture the characteristics of regional wetland systems is tested using a Monte Carlo approach. Here, we examine the impact of wetland network properties on the hydrological response of wetland-dominated landscapes. The findings of this study can contribute to our comprehension of wetland characteristics and potential approaches for enhanced hydrological simulation of those features without requiring high resolution data or demanding computational efforts.

4.1 Introduction

The hydrology of many low gradient landscapes is extremely complex because of the presence of large numbers of depressions (Woo and Rowsell, 1993; Hayashi et al., 1998; Van der Kamp et al., 2003; Fang et al., 2010; Pomeroy et al., 2009). These depressions intermittently connect to the primary stream network, leading to storage-dependent contributing area dynamics, whereby the amount of runoff from a landscape is dependent upon the degree of connection within it. Multiple attempts have been made to include the depression storage of wetlands in hydrological models. For instance, the basic wetland module in the SWAT aggregates all wetlands into one large wetland referred to as a Hydrologic Equivalent Wetland (HEW), with a single overflow threshold. This lumping method ignores the inherent heterogeneity of these complex landscapes and the physical processes are oversimplified (Wang et al., 2008). To more capably represent isolated wetlands, Evenson et al. (2015, 2016) introduced a pothole module in SWAT, called the GIW Module which represents contributing areas of individual GIWs. While successful for smaller systems, the computational costs of this fully-discretized module made the application of this model challenging in larger areas. Muhammad et al. (2020) introduced a method in which wetlands with a capacity below a specific threshold are removed from the modeling process to reduce the number of GIW-HRUs in the basin, and the corresponding computational costs.

The explicit representation of wetland connectivity in fully-distributed models often requires high resolution elevation data and computationally expensive hydrological modeling efforts (e.g., Shook and Pomeroy (2011); Shaw et al. (2013a); Shook et al. (2013); Ameli and Creed (2017); Amado et al. (2018)). The simplest explicit treatment is as a network of independent reservoirs. For instance, Shaw et al. (2012) conceptualized each wetland as a simple reservoir in which water spills to the next wetland or stream network after passing a storage threshold. They applied this theoretical representation of fill-and-spill in a watershed with fewer than 10 wetlands. The application of these models in basins with large numbers of wetlands such as those found in prairies may be impracticable due to the need to characterise individual wetlands. However, the characteristics of a population of wetlands may instead be described statistically. For instance, Shook and Pomeroy (2011) delineated a dendritic drainage network to explicitly represent the connectivity of a statistically representative set of wetlands. In each time step, they added a constant depth of water to all wetlands and simply scaled that depth to account for the local contributing area and removed a uniform depth from the wetland water surface to account for evaporation.

To reasonably represent the role of thousands of wetlands in basins without oversimplification of the hydrological process, probabilistic models characterizing the wetland pop-

ulation as a distribution of storage areas have been proposed. Examples of such models include the PDMROF (Mekonnen et al., 2014) in the MESH land surface model, the PDLD (Mekonnen et al., 2016) model in SWAT, and the HYPR (Ahmed et al., 2020a). These models are inspired by the PDM (Moore, 1985, 2007), which proposed that soil storage on a landscape may be represented as a series of connected or isolated "bucket" stores with varying levels of storage capacity. However, these models do not include the effects of local contributing area or the connectivity between upstream and downstream wetlands. The previously introduced UWFS (Taheri et al., 2023) from Chapter 3, probabilistically handles the treatment of fill-and-spill phenomenon in systems represented by wetland cascades. This model simplifies the representation of wetlands in hydrological models subject to two influential assumptions: that wetlands are prismatic (i.e., those with constant areas at each depth) and that simple non-branching cascading networks of wetlands is sufficient to represent the hydrological connectivity between wetlands. These assumptions are relaxed in this chapter. We will also show that the concentrating factor of the UWFS model can be extended to represent the heterogeneous infiltration properties of wetland contributing areas.

4.2 Method

The UWFS model from Chapter 3 simulates runoff from thousands of wetlands in response to a series of precipitation or snowmelt events. In each time step (or for each individual event), the algorithm considers the water balance in each wetland as

$$O = \max\left(\frac{A_u}{A_w} \cdot R + P' - D, 0\right) = \max\left(\beta R + P' - D, 0\right) \tag{4.1}$$

where O [mm] is the actual outflow depth from a wetland, β is the local contributing area ratio which is equal to the ratio of wetland contributing area, A_u, over the wetland area, A_w, D is the wetland deficit depth, R is runoff from the local contributing area, and P' is precipitation over wetland area. The UWFS model characterizes the local contributing area ratio, β, and deficit, D, of wetlands probabilistically using truncated exponential distribution functions. One distribution must be defined for local contributing area ratios based on the average, β_{avg} and minimum values, β_{min}, and one distribution must be defined for initial deficit depths based on their average, D_{avg} and minimum values, D_{min}. To upscale the runoff from a single wetland to the runoff from a basin with thousands of wetlands, an upscaling approach based on the derived distribution approach is used (For more information about the UWFS method refer to Chapter 3 or Taheri et al. (2023)). The

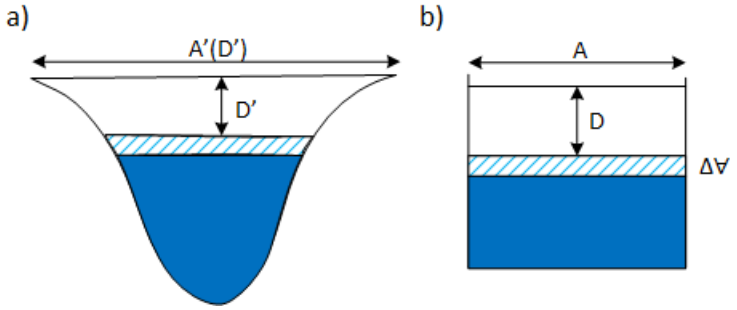

Figure 4.1: Schematic representation of a) a non prismatic wetland and b) the equivalent prismatic form. $A'(D')$ and A represent the wetland surface area at top in non-prismatic and prismatic wetland, respectively. Deficit depth in non-prismatic and prismatic wetland are shown by D' and D, respectively. $\Delta\forall$ represents changes in water storage after precipitation.

basic probabilistic approach used in the UWFS method nominally assumes that wetlands are prismatic and non-branching cascading networks of wetlands may adequately represent different wetlands networks. In this paper we study the impacts of these assumptions on the simulated runoff by the help of a Monte Carlo approach. We here, show that we can relax these basic assumptions of UWFS model by adjusting one of the model parameters (i.e., local contributing area ratio) to account for system characteristics not addressed in the original model of Chapter 3.

4.2.1 Non-prismatic Wetlands

The storage capacity of wetlands is one of the important properties that is determinant of their role in the basin. In the derivation of the UWFS method, wetlands were assumed to be prismatic in shape, even though they may not be in reality. The available storage in wetlands is defined by the deficit depth, which is the vertical distance from the wetland's water surface to its overtopping height. The degrees of freedom required to define the characteristics of each wetland is thus decreased because the storage dimension is changed from volume, $[L^3]$, to depth, $[L]$. Here we first present a general non-prismatic form of wetlands and then we evaluate the impacts of assuming a non-prismatic trapezoidal wetland geometry.

The area of a non-prismatic wetland at each level is a function of the deficit depth as shown in Figure 4.1. The geometry of the equivalent prismatic wetland is defined such that

its deficit (or void) volume is equivalent to that of the non-prismatic wetland and that can be determined as,

$$\forall_v = D \cdot A = \int_0^{D'} A'(D') \cdot dD' \tag{4.2}$$

and changes in the volume due to receiving water may be found as,

$$\Delta\forall = \Delta D \cdot A = \int_{D'}^{D'+\Delta D'} A'(D') \cdot dD' \tag{4.3}$$

where $A'(D')$ and A represent the wetland surface area at overtopping level where the deficit depths are D' in non-prismatic and D in equivalent prismatic wetland. By rearranging Equation 4.2 and 4.3, the deficit depth in the equivalent prismatic wetland may be found as,

$$D = \frac{1}{A} \int_0^{D'} A'(D') \cdot dD' \tag{4.4}$$

and deficit depth change may be found as,

$$\Delta D = \frac{1}{A} \int_{D'}^{D'+\Delta D'} A'(D') \cdot dD' \tag{4.5}$$

Figure 4.2 shows the relation between area and the deficit depth in non-prismatic wetlands in general shape and trapazoidal non-prismatic wetlands. As the deficit depth, which is the vertical distance between the overtopping level and the water surface level, increases, the area decreases. Knowing the function that relates area, A' to the deficit depth, D', we would be able to solve the integrals in Equation 4.4 and 4.5 to find the geometry of the equivalent prismatic wetland. For a trapezoidal non-prismatic wetland this function can be found as,

$$A'(D') = A(1 - bD') \tag{4.6}$$

where b is the side slope of the trapezoidal non-prismatic wetland. Then, the relation between initial deficit and the equivalent deficit depth may be as,

$$D = \frac{1}{A} \int_0^{D'} A(1 - bD')dD' = \int_0^{D'} dD' - b \int_0^{D'} D'dD' = D' - b\frac{D'^2}{2} \tag{4.7}$$

It should be noted that for a non-trapezoidal wetland b is changing with depth.

Based on Equation 4.7 and transforming the deficit depth distribution in trapezoidal wetland, the deficit depth distribution in the equivalent prismatic wetland may be found as shown in Figure 4.3 where the deficit distribution of wetland in non-prismatic form is a

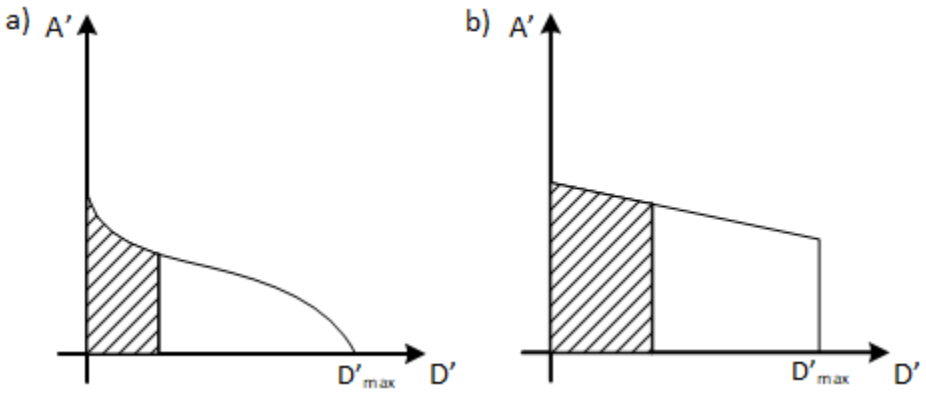

Figure 4.2: The relationship between deficit depth and area in a) a non prismatic wetland and b) the non-prismatic trapezoidal wetland. Dashed area shows the void volume in the wetland.

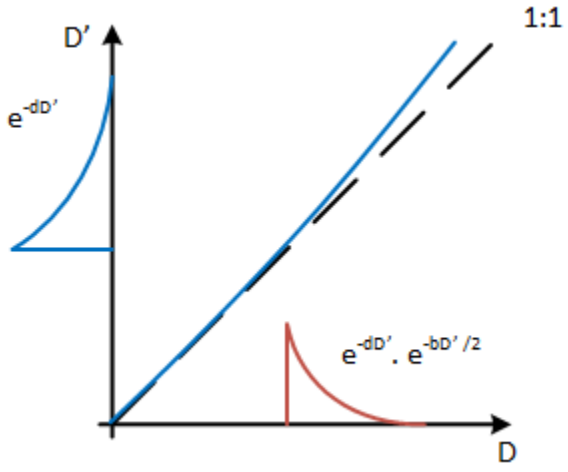

Figure 4.3: The relation between deficit depth at non-prismatic wetland, D', and equivalent wetland, D, and their distributions

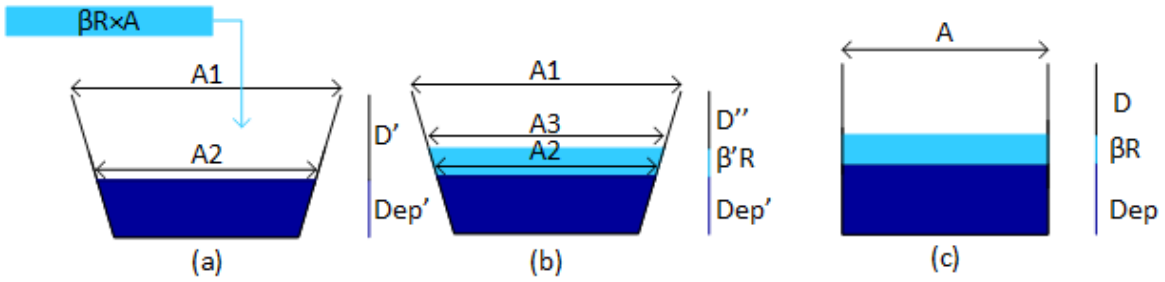

Figure 4.4: Schematic representation of a) a non prismatic wetland before applying the excess runoff, b) a non-prismatic wetland after applying the excess runoff, and c) the equivalent prismatic wetland. A_1, A_2, and A_3 represent the wetland surface area at overtopping level, water surface before excess runoff, and after excess runoff applied, respectively. D' and D'' represent deficit depth before and after excess runoff applied in non-prismatic wetland. D represent equivalent deficit depth in prismatic wetland. βR and $\beta' R$ are the excess runoff depth. Dep and Dep' represent the initial water level stored in prismatic and non-prismatic wetland, respectively.

truncated exponential distribution and the one at the equivalent wetland is a truncated non-exponential distribution with larger domain coverage. The equivalent deficit distribution can be found from the notes on Chapter 3 about the derived distribution approach and Equation 4.7.

Here we evaluate the response of a non-prismatic trapezoidal wetland of Figure 4.4-a in details to compare that with the equivalent form of Figure 4.4-c. The void volume of the trapezoidal wetland, $\forall_v$, may be found from

$$\forall_v = D' \cdot \frac{(A_1 + A_2)}{2} \tag{4.8}$$

where A_1, A_2, and D' represent the wetland's area at the overtopping point and at the water surface, the deficit depth, and water storage depth, respectively.

Assume the excess runoff from precipitation over local contributing area, $\beta R \cdot A$, shown by a block at the top left of Figure 4.4-a, is added to this wetland. The added water may fill the wetland completely or to the depth of $\beta' R$ as shown in Figure 4.4-b. In the second case, the volume of the added water, $\forall_f$, may be found from

$$\forall_f = \beta' R \cdot \frac{(A_2 + A_3)}{2} \tag{4.9}$$

where A_3 is the area of the wetland at the new deficit depth, D''. This wetland can be represented by an equivalent prismatic wetland as in Figure 4.4-c with a new initial deficit volume, $\forall'_v$, which can be found from

$$\forall'_v = D \cdot A \tag{4.10}$$

where A is the area of the equivalent prismatic wetland and D is a new deficit depth in the equivalent wetlands. Since the volume of the filled part in prismatic and non-prismatic wetland needs to be the same, according to the conservation of mass, the relationship between β values in both cases can be found from,

$$\forall_f = \beta R \cdot A = \beta' R \cdot \frac{A_2 + A_3}{2} \tag{4.11}$$

where $\beta' R$ is the new filled depth. It can be concluded that β and β' are equal as

$$\beta' = \frac{A}{(A_2 + A_3)/2} \cdot \beta = \beta \quad \text{where} \quad A = \frac{A}{(A_2 + A_3)/2} \tag{4.12}$$

Also, because the void volume in transformed and non-transformed forms are equal, the relationship between D' and D'' may be shown as:

$$A \cdot D = \frac{(A_1 + A_3)}{2} \cdot D'' \quad \text{therefore} \quad D = \frac{(A_1 + A_3)}{2A} \cdot D'' \tag{4.13}$$

It shows that to replicate the results from a non-prismatic wetland with an equivalent prismatic wetland the deficit depth is scaled by $\frac{(A_1+A_3)}{2A}$. Here, we suggest instead of scaling the deficit depth values by adjusting the local contributing area parameter, β, via the calibration process, we can replicate runoff from non-prismatic wetland using prismatic wetlands conceptualization. In this case, the deficit depth, D, should not be interpreted as the vertical difference between threshold and water level. Rather, it is an equivalent (smaller) depth in a prismatic wetland. This will also impact how the initial deficit distribution should be interpreted. One important consideration is that the re-conceptualization indicates that non-prismatic wetlands can be handled with UWFS. However, it is important to note that only non-prismatic wetlands with uniform slopes can be handled in this manner. It is not possible to mix prismatic and non-prismatic wetlands in a straightforward manner. While the assumption the specific functional form of the deficit distribution is now violated, it retains its essential features: that it is truncated and that the wetland system has some variance in deficit.

4.2.2 Handling Branching Networks

The initial UWFS model of Chapter 3 assumes a linear cascading network of wetlands as in Figure 4.5a in which wetlands in a cascading network receive water from precipitation over their land area, the excess runoff from local contributing area, and a single upstream wetland which is producing runoff. Therefore, The expected outflow from the cascading depth of two (i.e., where there are two wetlands in each cascade) is calculated as,

$$O_2 = \max(0, \beta_2 R + P' - D_2 + O_1) \tag{4.14}$$

where O_1 and O_2 represent runoff from the first (upstream) and second (downstream) wetland in a cascade, respectively. Here, β_2 is the local contributing area ratio and D_2 is the deficit depth of the second wetland. Wetland complexes may also be defined in branching networks as shown in Figure 4.5b. Branching networks are defined by cascade depth and branching ratio (i.e., the ratio of the number of wetlands upstream over downstream). The outflow produced from a simple branching network with branching ratio and cascading depth of two, can be found from,

$$O_2 = \max(0, \beta_2 R + P' - D_2 + O_{1,1} + O_{1,2}) \tag{4.15}$$

where $O_{1,1}$ and $O_{1,2}$ represent the outflow released from wetland 1 and 2 at the upstream cascade depth, respectively. Outflow released from wetlands in a branching network can be calculated via repeated application of UWFS basic rules using a Monte Carlo approach instead of a closed-form analytical solution which is mathematically demanding. To test the impact of branching, 100000 initial deficit and local contributing area ratio values are repeatedly sampled from their exponential distributions and substituted in the water balance equation, i.e., Equation 4.15. Results between branching and non-branching methods of cascade depth of two are evaluated.

4.3 Results and Discussion

In Section 4.2.1, it had been hypothesized with some mathematical support that a model with prismatic wetland configuration and the scaled local contributing area ratio can accurately simulate the runoff from non-prismatic wetlands. To test this statement and find the minimum local contributing area ratio of prismatic wetland, β'_{min}), the "fminsearch" function in MATLAB was used which is able to minimize the difference between the runoff generated from non-prismatic wetlands and the equivalent prismatic wetland using the

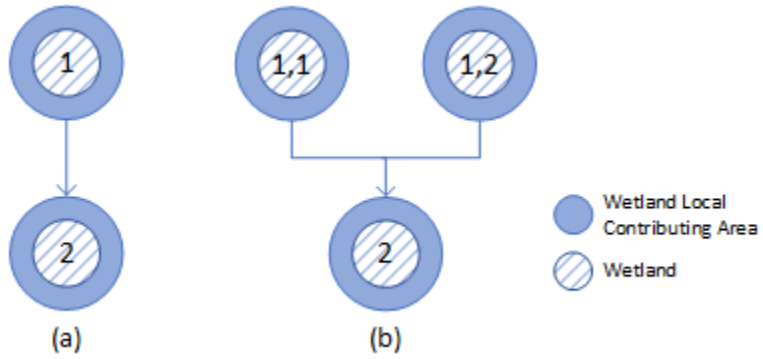

Figure 4.5: Wetlands in a) linear cascading network with cascading depth of two, and b) branching network with both cascade depth and branching ratio of two

Nelder-Mead simplex algorithm (Nelder and Mead, 1965). Therefore, the objective function here is to minimize the error defined as,

$$Error(\beta_{min}) = \sum_{i=1}^{n}\sum_{j=1}^{m} \frac{O_p(P'_i, D_j, \beta_j(\beta_{min}, \beta_{avg})R_i) - O_{np}(P'_i, D''_j, \beta'_j(\beta'_{min}, \beta'_{avg})R_i)}{O_{np}((P'_i, D''_j, \beta'_j(\beta'_{min}, \beta'_{avg})R_i))} \tag{4.16}$$

where O_{np} represents generated runoff from non-prismatic wetlands with β' and D'' discussed in Section 4.2.1. O_p represents generated runoff from equivalent prismatic wetlands with an scaled deficit, D, and local contributing area ratio, β which itself is a function of β_{min} and β_{avg}. n is the number of studied precipitation events (i.e., 150), and m is the number of Monte Carlo trials (i.e., the number of samples from deficit and local contributing area ratio distributions, which is 100000 here). Figure 4.6 compares the simulated runoff ratio for three different cases of prismatic wetlands with initial deficit depth of D''_i (i.e., the deficit in non-prismatic wetland), prismatic wetlands with scaled deficit depth of D_i (shown in Figure 4.4-c as an equivalent form of non-prismatic wetland), and the prismatic wetlands with deficit of D''_i and scaled local contributing area ratio of β_{min} (found from the optimization discussed in Equation 4.16). It can be concluded that non-prismatic trapezoidal wetland responses can be replicated by a prismatic wetland configuration with a scaled local contributing area ratio while the deficit depth remains constant. This is important because it is not necessary to simulate the exact bathymetry of wetlands to capture their responses correctly. The fact that the local contributing area ratio is capable of compensating for the deficiency of the model reduces the complexity of solving this problem. It can be concluded that a prismatic wetland configuration with a scaled local contributing area ratio can replicate the response of non-prismatic trapezoidal wetlands,

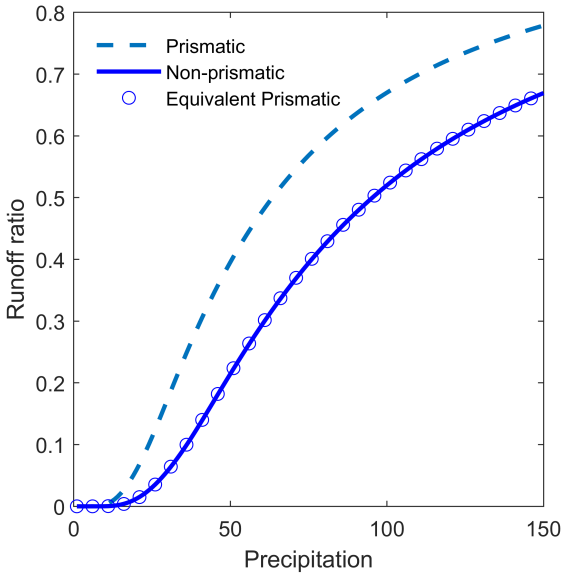

Figure 4.6: Runoff ratio generated from prismatic wetland (dashed line) with values of $D_{min} = 50$, $D_{avg} = 100$, $\beta_{avg} = 3$ and $\beta_{min} = 1.5$, equivalent form of non-prismatic wetland by prismatic configuration (solid line) with scaled deficit values of $D_{min} = 75$ and $D_{avg} = 150$ and constant values of local contributing area, and equivalent form of non-prismatic wetland (circle) with scaled local contributing area ratios, $\beta_{avg} = 2$, and $\beta_{min} = 1.3$, and the same deficit depths as the initial prismatic wetland (i.e., $D_{min} = 50$, $D_{avg} = 100$)

provided that the deficit depth remains the same. This is useful because it means that it might not be necessary to simulate the exact bathymetry of wetlands in order to accurately capture their responses. The ability of adjustments to the local contributing area ratio to compensate for the model's deficiencies reduces the need to explicitly incorporate complexity of wetland network geometry in the hydrologic model.

The next objective is to find an adjustment to the local contributing area ratio which can replicate the outflow from wetland networks with a branching ratio of two using an equivalent linear cascading wetland of depth two. The runoff produced by wetlands with linear cascading depths of two and branching ratios of two differ less than 1%. The percentage of the differences between runoff ratio (i.e., percentage of precipitation which runs off) generated from linear cascade depth of two and branching ratio of two for various minimum local contributing area ratios is presented in Figure 4.7-a. It can be concluded that the higher range of differences is observed in smaller values of local contributing area ratio. For larger local contributing area ratio the two structures respond similarly, since water is concentrated more intensely into the wetlands area. Consequently, wetlands may be filled up more quickly and smaller storage deficit remains. The likelihood of a wetland filling in response to a constant precipitation depth is lower for wetlands with smaller local

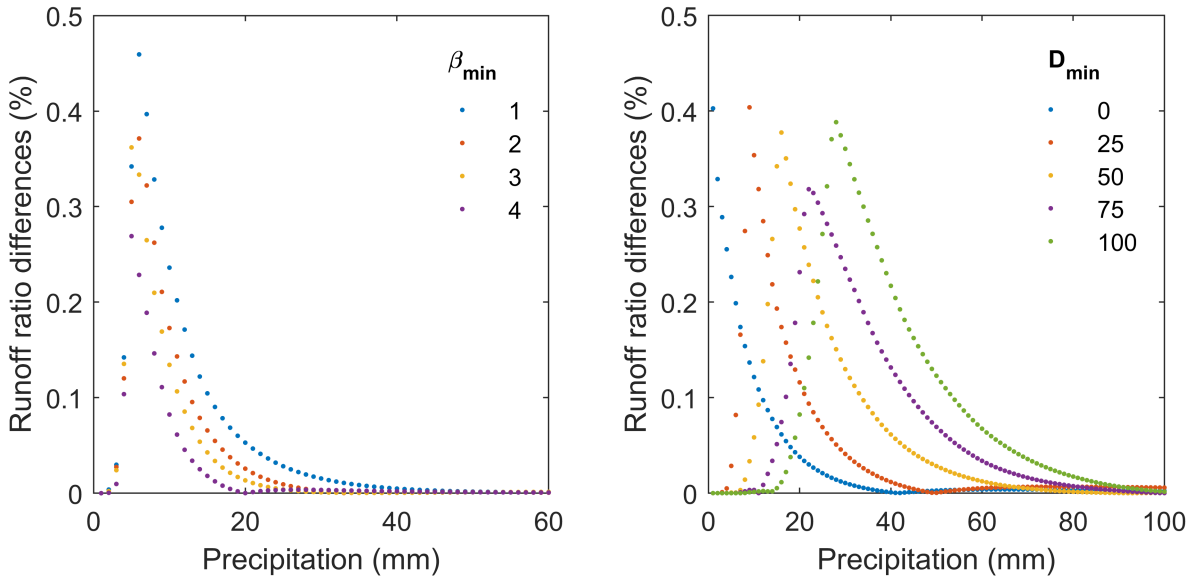

Figure 4.7: Runoff ratio differences (%) between wetlands in branching ratio of two and linear cascading depth of two for varying a) local contributing area ratios (i.e., $\beta_{avg} = 3 : 6$, $\beta_{min} = 1 : 4$, $D_{min} = 50$, $D_{avg} = 100$) and b) deficit depths (i.e., $D_{min} = 0 : 25 : 100$, $D_{avg} = 50 : 25 : 150$), $\beta_{avg} = 2$, $\beta_{min} = 1$)

contributing area ratios compared to wetlands with larger local contributing area ratios. Therefore, the storage effect of wetlands and the impact of their structures on the generated runoff is greater where local contributing area is smaller. Figure 4.7-b compares the percentage difference between runoff ratio generated from linear cascade depth of two and branching ratio of two for various minimum deficit depths. It can be concluded that the maximum differences for all cases, remain a roughly constant proportion of runoff ratio, hovering around 0.4%. However, the maximum difference for larger deficit occurs at higher precipitation depth. This might be caused by the fact that wetlands with smaller deficit depths are filled up at lower precipitation depths; consequently, at higher precipitation depths, the effects of their storage and structures on generated runoff are less significant. Here, it is suggested that by adjusting the local contributing area ratio during calibration process, we can replicate the outflow released from branching network using the linear cascading network.

In this case, another optimization process is used similar to the one discussed above.

Here, the purpose is find a suitable $\beta_{c_{min}}$ to minimize the following error,

$$Error(\beta_{c_{min}}) = \sum_{i=1}^{n}\sum_{j=1}^{m} \frac{O_c(P'_i, D_{cj}, \beta_{cj}(\beta_{c_{min}}, \beta_{c_{avg}})R_i) - O_b(P'_i, D_{bj}, \beta_{bj}(\beta_{b_{min}}, \beta_{b_{avg}})R_i)}{O_b((P'_i, D_{bj}, \beta_{bj}(\beta_{b_{min}}, \beta_{b_{avg}})R_i))} \tag{4.17}$$

where O_b and O_c are outflow from branching and cascading wetlands. D_b and β_b are deficit depth and local contributing area ratio of branching network, respectively. D_c and β_c are deficit depth and local contributing area ratio of cascading network, respectively. Note that β_b and β_c are functions of average and minimum local contributing area ratio. We can find the optimal $\beta_{c_{min}}$ value for the cascading network that can simulate runoff in close proximity to the runoff simulated from the branching network by minimising the error in Equation 4.17. Figure 4.8 depicts the error value that reflects the variation between the runoff simulation from the branching and equivalent non-branching network before and after optimization. The variations between two configurations after optimization are insignificant and this concludes that by calibrating the local contributing area ratio, it is straightforward to simulate the runoff produced by branching wetlands using the simpler mathematical formulation of Chapter 3. That means without the need for advanced mathematical techniques or extensive computational resources, we can adequately simulate complex wetland network using simple wetland cascades.

4.4 Conclusions

Explicit representation of wetland network geometry and bathymetry in hydrological models is often impractical in large basins because such models require (typically unavailable) high resolution data and/or are computationally expensive. The degree of complexity that is required to be considered in wetland modeling is changing because wetland complexes serve different functions of either storage or runoff generation depending upon weather condition. The UWFS model is an analytical upscaled algorithm that represents the fill-and-spill hydrological processes in landscapes dominated by wetlands. Two initial assumptions about wetlands used in the derivation were that first, wetlands were prismatic and second, wetland networks were linear and non-branching. We examine the flexibility of the model under conditions where these assumptions were violated, using Monte Carlo methods. It can be concluded that adjusting the local contributing area ratio as an effective parameter during model calibration can capture the effects of non-prismatic wetlands and branching wetland networks with the simple configuration of linear cascading network of prismatic wetlands. This implies that in a conceptual model where parameters represent

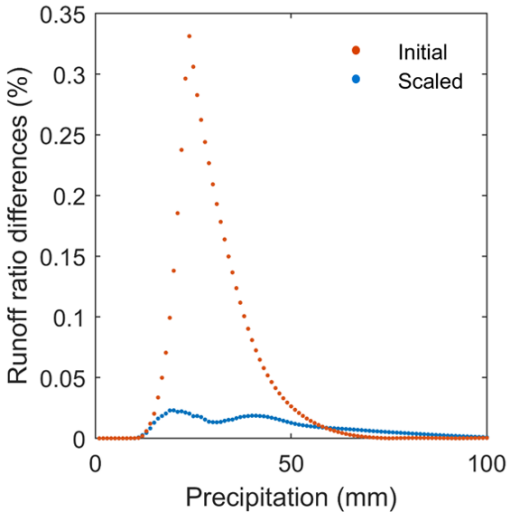

Figure 4.8: Runoff ratio differences between wetlands in branching ratio of two and linear cascading depth of two versus precipitation for a) the initial value of $\beta_{c_{min}}$ and b) the optimized value of $\beta_{c_{min}}$

more than what they physically mean, the calibration process is advantageous since it can compensate for these two model assumptions. The results from this study indicate that we can use UWFS to simulate studying the hydrological responses of wetland-dominated landscapes without explicit consideration of all of their characteristics, such as their precise bathymetry or network geometry.

Chapter 5

Quantifying Simultaneous Land Cover and Climate Change Impacts in a Northern Watershed

Wetland complexes in Northern Canada are rapidly changing due to the impacts of permafrost thaw. One of the main transformations observed in these landscapes is the rapid transition from permafrost plateaus to hydrologically connected fens and collapse scar bogs. These changes can significantly affect the connection between fens and bogs, the stored water in the basin, and consequently the runoff responses at the basin scale. The UWFS method implemented in the Raven hydrological modelling framework is here coupled to a land cover change model to assess the long-term effects of climate warming on the hydrological responses of these peatland systems. This model is evaluated in its ability to simulate streamflow in the Scotty Creek basin, and then deployed to understand the joint impacts of climate and land cover change. The response of this basin to climate change induced land cover transition is evaluated for three different land cover change scenarios over the next 80 years corresponding to the RCP2.6, RCP4.5, and RCP8.5 climate scenarios as estimated by three climate change models. This approach is expected to provide insight into potential long-term hydrological impacts of climate change and permafrost thaw in these regions.

5.1 Introduction

Permafrost thaw as a result of climate warming is drastically modifying the distribution of permafrost plateaus, fens, and isolated bogs in regions of northern Canada. These changes influence the hydrological behaviour of wetlands in the discontinuous permafrost zone. The pattern of hydrologically-important land cover in discontinuous permafrost regions is affected by topography, hydrology, and the local surface and subsurface characteristics (Tedesco, 2015; Schuur et al., 2008). Each land cover type plays a unique function in the hydrology of the region (Quinton et al., 2003). Channel fens are typically water conveyors and bogs can act as storage features or water conveyors (Woo, 2012). The boundaries between fens, bogs, and permafrost plateaus are changing as permafrost is thawing continuously in the NWT (Payette et al., 2004; Quinton et al., 2011). Degradation of permafrost plateaus around a channel fen or a chain of isolated bogs increases the runoff contributing area (Walvoord and Kurylyk, 2016), leads to transition from bog to fen (termed "bog capture" by Connon et al. (2014)), influences the wetting-drying cycles of the ground, and changes the primary and secondary runoff characteristics of the landscape. Therefore, the thaw-induced alterations of these land covers can drastically change the hydrological responses to precipitation and snowmelt events.

The annual runoff ratio and river discharge have increased in the Taiga Plains, while there has not been a significant change in precipitation pattern and magnitude (Mack et al., 2021). Connon et al. (2014) proposed that the main factor behind the rise in river discharge is land-cover change caused by permafrost thaw. Other factors include increased plateau runoff areas and increased hydrological connectivity due to formation of new channels between bogs and fens, as well as changing water contribution from melting permafrost ice and increased baseflow (Connon et al., 2015). To accurately predict the long-term impact of climate change on discharge, the information on permafrost thaw-induced land cover transitions must be incorporated into hydrological models.

Each land cover in a basin, such as fen and bog, has a unique influence on the water balance of the basin and the seasonal connectivity between the basin's hydrological features. Two main runoff generating areas, i.e., primary and secondary areas, can be taken into consideration in order to better comprehend the functions of the various land cover types, as suggested by Connon et al. (2014). The secondary contributing area contains bogs (Quinton et al., 2003) and their local contributing areas. These have been regarded as storage features in the landscape and can generate runoff only if a certain storage threshold in bogs is exceeded. The primary contributing area includes channel fens that convey runoff to the outlet of the basin (Hayashi et al., 2004) and the local contributing area to these fens. The fill-and-spill hydrological process (Spence, 2007) determines the threshold based

runoff generation in the secondary contributing area. The relationship between the primary and secondary contributing runoff areas changes when permafrost thaws. Fen and bog coverage has increased over the past 50 years as a result of the fast permafrost thaw that has deteriorated subarctic peatlands (Payette et al., 2004). The reduction of the hydraulic gradient between the permafrost plateau and the neighbouring bog or fen, as well as the conversion of permafrost plateaus into wetland, may reduce the basin capacity to generate runoff (Quinton and Baltzer, 2013). However, permafrost breaches close to bogs have enhanced wetland hydrological connection and made it simpler for water to travel between adjacent bogs and channel fens, which has boosted runoff to drainage networks (Connon et al., 2014, 2015; Haynes et al., 2018). Transitions between bog, fen, and permafrost plateaus, and thaw-induced increase in flow rate have a significant impact on the response of discontinuous permafrost watersheds to a changing climate (Connon et al., 2014; Haynes et al., 2018).

Hydrological models are essential tools for evaluating the consequences of climate change. Due to the region's extreme weather patterns, distinctive hydrological processes, and challenges with data collection, care should be given while selecting appropriate hydrological model(s) for the colder regions of the Canadian North (Bui et al., 2020). For studying the surface hydrological processes in Northern regions, hydrological models including TopoFlow (Schramm et al., 2007), HBV by Bergström et al. (1995), SWAT (Arnold and Fohrer, 2005), ECOMAG (Ecological Model for Applied Geophysics by Motovilov (2013)), and the Cold Regions Hydrological Model (CRHM) (Pomeroy et al., 2007) have been used. None of these models are capable of explicitly simulating the land cover change impacts discussed above. The magnitude and timing of the simulated streamflow hydrograph are highly related to the accurate classification of the land cover types and connected areas (Stadnyk et al., 2005), the extent and proportional coverage of land cover types such as fens and bogs (Quinton et al., 2003), understanding the transitions and interactions between the major land cover types (Stone et al., 2019), and an accurate transfer of the understanding from field observations to the hydrological models. These controls on streamflow are all changing.

Some studies have been conducted to pair hydrological models with land use change models in order to provide a valuable tool for decision-making, specially for better land-use decision support (McColl and Aggett, 2007). A common shortcoming of land-use-hydrology interaction models is that they assume a steady land use throughout the simulation period (Yalew et al., 2018). For example, Stone et al. (2019) evaluated the hydrological response of a channel fen sub-basin in the Scotty Creek basin, Northwest Territories, Canada, which is characterised by permafrost plateau-bog complexes using the CRHM platform. To accommodate changes in wetland area, different decreasing ratio of wetland to plateau were

assumed rather than predicted. These modelling attempts are helpful in determining a watershed's vulnerability to climate change impacts, but they cannot provide a forecast of the watershed's future. Also, there is a lack of research that differentiates between secondary and primary runoff area function when simulating the hydrological responses of wetland systems in discontinuous permafrost zones to climate warming. That research gap is not only a result of the challenges associated with identifying the roles played by various types of land cover in hydrological models, but also a historical difficulty in simulating the fill-and-spill response in complex systems.

To comprehend the consequences of climate change, a thorough analysis of the land cover development process in hydrological models is desirable. In this study, information about the magnitude and pace of landscape changes derived from a land cover evolution model is included in a hydrologic model of Scotty Creek basin in the southern NWT. Here, we employed the upscaled fill-and-spill algorithm of Chapter 3 to runoff simulation within secondary contributing areas. Finally, to quantify the effects of permafrost thaw on the hydrological response of the study basin, the streamflow responses to various land cover transitions and climatic forcing from various climate change scenarios were analysed.

5.2 Case Study and Data

The Scotty Creek basin has a drainage area of 129 km^2, and is located 50 km south of Fort Simpson in the Northwest Territories (WSC, 2022b), as illustrated in Figure 5.1. The main land cover types in this basin are permafrost plateaus covered by pima, bogs covered by sphagnum, channel fens covered by grass, small lakes, and uplands covered by deciduous forest. The average daily temperature for the basin is around -2.8 °C and the annual average precipitation is 388 mm; half of this is snow (ECCC, 2017). The meteorological data, precipitation and temperature, were obtained from Fort Simpson gauge (Gauge ID 2202103, located at 121°14'12" W and 61°45'37" N) for 1995 to 2016 (ECCC, 2020). The streamflow observations were obtained from Mackenzie River at Fort Simpson gauge (Gauge ID 10ED009, located at 121° 21' 32" W and 61° 52' 06" N) for 1995 to 2016 (WSC, 2020).

As a result of permafrost thaw, the areal coverage of permafrost plateaus has decreased over time in the Scotty Creek basin. Permafrost plateaus are located at higher elevation than the adjacent unfrozen bogs and fens. This higher elevation increases the thermal conductivity and the potential to melting (Quinton et al., 2011; Chasmer et al., 2010). Previous studies reported that the plateaus covered 22% of the basin and this amount is predicted to decline to 17% by 2055 (Smith et al., 2005). In this study, the land cover data

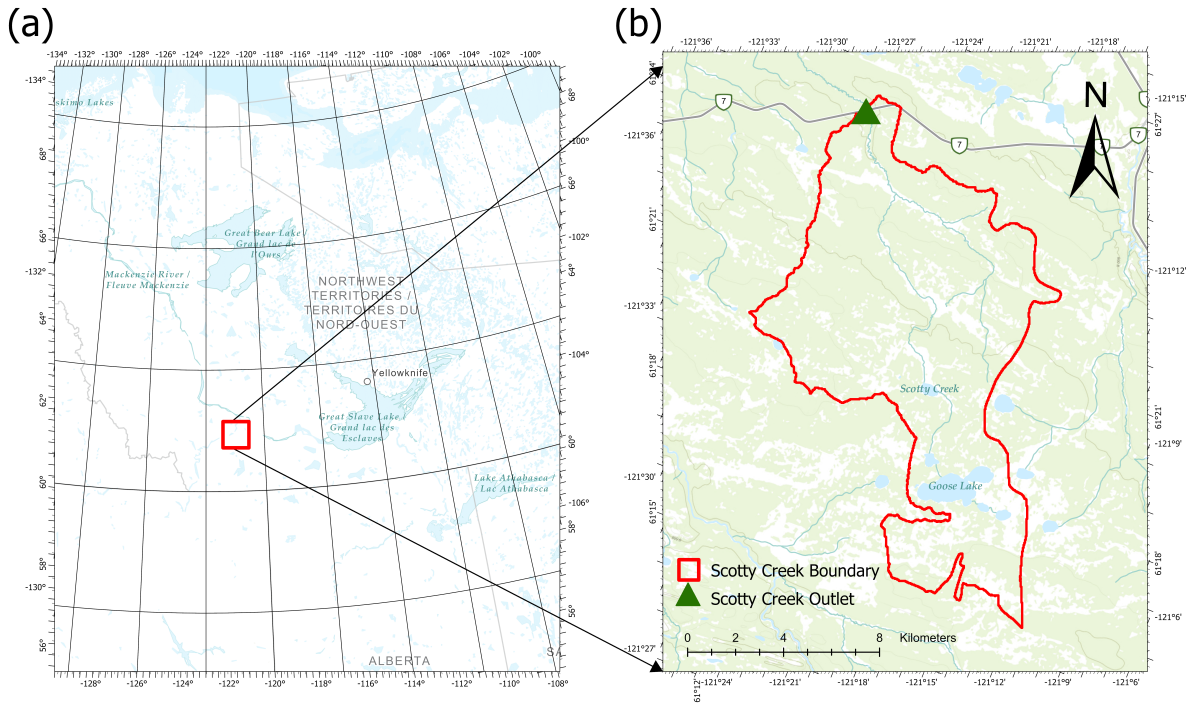

Figure 5.1: The location of the Scotty Creek basin within the Taiga Northwest Territories, Canada

and transitions in response to climate change are derived from a classification model (for historical data) and by a machine-learning land cover change model (for future prediction).

5.3 Methods

To estimate changes in runoff, recharge, storage, and other watershed processes by hydrological models under different land cover change scenarios, we need classified maps of the Scotty Creek watershed for present and future time. Under the proposed coupling framework, the hydrologic model simulates the runoff process, while the TSLCM model estimates the land cover change, and the Taiga PlainsWetland Identification Neural Network (TWINN) solution delineates the runoff contributing area input to the hydrological model. The purpose of this section is to describe the methodology for calibration, building, and incorporating land cover change model into a hydrological model to determine how Scotty Creek basin may respond to land cover transitions caused by permafrost thaw.

5.3.1 Raven-UWFS Hydrological Model

A hydrological model of Scotty Creek was developed in Raven (Craig et al., 2020), a semi-distributed flexible hydrological modelling framework. The Raven framework offers a selection of more than 100 hydrological processes. In this study, first, the basin was discretized into five HRUs corresponding to land classes with similar hydrological functions. The five main land classes defined in this basin are open water, upland, fen, secondary, and primary area. The primary area includes the portion of permafrost plateaus draining directly to the fen, while the secondary area includes permafrost plateaus draining to bogs. The UWFS algorithm from Chapter 3, a modified version of the HBV model, was used to simulate the abstraction process in the secondary runoff area, which includes redirecting the rainfall and rainfall excess including snowmelt and runoff from peat secondary contributing area to bog area of this basin. The process requires information about local contributing area ratio of secondary contributing area to bog area. The Raven-UWFS model requires forcing inputs including daily precipitation, maximum and minimum temperature, and land cover transition data. Snowmelt and refreezing of the snow pack are modeled using the degree day method. The evaporation process from the secondary area is modeled by UWFS open water evaporation algorithm which updates bog deficit depth at each time step. The evaporation from soil is modeled by the GR4J soil evaporation method (Perrin et al., 2003). The infiltration process at primary runoff area and fen is modeled by partition coefficient method which is a simple linear relationship between precipitation and runoff based on the partition coefficient parameter. For detailed information about the UWFS algorithm and Raven model see Chapter 3, and Craig et al. (2020). The initial Scotty Creek lumped model was developed using the historical meteorological data recorded at the Fort Simpson gauge from 1995 to 2015 with five HRUs. The historical classified land cover maps of the Scotty Creek basin for every five years from 1995-2015 has been generated by the TWINN solution (Akbarpour et al., view). TWINN solution generates classified land cover maps using RGB bands of Landsat Collection with a spatial resolution of 30 m. The extent of primary and secondary runoff area extracted from TWINN are used to define HRUs areas in Raven. Every five years during the historical period of hydrologic simulation, the area of the dominant land cover types in the basin is updated and introduced to the model as indicated in Table 5.3. The simulation period was divided into the two periods of 1995-2010 and 2010-2015 for the purpose of calibration and validation, respectively. The list of parameters used in the model and their definition is provided in Table 5.1. The values of parameters are estimated based on an automatic calibration process. The Dynamically Dimensioned Search (DDS) algorithm (Tolson and Shoemaker, 2007) in OSTRICH (Matott, 2017) with 2,000 iterations and 10 replicates is used to find the set of parameters which provides the best performance of the model in streamflow simulation during the calibration period. To

evaluate the model performance, the KGE metric (Gupta et al., 2009) has been calculated as,

$$KGE = \sqrt{(r-1)^2 + (\frac{\mu_{sim}}{\mu_{obs}} - 1)^2 + (\frac{\sigma_{sim}}{\sigma_{obs}} - 1)^2} \tag{5.1}$$

where r is the correlation between simulated and observed streamflow, $\frac{\mu_{sim}}{\mu_{obs}}$ is the ratio of the mean simulated to mean observed streamflows, and $\frac{\sigma_{sim}}{\sigma_{obs}}$ is the ratio of the simulated to observed streamflow variance.

Table 5.1: UWFS parameter ranges for calibration of the Scotty Creek hydrologic model

Parameter name	Description	Units	Min	Max
RAIN_CORR	Rain bias correction factor	[-]	0.8	1.2
SNOW_CORR	Snow bias correction factor	[-]	0.8	1.2
RAIN_ICEPT_PCT	Relates percentage of throughfall of rain to LAI+SAI	[-]	0.02	0.2
SNOW_ICEPT_PCT	Relates percentage of throughfall of snow to LAI+SAI	[-]	0.02	0.2
MELT_FACTOR	Maximum snow melt factor used in degree day models	mm/d/°C	1	3.5
SNOW_SWI	Water saturation fraction of snow	[-]	0	0.4
RAINSNOW_TEMP	Rain/snow halfway transition temperature	°C	-3	3
PARTITION_COEFF	Runoff fraction	[0..1]	0.5	1
GAMMA_SCALE	Gamma unit hydrograph scale parameters	[1/d]	0.1	20
MAX_PERC_RATE	Percolation rate	[mm/d]	0.01	1000
FIELD_CAPACITY	Field capacity saturation of the soil	[0..1]	0	1
BASEFLOW_COEFF	Linear baseflow storage/routing coefficient	1/d	0.01	1
FOREST_COVERAGE	Fraction of land covered by vegetation canopy	[0..1]	0	1
LAKE_PET_CORR	Fraction of PET to apply to lake evaporation	[-]	0.8	1.2
Parameters for secondary area:				
OW_PET_CORR	Fraction of PET to apply to open water evaporation	[-]	0.8	1.2
DEP_{max}	Maximum amount of water that stored in depressions	mm	100	450
DEP_{frac}	Percent of landscape covered by depressions when full	[0..1]	0.1	0.8
β_{min}	Minimum local contributing area ratio	[-]	0	4
b	Shape factor of local contributing area ratio distribution	[-]	0.01	10
Initial Parameters for secondary area:				
DEPRESSION	Initial amount of water that is stored in depressions	mm	50	250
D_{min}	Minimum amount of deficit in each depression	mm	0	250

5.3.2 Climate Change Scenarios

To investigate the long-term effects of continuous climate warming in the Scotty Creek basin, specifically permafrost plateau transition to wetlands, the precipitation and temperature data were retrieved from three Global Climate Models (GCMs) under the three Representative Concentration Pathways (RCPs) from the Coupled Model Intercomparison Project 5 (CMIP5; Pacific Climate (2022)). Table 5.2 includes information about the selected models. The choice of using three global climate models to address climate model

Table 5.2: Attributes of the selected CMIP5 GCMs (Lakku and Behera, 2022)

Acronyms	Model	Institution	Atmospheric Spatial Resolution
BCC-CSM1.1	Beijing Climate Center Climate System Model with Moderate Resolution	Beijing Climate Center, China Meteorological Administration	1.1215° × 1.125°
MIROC5	Model for Interdisciplinary Research on Climate 5	Atmosphere and Ocean Research Institute, National Institute for Environmental Studies, and Japan Agency for Marine-Earth Science and Technology	1.4008° × 1.4063°
GFDL-CM3	GFDL Coupled Model version 3	Geophysical Fluid Dynamics Laboratory	2.0° × 2.5°

uncertainty is based on practical considerations such as computational resources and time constraints. Running a large number of models for each scenario would be prohibitively time-consuming and resource-intensive specially for the TSLCM model. While using only three models does not completely capture the range of possible outcomes, it provides a reasonable estimate of the range of uncertainties associated with the modeled climate projections. The RCP 2.6, 4.5, and 8.5 representing a low, moderate, and high emission of Greenhouse Gas (GHG) are selected. The changing pattern of dominant hydrologic land covers based on the forecasted temperature data from these climate scenarios and models are predicted by the TSLCM model over 2010–2100 period using classified imagery from 2010 as an initial condition. Then, the estimated land cover change information is used in the hydrological model along with the forecasted precipitation and temperature from the GCMs to analyze the effect of climate warming and land cover transitions on the generated streamflow in the Scotty Creek basin.

For hydrological simulation during 2016-2100, the land cover transitions information is provided by the TSLCM model which predicts the transitions between different land cover in 2040, 2070, and 2100. The classified and predicted land cover information from TSLCM and TWINN along with the temperature and precipitation data from GCMs are used in the hydrological model to predict the simultaneous effect of climate change and land cover transition on the generated runoff.

For the future scenarios, the classified map of the Scotty Creek basin in 2010 and the temporal input data includes time increments and accumulated temperature degree from the selected GCMs are used in the TSLCM to predict land cover change from 2010 to 2100. The input data of the trained TSLCM includes a set of spatio-temporal variables obtained by remote sensing including the estimated summertime land surface temperature anomaly (LST), the distance to land cover interfaces, time horizon, time-accumulated temperature, and classified land cover maps. The TSLCM is able to capture the spatial patterns of change over time and generate land cover maps that represent the spatial distribution of

fen, bogs, and permafrost plateaus.

5.4 Results

5.4.1 Calibration

Figure 5.2 compares the simulated and observed streamflow for selected time increments during calibration and validation periods. Figure 5.2-a shows that the model is capable of simulating high flows accurately. The KGE metric of 0.77 and percentage of bias of 5.44 for the full calibration period (i.e., 1995-2010) confirms a good performance of the hydrological model, although the model overestimates the peak during low-flow events. The simulated streamflow during 2014 in Figure 5.2-b illustrates an example of the overestimation of peak during low-flow year. A similar quality result is reached for the validation period with a KGE of 0.65 and percentage of bias of -1.47. These KGE values are about what is typically considered acceptable for hydrological model (Knoben et al., 2019).

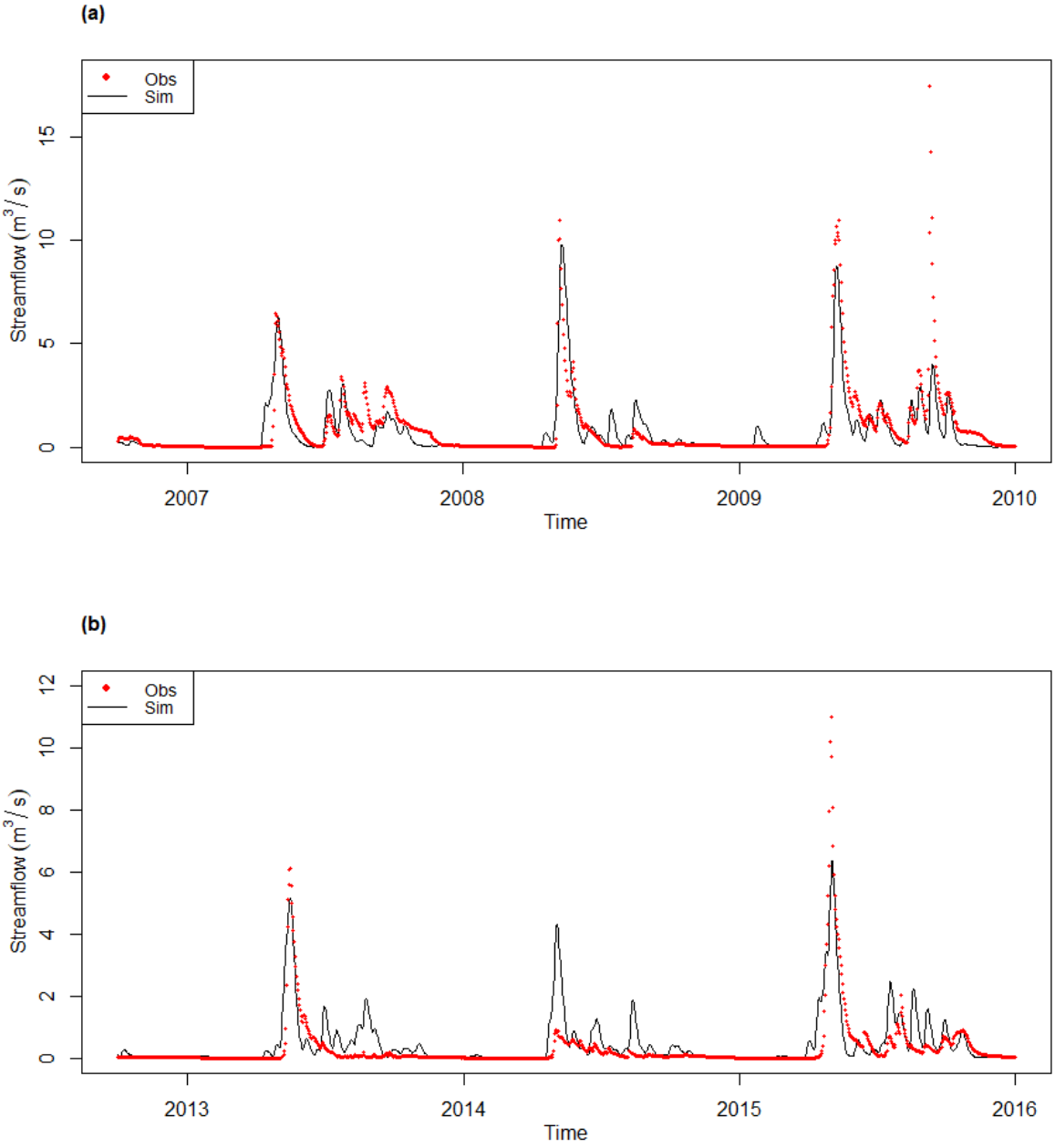

Figure 5.2: Streamflow hydrograph for a) a portion of the calibration period from 2006 to 2009 and b) a portion of the validation period from 2012-2016

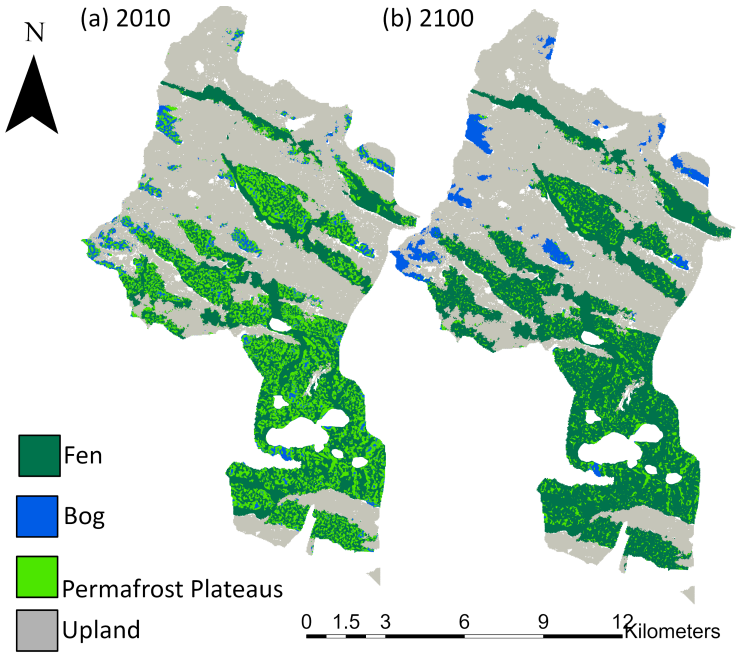

Figure 5.3: Prediction of land cover change over a 100 years time step (2010-2100) simulated for RCP8.5: (a) The distribution of land covers in 2010; (b) The distribution of land covers simulated by TSLCM for 2100 (Akbarpour, 2023).

5.4.2 Climate Scenarios: Land Cover Change

Figure 5.3 illustrates the simulated land cover change from 2010 to 2100 from the TSLCM model under RCP8.5. The predicted time series land cover maps generated up to the year 2100 suggest that permafrost plateaus are transforming to fens and the increase in the proportion of the landscape covered in fen is accelerating.

Table 5.3 and 5.4 report the area of historical and forecasted dominant hydrological land covers under each climate scenarios that has been generated from the TWINN and TSLCM solutions to define HRUs in the Raven-UWFS model. It can be concluded that the rate of land cover change simulated for RCP8.5 is greater than other selected RCPs. The overall trend of simulated land cover change for all RCPs shows a decreasing trend in secondary runoff area distribution and an increasing trend in primary runoff area distribution; considering these trends, streamflow is expected to rise as a result of climate change in the future because the storage would decrease and the extent of primary contributing area would increase.

Table 5.3: The percentage of each land cover type area, relative to the total land area, for a historical simulation period derived from the TWINN model

Year	Fen	Primary	Secondary	Upland	Water
1995	17.78	12.22	24.68	42.66	2.65
2000	19.39	13.89	21.41	42.66	2.65
2005	24.60	11.95	18.13	42.66	2.65
2010	27.51	10.23	16.95	42.66	2.65
2015	27.67	10.48	16.53	42.66	2.65

5.4.3 Climate Scenarios: Hydrological Simulations

To investigate the impacts of climate change on the hydrological responses of Scotty Creek basin, the simulated streamflow for the three climate models (BCC-CSM, GFDL-CM3, and MIROC5) and three scenarios (RCP 2.6, 4.5, and 8.5) have been compared. Figure 5.4 shows the streamflow values in each day of the year averaged over 1995-2016, indicated as pre-2016, and over 2016-2100, indicated as Post-2016. It can be concluded from all nine cases that the highest daily streamflow occurs earlier for simulations post-2016. Moreover, the leftward shift in streamflow for post-2016 indicates that the spring freshet may occur earlier in future scenarios. The estimated 90% quantile for Post-2016 is generally greater than pre-2016 in each climate scenario confirming the expected impacts of climate change. The majority of the basin serves as a primary runoff area during high-flow (i.e., April and May during the spring freshet), and the fill-and-spill process not happening in secondary runoff area impedes the generated runoff magnitude during the low-flow. The importance of climate induced land cover change, specially, the transition of secondary runoff area to primary runoff during low-flow can be noticed in Figure 5.4 after the spring freshet (i.e., day 150). The higher mid-summer flows can be attributed to less water stored in bogs and lost as evaporation.

The 10-year moving average of precipitation, temperature, annual peak streamflow, and annual volume for three climate scenarios is shown in Figure 5.5 and 5.6 where each column reports the maximum, minimum, and average of the three selected climate models and observations in each scenario from 1995-2100, i.e., the range represents GCM uncertainty. A gradual increase is observed in the predicted annual peak streamflow for RCP2.6, and RCP4.5 during the 100 years time increment (Figure 5.6-a), while there is a sharp rise in predicted streamflow for RCP8.5 after 2070. A similar behaviour is seen on estimated annual volume of streamflow (Figure 5.6-b) which might be related to the trend of precipi-

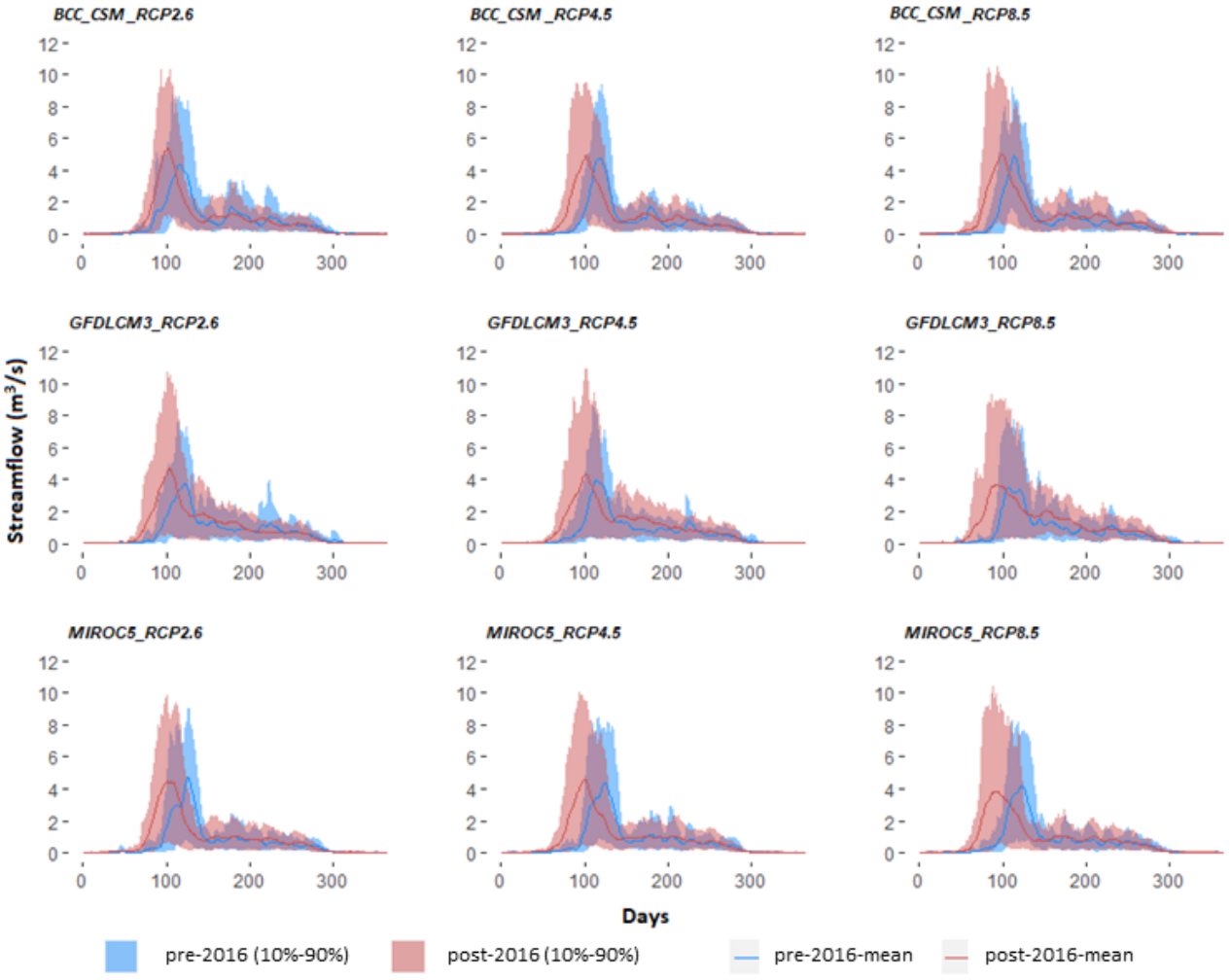

Figure 5.4: Comparison of Julian day stream flow distribution before and after 2016 for different climate models and scenarios

Table 5.4: The percentage of predicted dominant land cover area, relative to the total land area derived from TSLCM model

Year	Fen	Secondary	Primary	Fen	Secondary	Primary	Fen	Secondary	Primary
	BCCCSM_RCP2.6			BCCCSM_RCP4.5			BCCCSM_RCP8.5		
2040	29.20	15.94	9.89	29.20	15.94	9.89	29.40	15.95	9.69
2070	33.73	11.21	10.09	33.73	11.21	10.09	34.52	10.41	10.12
2100	39.78	7.21	8.06	39.78	7.21	8.06	41.24	6.51	7.29
	GFDLCM3_RCP2.6			GFDLCM3_RCP4.5			GFDLCM3_RCP8.5		
2040	29.38	15.80	9.86	29.52	15.69	9.83	29.57	15.65	9.81
2070	34.27	10.68	10.08	34.50	10.47	10.07	34.90	10.13	10.01
2100	40.48	6.84	7.72	40.95	6.64	7.45	41.99	6.19	6.86
	MIROC5_RCP2.6			MIROC5_RCP4.5			MIROC5_RCP8.5		
2040	29.34	15.74	9.95	29.36	15.74	9.92	29.47	15.68	9.88
2070	43.96	14.04	13.00	44.10	13.91	12.99	44.88	13.16	12.96
2100	51.68	9.08	10.23	52.31	8.78	9.91	54.09	8.03	8.88

tation and temperature generated for the selected RCPs shown in Figure 5.6-a and b. The observed streamflow are more closely aligned with the maximum values of the predicted annual peak streamflow and the average values of the annual volume streamflow for the three climate models. To gain a better understanding of the streamflow variations, the 10-year moving average of maximum, minimum, and average of runoff ratio simulated for the three climate change models and scenarios have been shown in Figure 5.6-c. It can be concluded that the runoff ratio is increasing about 20% to 25% in each of the three RCPs through 2010 to 2100. These increase mostly caused by precipitation increase as seen in Figure 5.5-a. Precipitation increases as the climate warms because the atmosphere can hold more moisture. The earlier snowmelt and change from snow to rain caused by the warmer temperatures can also result in an increase in streamflow.

To investigate the impact of land cover transitions on the predicted streamflow under three climate scenarios, the simulated summer peak and summer volume of streamflow with and without considering land cover change is compared for BCC-CSM1.1 under three different RCPs. For the case without land cover change, the Raven-UWFS model uses the fixed land cover from 2010. The impact of land cover transition on the simulated streamflow is estimated by an average difference percentage (ADP) calculated as,

$$ADP = \sum_{1}^{n} \frac{F_{withLCC} - F_{withoutLCC}}{F_{withLCC}} \tag{5.2}$$

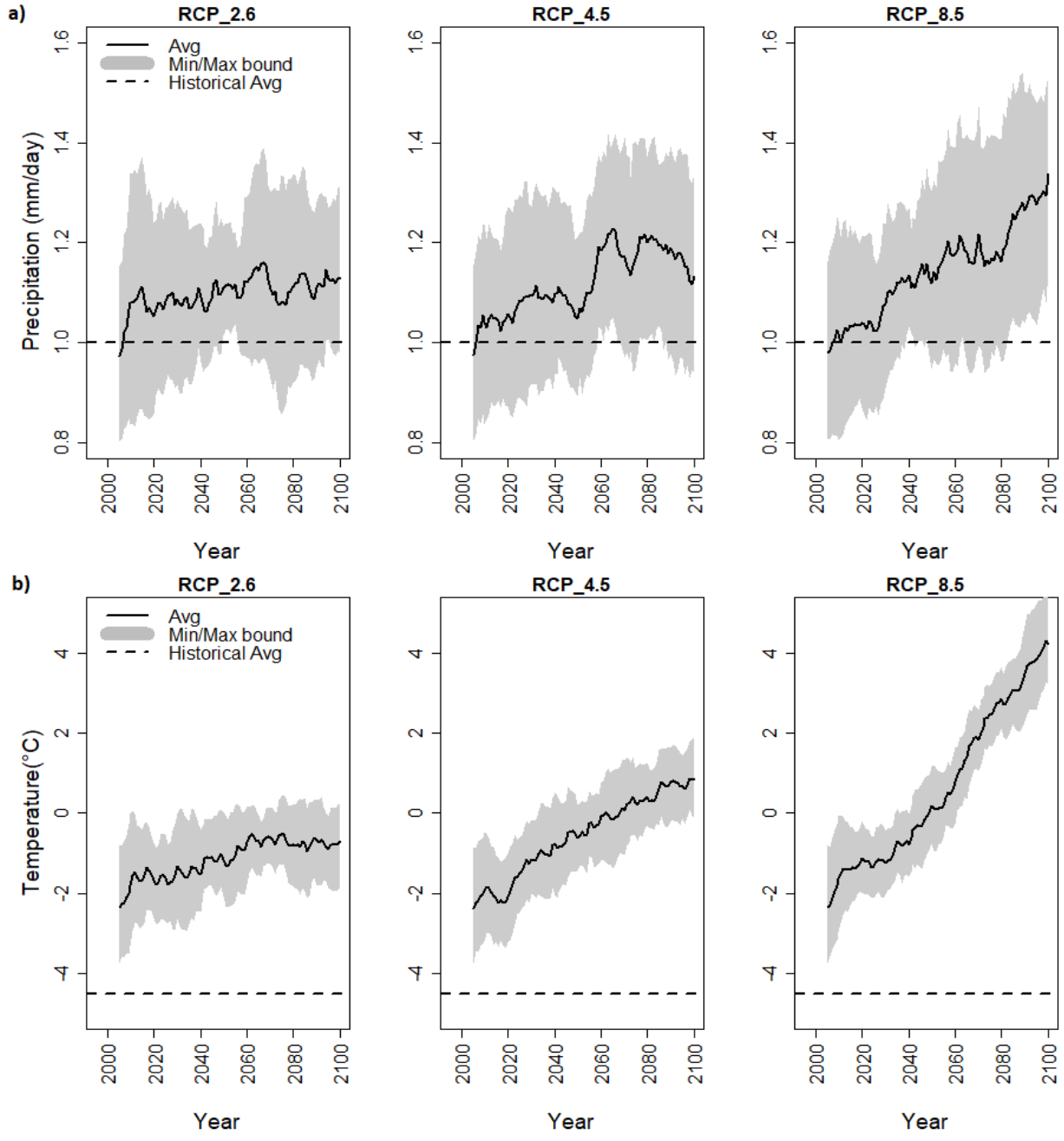

Figure 5.5: 10-year moving average of a) mean annual precipitation b) mean annual temperature from the three climate scenarios and models (Akbarpour, 2023)

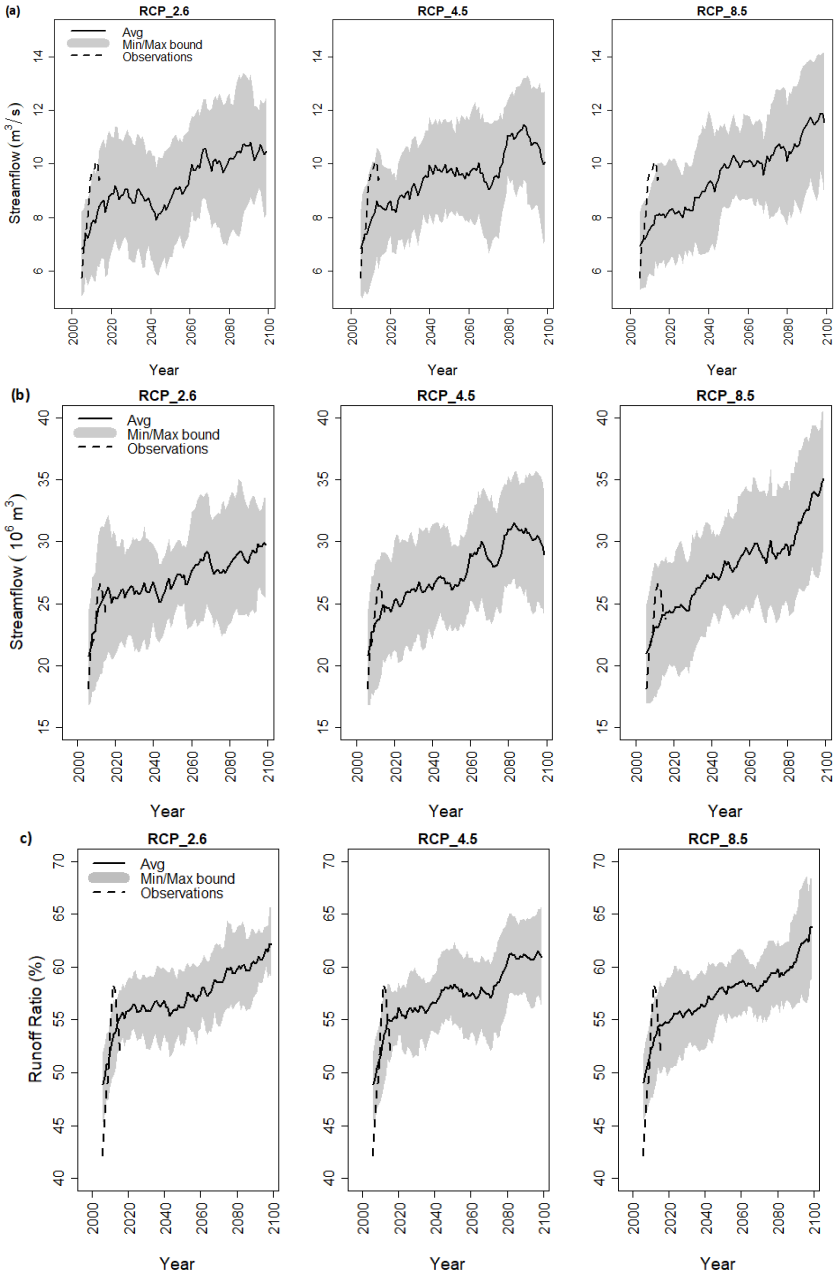

Figure 5.6: 10-year moving average of simulated a) annual peak, b) annual volume, and c) annual runoff ratio of streamflow in response to climatic forcings of three climate scenarios and models.

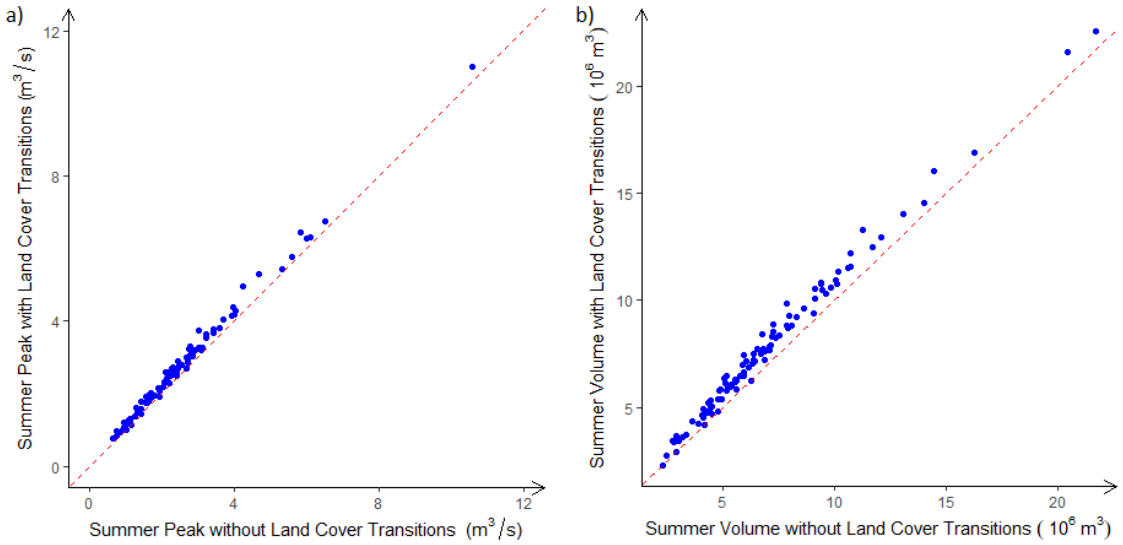

Figure 5.7: Comparison of a) the summer peak streamflow and b) the summer volume of streamflow magnitude with and without considering land cover transitions in the hydrological model (Akbarpour, 2023)

where $F_{withLCC}$ and $F_{withoutLCC}$ represent the simulated streamflow by the hydrological model with and without land cover evolution information as input, respectively, and n is the number of data. The ADP values for summer peak streamflow have been estimated as 9%, 9.3%, and 9.8%, under RCP2.6, RCP4.5, and RCP8.5 for BCC-CSM1.1 model, respectively. The ADP values for summer streamflow volume have been estimated as 10.5%, 10.8%, and 11%, under RCP2.6, RCP4.5, and RCP8.5 for BCC-CSM1.1 model, respectively. This implies that a primary driver of the streamflow increase is attributed to the increased in the rainfall. The ADP value for annual peak and annual volume streamflow has been estimated around 7% and 5.6%, respectively, which shows the higher impact of fill-and-spill process in runoff generation of secondary area during summer time. The one to one comparison of summer peak and summer volume of streamflow simulated for BCC-CSM1.1 climate model under RCP4.5 has been shown in Figure 5.7 as an example. The majority of land cover transitions are from secondary to primary runoff areas and the decrease in the storage capacity of the basin during this transition results in an increase in the generated streamflow.

5.5 Conclusions

Permafrost thaw is accelerating the evolution of hydrologically-important land covers and transforming their hydrological roles in the discontinuous permafrost zones of Northwest Territories. It has been observed that permafrost thaw reduces the extent of secondary runoff area and storage capacity, accelerates the transition to primary runoff area, increases the hydrological connectivity, and therefore streamflow in a basin. To investigate the effects of the thaw-induced land cover transitions on the hydrological responses of a wetland-permafrost plateau complex, a land cover classification model, TWINN, a land cover change prediction model, TSLCM, and a hydrological model, UWFS, were coupled. TWINN method is a method which uses remotely sensed imagery to classify the basin into five main land covers including primary and secondary contributing area for each five years during historical simulation period. The TSLCM is a machine learning-based model able to estimate the long-term evolution of hydrologically-important land cover, and simulate spatial patterns and pace of change every 30 years from 2010 to 2100. The UWFS algorithm implemented in Raven differentiates between runoff generation processes in secondary and primary contributing area and simulates the streamflow from the basin in response to climatic forcings. The proposed framework informs the UWFS model with the extent of main land cover types generated from TWINN and transition data generated by the TSLCM to simulate the past as well as project the long-term impacts of land cover evolution on the streamflow generation in the Scotty Creek basin. The simulation of streamflow using the selected model and scenarios concludes that there is a likelihood of an earlier spring freshet occurring in the future, which can be attributed to the rising temperatures. Comparing the trend in runoff ratio shows that about 20 to 25% of increase is predicted in future under the selected climate models and scenarios. This is aligned with the increase in streamflow volume caused by rainfall increase in the basin and bog capture mainly caused by transition of secondary runoff area to primary runoff area.

The impact of land cover transition on predicted streamflow for the BCC-CSM1.1 model under different RCPs is estimated to be approximately 10% according to the coupling framework. Similar behavior is observed in other selected GCMs, indicating low uncertainty in the estimation of land cover's impact on streamflow. This value is comparable to the range estimated by Connon et al. (2015), who found that neglecting to represent connected bogs as dynamic transmission features in the landscape can lead to an underestimation of water available for streamflow by 5-15%. Therefore, these systems are a crucial component of the water balance in regions with discontinuous permafrost. Overall, the results suggest that land cover transitions were a primary driver of increased streamflow in the past. However, in the future, precipitation is expected to play a more dominant role in increasing

streamflow due to the decline in the extent of the secondary runoff area and the transitions to primary runoff area.

This study's findings provide valuable insights understanding long-term changes in Canadian wetland-dominated basins, which can be used to inform policy and management decisions. Further application and evaluation of the presented machine learning-informed hydrologic model coupling framework on other areas of interest would strengthen understanding the impacts of permafrost thaw-induced land cover transitions on streamflow generation. This study is focused on the forcing data from only three climate change models under three RCPs to simulate streamflow trends; future studies may benefit from including an ensemble of more climate change models.

Chapter 6

Conclusions

6.1 Summary

The hydrology of low gradient landscapes can be highly influenced by the presence of hundreds to thousands of wetlands. Wetlands can serve as storage features or contribute to runoff when the water level within exceeds a certain threshold. An understanding of the role of wetlands on hydrological behavior of a basin and interactions between them and other hydrological features is required to determine the basin-scale response to precipitation or snowmelt events both historically and under future climate change scenarios.

The first and main objective of this study was **to develop and test a probabilistic-analytic model for cascades of wetlands, and provide an upscaling approach to understand and characterize system runoff responses**. Chapter 3 describes the model development. First, a probabilistic-analytic solution of fill-and-spill events in a single wetland was proposed. In this algorithm, the water balance in a wetland is defined based on basic characteristics of a single wetland, i.e., deficit depth and local contributing area. Then using a derived distribution approach, the response of a single wetland to precipitation or snowmelt events is upscaled to find the total outflow from a basin including thousands of wetlands. The detailed analytical solution for wetlands in cascade sequence depths of one, two, three, and four has been provided in Appendix A.1, A.2, A.3, and A.4, respectively. A Monte Carlo based approach was used for testing the accuracy of the derived analytical solution and evaluate extensions of the model's ability to simulate different networks. The utilization of probabilistic characteristics of wetland properties and a Monte Carlo based approach has enabled the first comprehensive examination of the influence of cascade depth on landscapes containing hundreds to thousands of wetlands. The fact that there is little

variation in the runoff produced by higher cascade depths indicates that simulating a small sequence of cascades (such as four) can effectively capture the runoff generated by a basin, even if it possesses deeper cascade networks. Given the high computational cost and impracticality of obtaining analytical solutions for deeper networks, as demonstrated in Appendix A.4, it is sensible to refrain from using a larger number of cascades.

The second objective of this study was **to implement the proposed UWFS algorithm into an existing two-dimensional semi-distributed hydrologic model, Raven, to test the ability of the upscaling method in the lumped runoff simulation of wetland-dominated basins influenced by fill-and-spill hydrology**. The event based algorithm has been extended to a continuous model to evaluate the continuous response of a heterogeneous wetland complex to rainfall and snowmelt events by evolving the wetland deficit distribution based on time-varying evaporation and continuous time series of precipitation. The performance of the Raven-UWFS model in simulation of runoff at 10 subbasins inside the QRB in the PPR of Saskatchewan and comparison of the simulation results with an existing prairie model named HYPR has been discussed in Chapter 3 and Appendix B.1. The comparison results demonstrate that the UWFS algorithm is capable of accurately representing the influence of wetland properties and overcoming the challenges of parameterizing numerous wetlands. This method has the potential to enhance the accuracy of streamflow simulation by existing hydrological models in basins with heterogeneous conditions by incorporating lateral flow from the local contributing area and enabling the representation of various wetland networks. It is expected that the model may be applied successfully to various similar wetland-dominated landscapes, which includes the boreal plains of northern British Columbia, Manitoba, and Ontario, the taiga plains, southern parts of the PPR extending down into Montana, and many regions of western China and central Russia.

The third objective of this study was **to use the analytical model and numerical model to explore the impacts of network depth, branching, and gatekeeping on fill-and-spill network responses**. The impact of the network depth and gatekeepers, and the sensitivity of the proposed upscaled fill-and-spill model to the properties of wetlands have been studied in Chapter 3. Using the proposed Monte Carlo approach, the role of network branching on the generated runoff from the basin has been studied in Chapter 4. In Chapter 4, it is demonstrated that, through calibration of the UWFS parameters, both branching networks and non-prismatic wetlands can be simulated adequately at the basin scale. The analysis indicates that the variation in the runoff generated by wetlands with a branching ratio of two and a cascade depth of two is less than 1%. Therefore, accounting for wetlands in cascade depth (i.e., in series) could sufficiently capture the runoff generated from wetland network, particularly if model calibration is used to adjust distribution

parameters. This finding can decrease the computational requirements and accelerate the modeling of the wetland network in hydrological models. It also indicates that even the simple analytical model with a cascade depth of one may be practically deployed in even complex systems, and effective properties may be determined which emulate the influence of more complex branching and network depth impacts.

The fourth objective of this study was **to investigate the impacts of permafrost thaw induced by climate change on a hydrological response of a basin in the NWT**. Chapter 5 provides a description of an approach to use the information about land cover transitions induced by climate change and permafrost thaw in conjunction with the UWFS model to predict future streamflow trends in a discontinuous permafrost region. Chapter 5 studies the simultaneous response of Scotty Creek basin to climate change (i.e., precipitation and temperature changes) simulated by three different climate models and climate change induced land cover transitions. This study implies that including the land cover transition in hydrological study of Scotty Creek basin may increase the generated runoff about 10 % during summer time and lead to a 6% increase in annual volume, in addition to runoff changes predicted due to increasing precipitation. This also indicates that the impacts of the secondary runoff area, which acts as a threshold-based runoff generator, may be higher during the summer when the wetlands are not as full compared to the rest of the year. As climate warms and permafrost thaws, the percent of the landscape covered with secondary runoff area will decrease. Thus, it is highly probable that the long-term increase in runoff ratio will be attributed to rising precipitation.

6.2 Contributions

The primary contributions from this study could be summarized as:

- The upscaled fill-and-spill model is the first closed-form probabilistic model that takes into account lateral flow from the local contributing area of wetlands and enables the representation of wetlands in different cascading depths.
- The probabilistic characterization of wetland properties was demonstrated to successfully simulate the runoff response of low gradient landscapes with hundreds to thousands of wetlands where limited high-resolution elevation data are available.
- The definition of water balance components in terms of units of depth reduces the dimensionality of the problem and eliminates the need to use wetland volume in runoff calculations.

- The use of local contributing area distribution as a key model input can be modified for extension to use cases not considered in the original UWFS model. The contributing area distribution parameters compensates for deficiencies and assumptions in the model, such as considering cascading networks instead of branching networks (even the impact of this assumption is shown to be negligible) and prismatic wetlands instead of non-prismatic wetlands, acting as a more comprehensive parameter in the conceptual model.

- This is the first model of this type of landscape and at this scale to simultaneously address land cover change and climate change. The ability to differentiate between primary and secondary runoff areas allows the model to simulate threshold-based runoff generation in basins and predict the primary factor in runoff generation for past and future scenarios.

6.3 Future Research

The UWFS method enables hydrological models to simulate fill-and-spill responses of wetland-dominated landscapes. In spite of the valuable insights this method has provided on characteristics of wetland systems and their influence on runoff response, there are some limitations within this method. The limitations and assumptions of the UWFS method and its application have been discussed in detail in Chapter 3 and 4. The most important limitations are summarized here:

- Wetlands are assumed uniform in size, at least within a given cascade.

- The wetland deficit in a single cascade is independent of upstream wetland characteristics.

- For cascade depths greater than four, the complex analytical solution is mathematically intractable.

- The wetland response is considered to be fast enough to ignore transient effects during an event.

- An exponential distribution is assumed for deficit and local contributing area ratio. This was found to be appropriate from calibration to one GIS-generated local contributing area ratio distribution. However, we have no field data to inform selection of a specific deficit distribution.

- Only the analytical solution of wetlands with cascade depth of one has been implemented for continuous simulation in Raven.
- The loss of water from wetlands is all considered to be surface flow, ignoring the impact of subsurface flow.
- To study the impact of landcover transition on the hydrological response of a discontinuous permafrost region, the information about landcover transition has been introduced at discrete intervals without consideration of gradual change.
- The climate change models have been sampled randomly and only three general climate models were considered.

It should be noted that the purpose of this research is to improve our ability to simulate lumped wetland systems while considering a degree of internal heterogeneity. It was not intended to be a perfect assumption-free rendering of reality. Future studies may include the implementation and testing of the detailed analytical solution for cascade depths of more than one in the hydrological model. Different distributions could be fitted to the observed contributing area data to find the best representation of local contributing area ratio. More climate models should be considered in evaluating the impacts of land cover transition on predicted streamflow. Improved land cover change representation in Raven, such as the ability to include gradual land cover transitions in the model, may improve the reliability of this study's findings.

6.4 Publication and Presentations

6.4.1 Peer-reviewed Journal

- Taheri, M., Ranjram, M., and Craig, J.R., An upscaled model of fill-and-spill hydrological response. Under review (second round) in Water Resources Research
- Ahmed, M., Stadnyk, T., Pietroniro, A., Awoye, H., Bajracharya, A., Mai, J., Tolson, B., Shen, H., Craig, J., Gervais, M., Sagan, K., Wruth, S., Koenig, K., Lilhare, R., Déry, S., Pokorny, S., Venema, H., Muhammad, A., Hallborg, C., Taheri, M., Learning From Hydrological Models' Challenges: A Case Study from the Nelson Basin Model Intercomparison Project. Submitted to the Journal of Hydrology.

6.4.2 Conference

This research was presented in parts at the following conferences:

- Taheri, M. and Craig, J.R., 2022, December. Fill-and-spill runoff representation within discontinuous permafrost wetlands. ArcticNet, 4-8 Dec., 2022.
- Taheri, M. and Craig, J., 2022, May. Implementation of an upscaled probabilistic fill-and-spill method to simulate wetland-dominated landscapes. In EGU General Assembly Conference Abstracts (pp. EGU22-6239).
- Ahmed, M., Stadnyk, T., Pietroniro, A., Awoye, H., Bajracharya, A., Mai, J., Tolson, B., Shen, H., Craig, J., Gervais, M., Sagan, K., Wruth, S., Koenig, K., Lilhare, R., Déry, S., Pokorny, S., Venema, H., Muhammad, A., Hallborg, C., Taheri, M., 2022, May. Multi-model Intercomparison Project on the Saskatchewan-Nelson-Churchill River Basin (Nelson-MiP). Proceedings of the GWF Annual Open Science Meeting.
- Taheri, M. and Craig, J., 2021, December. Simulating the Upscaled Hydrologic Response of Wetland Cascades in Prairie Regions. In AGU Fall Meeting Abstracts (Vol. 2021, pp. H13E-06).
- Taheri, M., Ranjram, M. and Craig, J.R., 2020, December. Upscaling Fill-and-Spill Hydrological Process in Cascading Wetland Networks. In AGU Fall Meeting Abstracts (Vol. 2020, pp. H212-09).
- Taheri, M., Quinton, W.L. and Craig, J.R., 2020, December. Investigating Climate Change Impacts Upon Runoff from Wetland Cascades in Discontinuous Permafrost Landscapes. Hosted virtually by ArcticNet.

References

Ahmed, M. I., Elshorbagy, A., and Pietroniro, A. (2020a). A novel model for storage dynamics simulation and inundation mapping in the prairies. *Environmental Modelling & Software*, 133:104850.

Ahmed, M. I., Elshorbagy, A., and Pietroniro, A. (2020b). Toward simple modeling practices in the complex canadian prairie watersheds. *Journal of Hydrologic Engineering*, 25(6):4020024.

Ahmed, M. I., Elshorbagy, A., Pietroniro, A., and Princz, D. (2021). Improving the representation of the non-contributing area dynamics in land surface models for better simulation of prairie hydrology. *Journal of Hydrology*, 600:126562.

Akbarpour, S. (2023). *Using machine learning to understand the hydrologic impacts of permafrost thaw-Driven land cover change*. University of Waterloo.

Akbarpour, S., Chasmer, L., and Craig, J. (in review). Hydrological classification of isolated wetlands in discontinuous permafrost regions using rgb imagery. *Under review in International Journal of Applied Earth Observation and Geoinformation*.

Akbarpour, S. and Craig, J. R. (2022). Simulating thaw-induced land cover change in discontinuous permafrost landscapes. *Remote Sensing Applications: Society and Environment*, 28:100829.

Ali, G., Oswald, C. J., Spence, C., Cammeraat, E. L., Mcguire, K. J., Meixner, T., and Reaney, S. M. (2013). Towards a unified threshold-based hydrological theory: Necessary components and recurring challenges. *Hydrological Processes*, 27(2):313–318.

Almendinger, J. E., Murphy, M. S., and Ulrich, J. S. (2014). Use of the Soil and Water Assessment Tool to Scale Sediment Delivery from Field to Watershed in an Agricultural Landscape with Topographic Depressions. *Journal of Environmental Quality*, 43(1):9–17.

Amado, A. A., Politano, M., Schilling, K., and Weber, L. (2018). Investigating Hydrologic Connectivity of a Drained Prairie Pothole Region Wetland Complex using a Fully Integrated, Physically-Based Model. *Wetlands*, 38(2):233–245.

Ameli, A. A. and Creed, I. F. (2017). Quantifying hydrologic connectivity of wetlands to surface water systems. *Hydrology and Earth System Sciences*, 21(3):1791–1808.

Annand, H. et al. (2022). *The influence of climate change and wetland managment on prairie hydrology-insights from Smith Creek, Saskatchewan*. PhD thesis, University of Saskatchewan.

Arfken, G. B. and Weber, H. J. (1999). Mathematical methods for physicists.

Arnold, J. G. and Fohrer, N. (2005). Swat2000: current capabilities and research opportunities in applied watershed modelling. *Hydrological Processes: An International Journal*, 19(3):563–572.

Arnold, J. G., Srinivasan, R., Muttiah, R. S., and Williams, J. R. (1998). Large area hydrologic modeling and assessment part i: model development 1. *JAWRA Journal of the American Water Resources Association*, 34(1):73–89.

Bartlett, M. S., Parolari, A. J., McDonnell, J. J., and Porporato, A. (2016a). Beyond the SCS-CN method: A theoretical framework for spatially lumped rainfall-runoff response. *Water Resources Research*, 52(6):4608–4627.

Bartlett, M. S., Parolari, A. J., McDonnell, J. J., and Porporato, A. (2016b). Framework for event-based semidistributed modeling that unifies the SCS-CN method, VIC, PDM, and TOPMODEL. *Water Resources Research*, 52(9):7036–7052.

Benjamin, J. R. and Cornell, C. A. (2014). *Probability, statistics, and decision for civil engineers*. Courier Corporation.

Bergström, S. et al. (1995). The hbv model. *Computer models of watershed hydrology.*, pages 443–476.

Beven, K. J. and Kirkby, M. J. (1979). A physically based, variable contributing area model of basin hydrology / Un modèle à base physique de zone d'appel variable de l'hydrologie du bassin versant. *Hydrological Sciences Bulletin*, 24(1):43–69.

Beven, K. J., Kirkby, M. J., Freer, J. E., and Lamb, R. (2021). A history of topmodel. *Hydrology and Earth System Sciences*, 25(2):527–549.

Blöschl, G. and Sivapalan, M. (1995). Scale issues in hydrological modelling: A review. *Hydrological Processes*, 9(3-4):251–290.

Bonnaventure, P. P. and Lamoureux, S. F. (2013). The active layer: A conceptual review of monitoring, modelling techniques and changes in a warming climate. *Progress in Physical Geography*, 37(3):352–376.

Bowling, L. C. and Lettenmaier, D. P. (2010). Modeling the effects of lakes and wetlands on the water balance of arctic environments. *Journal of Hydrometeorology*, 11(2):276–295.

Bracken, L. J. and Croke, J. (2007). The concept of hydrological connectivity and its contribution to understanding runoff-dominated geomorphic systems. *Hydrological Processes: An International Journal*, 21(13):1749–1763.

Bui, M. T., Lu, J., and Nie, L. (2020). A review of hydrological models applied in the permafrost-dominated arctic region. *Geosciences*, 10(10):401.

Bullock, A. and Acreman, M. (2003). The role of wetlands in the hydrological cycle. *Hydrology and Earth System Sciences*, 7(3):358–389.

Chasmer, L., Hopkinson, C., and Quinton, W. (2010). Quantifying errors in discontinuous permafrost plateau change from optical data, Northwest Territories, Canada: 1947–2008. *Canadian Journal of Remote Sensing*, 36(sup2):S211–S223.

Clark, M. P. and Shook, K. R. (2022). The numerical formulation of simple hysteretic models to simulate the large-scale hydrological impacts of prairie depressions. *Water Resources Research*, page e2022WR032694.

Coles, A. E. and McDonnell, J. J. (2018). Fill and spill drives runoff connectivity over frozen ground. *Journal of Hydrology*, 558:115–128.

Connon, R., Devoie, É., Hayashi, M., Veness, T., and Quinton, W. (2018). The influence of shallow taliks on permafrost thaw and active layer dynamics in subarctic canada. *Journal of Geophysical Research: Earth Surface*, 123(2):281–297.

Connon, R., Quinton, W., Craig, J., Hanisch, J., and Sonnentag, O. (2015). The hydrology of interconnected bog complexes in discontinuous permafrost terrains. *Hydrological Processes*, 29(18):3831–3847.

Connon, R., Quinton, W., Craig, J. R., and Hayashi, M. (2014). Changing hydrologic connectivity due to permafrost thaw in the lower liard river valley, nwt, canada. *Hydrological Processes*, 28(14):4163–4178.

Cooper, M. (2010). Advanced Bash-Scripting Guide An in-depth exploration of the art of shell scripting Table of Contents. *Okt 2005 Abrufbar uber httpwww tldp orgLDPabsabs-guide pdf Zugriff 1112 2005*, 2274(November 2008):2267–2274.

Craig, J. (2020). Raven: User's and developer's manual v3. 0. *Computer software manual]. The Raven Development Team.*

Craig, J. R. (2018). Upscaled response of fill-and-spill wetland networks to runoff events. *Personal Communication.*

Craig, J. R., Brown, G., Chlumsky, R., Jenkinson, R. W., Jost, G., Lee, K., Mai, J., Serrer, M., Sgro, N., Shafii, M., Snowdon, A. P., and Tolson, B. A. (2020). Flexible watershed simulation with the Raven hydrological modelling framework. *Environmental Modelling & Software*, 129:104728.

Craig, J. R., Liu, G., and Soulis, E. D. (2010). Runoff-infiltration partitioning using an upscaled Green-Ampt solution. *Hydrological Processes*, 24(16):2328–2334.

Devoie, É. (2021). *The changing influence of permafrost on peatlands hydrology.* University of Waterloo.

Devoie, É. G., Craig, J. R., Dominico, M., Carpino, O., Connon, R. F., Rudy, A. C., and Quinton, W. (2021). Mechanisms of discontinuous permafrost thaw in peatlands. *Journal of Geophysical Research: Earth Surface*, 126(11):e2021JF006204.

ECCC (2017). Canadian climate normals 1981–2010 station data (Fort Simpson A) [Data file]. Retrieved from http://climate.weather.gc.ca/climate_normals/, accessed 2022-02-01.

ECCC (2020). Meteorological Data for Fort Simpson. Retrieved from https://climate.weather.gc.ca/climate_data/daily_data_e.html?StationID=52780, accessed 2020-10-10.

Evenson, G. R., Golden, H. E., Lane, C. R., and D'Amico, E. (2015). Geographically isolated wetlands and watershed hydrology: A modified model analysis. *Journal of Hydrology*, 529(P1):240–256.

Evenson, G. R., Golden, H. E., Lane, C. R., and D'Amico, E. (2016). An improved representation of geographically isolated wetlands in a watershed-scale hydrologic model. *Hydrological Processes*, 30(22):4168–4184.

Evenson, G. R., Jones, C. N., McLaughlin, D. L., Golden, H. E., Lane, C. R., DeVries, B., Alexander, L. C., Lang, M. W., McCarty, G. W., and Sharifi, A. (2018). A watershed-scale model for depressional wetland-rich landscapes. *Journal of Hydrology X*, 1:100002.

Fang, X., Pomeroy, J., Westbrook, C., Guo, X., Minke, A., and Brown, T. (2010). Prediction of snowmelt derived streamflow in a wetland dominated prairie basin. *Hydrology and Earth System Sciences*, 14(6):991–1006.

Fang, X. and Pomeroy, J. W. (2007). Snowmelt runoff sensitivity analysis to drought on the canadian prairies. *Hydrological Processes: An International Journal*, 21(19):2594–2609.

Fang, X. and Pomeroy, J. W. (2008). Drought impacts on Canadian prairie wetland snow hydrology. *Hydrological Processes: An International Journal*, 22(15):2858–2873.

Gasset, N., Fortin, V., Dimitrijevic, M., Carrera, M., Bilodeau, B., Muncaster, R., Gaborit, É., Roy, G., Pentcheva, N., Bulat, M., and Others (2021). A 10 km North American precipitation and land-surface reanalysis based on the GEM atmospheric model. *Hydrology and Earth System Sciences*, 25(9):4917–4945.

Gharari, S. and Razavi, S. (2018). A review and synthesis of hysteresis in hydrology and hydrological modeling: Memory, path-dependency, or missing physics? *Journal of hydrology*, 566:500–519.

Gibson, C., Cottenie, K., Gingras-Hill, T., Kokelj, S., Baltzer, J., Chasmer, L., and Turetsky, M. (2021). Mapping and understanding the vulnerability of northern peatlands to permafrost thaw at scales relevant to community adaptation planning. *Environmental Research Letters*, 16(5):055022.

Golden, H. E., Creed, I. F., Ali, G., Basu, N. B., Neff, B. P., Rains, M. C., McLaughlin, D. L., Alexander, L. C., Ameli, A. A., Christensen, J. R., Evenson, G. R., Jones, C. N., Lane, C. R., and Lang, M. (2017). Integrating geographically isolated wetlands into land management decisions. *Frontiers in Ecology and the Environment*, 15(6):319–327.

Goudarzi, S., Milledge, D., and Holden, J. (2023). A generalized multistep dynamic (gmd) topmodel. *Water Resources Research*, 59(1):e2022WR032198.

Gupta, H. V., Kling, H., Yilmaz, K. K., and Martinez, G. F. (2009). Decomposition of the mean squared error and NSE performance criteria: Implications for improving hydrological modelling. *Journal of hydrology*, 377(1-2):80–91.

Hayashi, M., Quinton, W., Pietroniro, A., and Gibson, J. J. (2004). Hydrologic functions of wetlands in a discontinuous permafrost basin indicated by isotopic and chemical signatures. *Journal of Hydrology*, 296(1-4):81–97.

Hayashi, M., van der Kamp, G., and Rosenberry, D. O. (2016). Hydrology of prairie wetlands: understanding the integrated surface-water and groundwater processes. *Wetlands*, 36(2):237–254.

Hayashi, M., Van Der Kamp, G., and Rudolph, D. L. (1998). Water and solute transfer between a prairie wetland and adjacent uplands, 1. water balance. *Journal of Hydrology*, 207(1-2):42–55.

Hayashi, M., van der Kamp, G., and Schmidt, R. (2003). Focused infiltration of snowmelt water in partially frozen soil under small depressions. *Journal of Hydrology*, 270(3-4):214–229.

Haynes, K., Connon, R., and Quinton, W. (2018). Permafrost thaw induced drying of wetlands at scotty creek, nwt, canada. *Environmental Research Letters*, 13(11):114001.

IPCC (2014). Intergovernmental panel on climate change. *Climate Change*.

Jayawardena, A. W. and Zhou, M. C. (2000). A modified spatial soil moisture storage capacity distribution curve for the Xinanjiang model. *Journal of Hydrology*, 227(1-4):93–113.

Knoben, W. J., Freer, J. E., and Woods, R. A. (2019). Inherent benchmark or not? comparing nash–sutcliffe and kling–gupta efficiency scores. *Hydrology and Earth System Sciences*, 23(10):4323–4331.

Lakku, N. K. and Behera, M. R. (2022). Skill and inter-model comparison of regional and global climate models in simulating wind speed over south asian domain. *Climate*, 10(6):85.

Lee, S., Yeo, I. Y., Lang, M. W., Sadeghi, A. M., McCarty, G. W., Moglen, G. E., and Evenson, G. R. (2018). Assessing the cumulative impacts of geographically isolated wetlands on watershed hydrology using the SWAT model coupled with improved wetland modules. *Journal of Environmental Management*, 223(June):37–48.

Leibowitz, S. G. (2003). Isolated wetlands and their functions: an ecological perspective. *Wetlands*, 23(3):517–531.

Leibowitz, S. G., Mushet, D. M., and Newton, W. E. (2016). Intermittent Surface Water Connectivity: Fill and Spill Vs. Fill and Merge Dynamics. *Wetlands*, 36:323–342.

Leibowitz, S. G. and Vining, K. C. (2003). Temporal connectivity in a prairie pothole complex. *Wetlands*, 23(1):13–25.

Liang, X., Lettenmaier, D. P., Wood, E. F., and Burges, S. J. (1994). A simple hydrologically based model of land surface water and energy fluxes for general circulation models. *Journal of Geophysical Research*, 99(D7).

Liu, G. and Schwartz, F. W. (2011). An integrated observational and model-based analysis of the hydrologic response of prairie pothole systems to variability in climate. *Water Resources Research*, 47(2):1–15.

Liu, Y., Yang, W., and Wang, X. (2008). Development of a swat extension module to simulate riparian wetland hydrologic processes at a watershed scale. *Hydrological Processes: An International Journal*, 22(16):2901–2915.

Mack, M., Connon, R., Makarieva, O., McLaughlin, J., Nesterova, N., and Quinton, W. (2021). Heterogenous runoff trends in peatland-dominated basins throughout the circumpolar north. *Environmental Research Communications*, 3(7):075006.

Mai, J., Kornelsen, K. C., Tolson, B. A., Fortin, V., Gasset, N., Bouhemhem, D., Schäfer, D., Leahy, M., Anctil, F., and Coulibaly, P. (2020). The Canadian surface prediction archive (CaSPAr): A platform to enhance environmental modeling in Canada and globally. *Bulletin of the American Meteorological Society*, 101(3):E341—-E356.

Mai, J., Shen, H., Tolson, B. A., Gaborit, É., Arsenault, R., Craig, J. R., Fortin, V., Fry, L. M., Gauch, M., Klotz, D., Kratzert, F., O'Brien, N., Princz, D. G., Rasiya Koya, S., Roy, T., Seglenieks, F., Shrestha, N. K., Temgoua, A. G. T., Vionnet, V., and Waddell, J. W. (2022). The Great Lakes Runoff Intercomparison Project Phase 4: The Great Lakes (GRIP-GL). *Hydrology and Earth System Sciences Discussions*, 2022:1–54.

Matott, L. S. (2017). OSTRICH: an Optimization Software Tool, Documentation and User's Guide, Version 17.10. 18. University at Buffalo. *Center for Computational Research, Buffalo, NY*.

McColl, C. and Aggett, G. (2007). Land-use forecasting and hydrologic model integration for improved land-use decision support. *Journal of environmental management*, 84(4):494–512.

McDonnell, J. (2009). Where does water go when it rains? conceptualizing runoff processes in headwater catchments (john dalton medal lecture). In *EGU General Assembly Conference Abstracts*, page 14071.

McDonnell, J. J., Spence, C., Karran, D. J., van Meerveld, H. J., and Harman, C. J. (2021). Fill-and-Spill: A Process Description of Runoff Generation at the Scale of the Beholder. *Water Resources Research*, 57(5).

McLaughlin, D. L., Diamond, J. S., Quintero, C., Heffernan, J., and Cohen, M. J. (2019). Wetland Connectivity Thresholds and Flow Dynamics From Stage Measurements. *Water Resources Research*, 55(7):6018–6032.

Mekonnen, B. A., Mazurek, K. A., and Putz, G. (2016). Incorporating landscape depression heterogeneity into the Soil and Water Assessment Tool (SWAT) using a probability distribution. *Hydrological Processes*, 30(13):2373–2389.

Mekonnen, B. A., Nazemi, A., Mazurek, K. A., Elshorbagy, A., and Putz, G. (2015). Hybrid modelling approach to prairie hydrology: fusing data-driven and process-based hydrological models. *Hydrological sciences journal*, 60(9):1473–1489.

Mekonnen, M. A., Wheater, H. S., Ireson, A. M., Spence, C., Davison, B., and Pietroniro, A. (2014). Towards an improved land surface scheme for prairie landscapes. *Journal of Hydrology*.

Mengistu, S. G. and Spence, C. (2016). Testing the ability of a semidistributed hydrological model to simulate contributing area. *Water Resources Research*, 52(6):4399–4415.

Moore, R. J. (1985). The probability-distributed principle and runoff production at point and basin scales. *Hydrological Sciences Journal*, 30(2):273–297.

Moore, R. J. (2007). The PDM rainfall-runoff model. *Hydrology and Earth System Sciences*, 11(1):483–499.

Moriasi, D. N., Arnold, J. G., Van Liew, M. W., Bingner, R. L., Harmel, R. D., and Veith, T. L. (2007). Model evaluation guidelines for systematic quantification of accuracy in watershed simulations. *Transactions of the ASABE*, 50(3):885–900.

Morse, P., Wolfe, S., Kokelj, S., and Gaanderse, A. (2016). The occurrence and thermal disequilibrium state of permafrost in forest ecotopes of the great slave region, northwest territories, canada. *Permafrost and Periglacial Processes*, 27(2):145–162.

Motovilov, Y. G. (2013). Ecomag: A distributed model of runoff formation and pollution transformation in river basins. *IAHS Publ*, 361:227–234.

Muhammad, A., Evenson, G. R., Stadnyk, T. A., Boluwade, A., Jha, S. K., and Coulibaly, P. (2019). Impact of model structure on the accuracy of hydrological modeling of a canadian prairie watershed. *Journal of Hydrology: Regional Studies*, 21:40–56.

Muhammad, A., Evenson, G. R., Unduche, F., and Stadnyk, T. A. (2020). Climate change impacts on reservoir inflow in the Prairie Pothole Region: Awatershed model analysis. *Water (Switzerland)*, 12(1):1–18.

Nash, J. E. and Sutcliffe, J. V. (1970). River flow forecasting through conceptual models part I—A discussion of principles. *Journal of hydrology*, 10(3):282–290.

Nelder, J. A. and Mead, R. (1965). A simplex method for function minimization. *The computer journal*, 7(4):308–313.

NRC (1995). Permafrost in Canada. Retrieved from http://geogratis.gc.ca/api/en/nrcan-rncan/ess-sst/d1e2048b-ccff-5852-aaa5-b861bd55c367, accessed 2023-01-01.

NRC (2022). Geospatial Data Extraction. Retrieved from https://maps.canada.ca/czs/index-en.html, accessed 2022-03-20.

Oudin, L., Hervieu, F., Michel, C., Perrin, C., Andréassian, V., Anctil, F., and Loumagne, C. (2005). Which potential evapotranspiration input for a lumped rainfall–runoff model?: Part 2—towards a simple and efficient potential evapotranspiration model for rainfall–runoff modelling. *Journal of hydrology*, 303(1-4):290–306.

Pacific Climate (2022). Canadian Downscaled Climate Scenarios - Univariate (CMIP5) [Data file]. Retrieved from https://data.pacificclimate.org/portal/downscaled_gcms/map/, accessed 2022-12-01.

Papoulis, A. (1965). *Random Variables and Stochastic Processes*. McGraw-Hill, Inc.

Papoulis, A. and Pillai, S. U. (2002). *Probability, random variables, and stochastic processes*. Tata McGraw-Hill Education.

Payette, S., Delwaide, A., Caccianiga, M., and Beauchemin, M. (2004). Accelerated thawing of subarctic peatland permafrost over the last 50 years. *Geophysical Research Letters*, 31(18):1–4.

Perrin, C., Michel, C., and Andréassian, V. (2003). Improvement of a parsimonious model for streamflow simulation. *Journal of hydrology*, 279(1-4):275–289.

Phillips, R. W., Spence, C., and Pomeroy, J. W. (2011). Connectivity and runoff dynamics in heterogeneous basins. *Hydrological Processes*, 25(19):3061–3075.

Pomeroy, J., Brown, T., Fang, X., Shook, K., Pradhananga, D., Armstrong, R., Harder, P., Marsh, C., Costa, D., Krogh, S., et al. (2022). The cold regions hydrological modelling platform for hydrological diagnosis and prediction based on process understanding. *Journal of Hydrology*, 615:128711.

Pomeroy, J., Fang, X., Shook, K., Westbrook, C., and Brown, T. (2012). Informing the vermilion river watershed plan through application of the cold regions hydrological model platform. Technical report, Centre for Hydrology Report.

Pomeroy, J., Fang, X., Westbrook, C., Minke, A., Guo, X., and Brown, T. (2009). Prairie hydrological model study final report, december 2009. Technical report, Citeseer.

Pomeroy, J., Gray, D., Brown, T., Hedstrom, N., Quinton, W., Granger, R., and Carey, S. (2007). The cold regions hydrological model: a platform for basing process representation and model structure on physical evidence. *Hydrological Processes: An International Journal*, 21(19):2650–2667.

Pomeroy, J. W., Shook, K., Fang, X., Dumanski, S., Westbrook, C., and Brown, T. (2014). *Improving and testing the prairie hydrological model at Smith Creek Research Basin*. Centre for Hydrology, University of Saskatchewan Saskatoon, TX, USA.

Quinton, W., Berg, A., Braverman, M., Carpino, O., Chasmer, L., Connon, R., Craig, J., Devoie, É., Hayashi, M., Haynes, K., et al. (2019). A synthesis of three decades of hydrological research at scotty creek, nwt, canada. *Hydrology and Earth System Sciences*, 23(4):2015–2039.

Quinton, W., Hayashi, M., and Chasmer, L. (2011). Permafrost-thaw-induced land-cover change in the canadian subarctic: implications for water resources. *Hydrological Processes*, 25(1):152–158.

Quinton, W. L. and Baltzer, J. (2013). The active-layer hydrology of a peat plateau with thawing permafrost (scotty creek, canada). *Hydrogeology Journal*, 21(1):201.

Quinton, W. L., Hayashi, M., and Pietroniro, A. (2003). Connectivity and storage functions of channel fens and flat bogs in northern basins. *Hydrological Processes*, 17(18):3665–3684.

Rains, M. C., Leibowitz, S. G., Cohen, M. J., Creed, I. F., Golden, H. E., Jawitz, J. W., Kalla, P., Lane, C. R., Lang, M. W., and Mclaughlin, D. L. (2016). Geographically isolated wetlands are part of the hydrological landscape. *Hydrological Processes*, 30(1):153–160.

Sahoo, B. (2005). the Xinanjiang Model and Its Derivatives for Modeling Soil Moisture Variability in the Land- Surface Schemes of the Climate Change Models : an Overview. *Proceedings of the International Conference on Hydrological Perspectives for Sustainable Development*, 1(April).

Schramm, I., Boike, J., Bolton, W. R., and Hinzman, L. D. (2007). Application of topoflow, a spatially distributed hydrological model, to the imnavait creek watershed, alaska. *Journal of Geophysical Research: Biogeosciences*, 112(G4).

Schuur, E. A. G., Bockheim, J., Canadell, J. G., Euskirchen, E., Field, C. B., Goryachkin, S. V., Hagemann, S., Kuhry, P., Lafleur, P. M., Lee, H., Mazhitova, G., Nelson, F. E., Rinke, A., Romanovsky, V. E., Shiklomanov, N., Tarnocai, C., Venevsky, S., Vogel, J. G., and Zimov, S. A. (2008). Vulnerability of Permafrost Carbon to Climate Change: Implications for the Global Carbon Cycle. *BioScience*, 58(8):701–714.

Seibert, J. (2005). Hbv light version 2, user's manual. *Department of Earth Sciences, Uppsala University, Uppsala*.

Shapiro, M. and Westervelt, J. (1992). R.MAPCALC: An Algebra for GIS and Image Processing. *Army Crops of Engineers, Construction Engineering Research Laboratories*.

Shaw, D. A., Pietroniro, A., and Martz, L. W. (2013a). Topographic analysis for the prairie pothole region of Western Canada. *Hydrological Processes*, 27(22):3105–3114.

Shaw, D. A., Pietroniro, A., and Martz, L. W. (2013b). Topographic analysis for the prairie pothole region of Western Canada. *Hydrological Processes*, 27(22):3105–3114.

Shaw, D. A., Vanderkamp, G., Conly, F. M., Pietroniro, A., and Martz, L. (2012). The fill–spill hydrology of prairie wetland complexes during drought and deluge. *Hydrological Processes*, 26(20):3147–3156.

Shook, K., Papalexiou, S., and Pomeroy, J. W. (2021a). Quantifying the effects of Prairie depressional storage complexes on drainage basin connectivity. *Journal of Hydrology*, 593:125846.

Shook, K. and Pomeroy, J. W. (2011). Memory effects of depressional storage in Northern Prairie hydrology. *Hydrological Processes*, 25(25):3890–3898.

Shook, K., Pomeroy, J. W., Spence, C., and Boychuk, L. (2013). Storage dynamics simulations in prairie wetland hydrology models: Evaluation and parameterization. *Hydrological Processes*, 27(13):1875–1889.

Shook, K., Spiteri, R. J., Pomeroy, J. W., Liu, T., and Sharomi, O. (2021b). Wdpm: the wetland dem ponding model. *Journal of Open Source Software*, 6(64):2276.

Shur, Y. L. and Jorgenson, M. T. (2007). Patterns of permafrost formation and degradation in relation to climate and ecosystems. *Permafrost and Periglacial Processes*, 18(1):7–19.

Sivapalan, M., Beven, K., and Wood, E. F. (1987). On hydrologic similarity: 2. a scaled model of storm runoff production. *Water Resources Research*, 23(12):2266–2278.

Sivapalan, M., Woods, R. A., and Kalma, J. D. (1997). Variable bucket representation of topmodel and investigation of the effects of rainfall heterogeneity. *Hydrological processes*, 11(9):1307–1330.

Smith, S. L., Burgess, M. M., Riseborough, D., and Nixon, F. M. (2005). Recent trends from Canadian permafrost thermal monitoring network sites. *Permafrost and Periglacial Processes*, 16(1):19–30.

Spence, C. (2007). On the relation between dynamic storage and runoff: A discussion on thresholds, efficiency, and function. *Water Resources Research*, 43(12):1–11.

Spence, C. (2010). A paradigm shift in hydrology: Storage thresholds across scales influence catchment Runoff Generation. *Geography Compass*, 4(7):819–833.

Spence, C., Guan, X. J., Phillips, R., Hedstrom, N., Granger, R., and Reid, B. (2010). Storage dynamics and streamflow in a catchment with a variable contributing area. *Hydrological Processes*, 24(16):2209–2221.

Spence, C., He, Z., Shook, K., Pomeroy, J., Whitfield, C., and Wolfe, J. (2022). Assessing runoff sensitivity of north american prairie pothole region basins to wetland drainage using a basin classification–based virtual modeling approach. *Hydrology and Earth System Sciences Discussions*, pages 1–43.

Spence, C. and Woo, M. K. (2003). Hydrology of subarctic Canadian shield: Soil-filled valleys. *Journal of Hydrology*, 279(1-4):151–166.

Spence, C. and Woo, M.-k. (2006). Hydrology of subarctic Canadian Shield: heterogeneous headwater basins. *Journal of Hydrology*, 317(1-2):138–154.

St. Jacques, J.-M. and Sauchyn, D. J. (2009). Increasing winter baseflow and mean annual streamflow from possible permafrost thawing in the northwest territories, canada. *Geophysical Research Letters*, 36(1).

Stadnyk, T., Amour, N. S., Kouwen, N., Edwards, T., Pietroniro, A., and Gibson, J. (2005). A groundwater separation study in boreal wetland terrain: The watflood hydrological model compared with stable isotope tracers. *Isotopes in Environ Health Studies*, 41(1):49–68.

Stone, L. E., Fang, X., Haynes, K. M., Helbig, M., Pomeroy, J. W., Sonnentag, O., and Quinton, W. (2019). Modelling the effects of permafrost loss on discharge from a wetland-dominated, discontinuous permafrost basin. *Hydrological Processes*, 33(20):2607–2626.

SugaWara, M. (1979). Automatic calibration of the tank model. *Hydrological Sciences Journal*, 24(3):375–388.

Taheri, M., Ranjram, M., and Craig, J. (2023). An upscaled model of fill-and-spill hydrological response. *Under review in Water Resources Research*.

Taylor, K. E., Stouffer, R. J., and Meehl, G. A. (2012). An overview of cmip5 and the experiment design. *Bulletin of the American meteorological Society*, 93(4):485–498.

Tedesco, M. (2015). Remote sensing and the cryosphere. *Remote Sensing of the Cryosphere*, pages 1–16.

Todini, E. (1996). The ARNO rainfall-runoff model. *Journal of Hydrology*, 175(1-4):339–382.

Tolson, B. A. and Shoemaker, C. A. (2007). Dynamically dimensioned search algorithm for computationally efficient watershed model calibration. *Water Resources Research*, 43(1).

Tromp-van Meerveld, H. J. and McDonnell, J. J. (2006). Threshold relations in subsurface stormflow: 2. The fill and spill hypothesis. *Water Resources Research*, 42(2).

van der Kamp, G. and Hayashi, M. (1998). The groundwater recharge function of small wetlands in the semi-arid northern prairies. *Great Plains Research*, pages 39–56.

Van der Kamp, G., Hayashi, M., and Gallen, D. (2003). Comparing the hydrology of grassed and cultivated catchments in the semi-arid canadian prairies. *Hydrological Processes*, 17(3):559–575.

Walvoord, M. A. and Kurylyk, B. L. (2016). Hydrologic impacts of thawing permafrost—a review. *Vadose Zone Journal*, 15(6).

Wang, D. (2018). A new probability density function for spatial distribution of soil water storage capacity leads to the SCS curve number method. *Hydrology and Earth System Sciences*, 22(12):6567–6578.

Wang, X., Yang, W., and Melesse, A. M. (2008). Using hydrologic equivalent wetland concept within SWAT to estimate streamflow in watersheds with numerous wetlands. *Transactions of the ASABE*, 51(1):55–72.

Watson, B. M., McKeown, R. A., Putz, G., and MacDonald, J. D. (2008). Modification of swat for modelling streamflow from forested watersheds on the canadian boreal plain. *Journal of Environmental Engineering and Science*, 7(S1):145–159.

Woo, M.-k. (2012). *Permafrost hydrology*. Springer Science & Business Media.

Woo, M.-K. and Marsh, P. (2005). Snow, frozen soils and permafrost hydrology in canada, 1999–2002. *Hydrological Processes: An International Journal*, 19(1):215–229.

Woo, M.-K. and Rowsell, R. D. (1993). Hydrology of a prairie slough. *Journal of Hydrology*, 146:175–207.

Wood, B. D. (2009). The role of scaling laws in upscaling. *Advances in Water Resources*, 32(5):723–736.

Wood, E. F., Lettenmaier, D. P., and Zartarian, V. G. (1992). A land-surface hydrology parameterization with subgrid variability for general circulation models. *Journal of Geophysical Research*, 97(D3):2717–2728.

Wright, N., Hayashi, M., and Quinton, W. (2009). Spatial and temporal variations in active layer thawing and their implication on runoff generation in peat-covered permafrost terrain. *Water Resources Research*, 45(5).

Wright, S. N., Thompson, L. M., Olefeldt, D., Connon, R. F., Carpino, O. A., Beel, C. R., and Quinton, W. (2022). Thaw-induced impacts on land and water in discontinuous permafrost: A review of the taiga plains and taiga shield, northwestern canada. *Earth-Science Reviews*, 232:104104.

WSC (2020). Hydrometric Data for Mackenzie River at Fort Simpson. Retrieved from https://wateroffice.ec.gc.ca/report/real_time_e.html?stn=10GC001, accessed 2020-10-10.

WSC (2022a). Historical Hydrometric Data Extracted from the Environment and Climate Change Canada Historical Hydrometric Data Website. Retrieved from https://wateroffice.ec.gc.ca/mainmenu/historical/data/index/e.html, accessed2022-02-01.

WSC (2022b). Watershed Drainage Areas. Retrieved from https://collaboration.cmc.ec.gc.ca/cmc/hydrometrics/www/HydrometricNetworkBasinPolygons/, accessed 2022-10-06.

Yalew, S., Pilz, T., Schweitzer, C., Liersch, S., van der Kwast, J., Van Griensven, A., Mul, M. L., Dickens, C., and van der Zaag, P. (2018). Coupling land-use change and hydrologic models for quantification of catchment ecosystem services. *Environmental Modelling & Software*, 109:315–328.

Yang, W., Wang, X., Liu, Y., Gabor, S., Boychuk, L., and Badiou, P. (2010). Simulated environmental effects of wetland restoration scenarios in a typical canadian prairie watershed. *Wetlands Ecology and Management*, 18(3):269–279.

Yuemei, H., Xiaoqin, Z., Jianguo, S., and Jina, N. (2008). Conduction between left superior pulmonary vein and left atria and atria fibrillation under cervical vagal trunk stimulation. *Colombia Medica*, 39(3):227–234.

Zehe, E., Becker, R., Bárdossy, A., and Plate, E. (2005). Uncertainty of simulated catchment runoff response in the presence of threshold processes: Role of initial soil moisture and precipitation. *Journal of hydrology*, 315(1-4):183–202.

Zeng, L., Shao, J., and Chu, X. (2020). Improved hydrologic modeling for depression-dominated areas. *Journal of Hydrology*, 590(May):125269.

Zhang, Y., Olthof, I., Fraser, R., and Wolfe, S. A. (2014). A new approach to mapping permafrost and change incorporating uncertainties in ground conditions and climate projections. *The Cryosphere*, 8(6):2177–2194.

Zhao, R.-J. (1980). The xinanjiang model. In *Proceedings of the Oxford Symposium*.

Zulkafli, Z., Yusuf, B., and Nurhidayu, S. (2021). Assessment of streamflow simulation for a tropical forested catchment using dynamic topmodel—dynamic fluxes and connectivity

for predictions of hydrology (decipher) framework and generalized likelihood uncertainty estimation (glue). *Water*, 13(3):317.

APPENDICES

Appendix A

Detailed analytical solution

A.1 Outflow distribution of cascade depth of one

Considering an Exponential distribution of initial deficit and concentrating factor (Equations 3.9 and 3.10) and substituting them into Equation 3.4, we can calculate the resultant distribution of $O^* = \beta R + P' - D$ via integration as,

$$f_{O^*}(O^*) = \begin{cases} \frac{ad}{a+d}(1-P_f)e^{d(O^*-P^*)} & \text{for } O^* < P^* \\ (\frac{ad}{a+d}(1-P_f) + aP_f)e^{-a(O^*-P^*)} & \text{for } O^* \geq P^* \end{cases} \tag{A.1}$$

where P^* is defined as $\beta_{min}R + P' - D_{min}$. The final outflow distribution may therefore be obtained by taking the maximum of O^* and zero, leading to,

$$f_{O_1}(O_1) = \delta(O_1)\int_{-\infty}^{0} f_{O_1^*}(x)dx + H(O_1)f_{O_1^*}(O_1) \tag{A.2}$$

The integral in Equation A.2 is defined as P_1, and represents the probability of zero outflow from wetlands (with cascade depths of one wetland) as follows,

$$P_1 = \int_{-\infty}^{0} f_{O^*}(x)dx = \begin{cases} \frac{a}{a+d}(1-P_f)e^{-d(P^*)} & \text{for } P^* > 0 \\ \frac{a}{a+d} + \frac{d}{a+d}\left(1-e^{aP^*}\right) & \text{for } P^* \leq 0 \end{cases} \tag{A.3}$$

P_1 also represents the probability of non-contributing area. Therefore, the fractional contributing area may be expressed as,

$$A_1 = 1 - P_1 \tag{A.4}$$

A.2 Outflow distribution of cascade depth of two

Here the outflow distribution of cascades with two wetlands is calculated considering,

$$O_2^* = \beta_2 R + P' - D_2 + O_1 \tag{A.5}$$

We will introduce a new term $\gamma_2 = \beta_2 R + P' - D_2$. We have already calculated the resultant distribution of this for single wetland cascades (where $\gamma_1 = O_1^*$). Then, for cascade depth of two, distribution of potential outflow can be found from solving the integral in Equation 3.6 where $n = 2$ as (for $P^* > 0$),

$$f_{O_2^*}(O_2^*) = P_1 \cdot f_{O_1^*}(O_2^*) + (1 - P_f)\left(\frac{ad}{a+d}\right)^2 \begin{cases} A_1 & \text{for } O_2^* < P^* \\ A_2 & \text{for } P^* \leq O_2^* < 2P^* \\ A_3 & \text{for } 2P^* \leq O_2^* \end{cases} \tag{A.6}$$

where

$$A_1 = e^{d(O_2^* - 2P^*)}[(1 - P_f)(P^* + \frac{1}{a+d}) + \frac{P_f}{d}] \tag{A.7}$$

$$A_2 = e^{d(O_2^* - 2P^*)}[\frac{2P_f}{d} + (2P^* - O_2^* + \frac{2}{a+d})(1 - P_f)] - \frac{(aP_f + d)}{d(a+d)} e^{(a-d)P^* - aO_2^*} \tag{A.8}$$

$$A_3 = P_f[((O_2^* - 2P^*)(\frac{a+d}{d})^2(\frac{P_f}{1-P_f} + \frac{2d}{a+d}) + \frac{2}{d})e^{a(2P^* - O_2^*)} - \frac{e^{a(P^* - O_2^*) - dP^*}}{d}] \tag{A.9}$$

For $P^* < 0$, we obtain the following expression:

$$f_{O_2^*}(O_2^*) = P_1 \cdot f_{O_1^*}(O_2^*) + \left(\frac{ad}{a+d}\right)^2 \begin{cases} [\frac{e^{(a+d)P^*}}{a+d}]e^{d(O_2^* - 2P^*)} & \text{for } O_2^* < P^* \\ [O_2^* - P^* + \frac{1}{a+d}]e^{-a(O_2^* - 2P^*)} & \text{for } O_2^* \geq P^* \end{cases} \tag{A.10}$$

and the final outflow distribution may be calculated as,

$$f_{O_2}(O_2) = \delta(O_2) \int_{-\infty}^{0} f_{O_2^*}(x)dx + H(O_2) f_{O_2^*}(O_2) \tag{A.11}$$

The integral in A.11, the probability of zero outflow from the second wetland in a cascade, can be calculated as,

$$P_2 = \int_{-\infty}^{0} f_{O_2^*}(x)dx = \begin{cases} (\frac{ad}{a+d})^2 \frac{1-P_f}{d} e^{-2dP^*} [\frac{P_f}{d} + (1-P_f)(\frac{1}{d} + \frac{1}{a+d} + P^*)] & \text{for } P^* > 0 \\ 1 - e^{aP^*} \frac{d(a+d)^2 + ad^2 e^{aP^*}(1-dP^s - aP^*)}{(a+d)^3} & \text{for } P^* \leq 0 \end{cases} \tag{A.12}$$

The average outflow from second wetland in a cascade may be found as,

$$\bar{O}_2 = P_1 \bar{O}_1 + \begin{cases} (\frac{ad}{a+d})^2 [(P^* + \frac{1}{a+d}) \frac{e^{-2dP^*}(e^{dP^*}(dP^*-1)+1)}{d^2} \\ + \frac{-(d^2 P^*((a+d)P^*+2) - 2(2d+a))e^{-dP^*} + 2dP^*(3d+a) - 2(2d+a)}{d^3(a+d)} \\ + \frac{2aP^*(d+3a) + 2(d+2a) - ae^{-dP^*}(aP^*+1)}{(a+d)a^3}] \\ + (1-P_f)P_f [\frac{2a^2(2dP^*-1) - e^{-dP^*}(d(aP^*(d+2a)+d) - 2a^2)}{d(a+d)^2} \\ + \frac{2(aP^*+1)}{a}(\frac{2d}{(a+d)^2} + \frac{P_f}{1-P_f}) + \frac{2d(2aP^*+1)}{(a+d)^2}] & \text{for } P^* > 0 \\ \\ \frac{e^{2aP^*}}{a^3}\left(\frac{a}{a+d} + 2 - aP^*\right) & \text{for } P^* \leq 0 \end{cases} \tag{A.13}$$

Note that the average outflow of Equation A.13 should be multiplied by the correction factor of $\frac{1}{2(\bar{\beta}+1)}$, to be normalized by the catchment area.

A.3 Outflow distribution of cascade depth of three

Here the outflow distribution of cascades with three wetlands is calculated considering,

$$O_3^* = \beta_3 R + P' - D_3 + O_1 + O_2 \tag{A.14}$$

We will introduce a new term $\gamma_3 = \beta_3 R + P' - D_3$. We have already calculated the resultant distribution of this for single wetland cascades (where $\gamma_1 = O_1^*$). Then, for

cascade depth of three, distribution of potential outflow can be found from solving the integral in Equation 3.6 where $n = 3$ as (for $P^* > 0$),

$$f_{O_3^*}(O_3^*) = P_2 \cdot f_{O_1^*}(O_3^*) + (\frac{ad}{a+d})^3 \begin{cases} B_1 & \text{for } O_3^* < P^* \\ B_2 & \text{for } O_2^* \leq P^* \leq 2O_2^* \\ B_3 & \text{for } 2O_2^* \leq P^* \leq 3O_2^* \\ B_4 & \text{for } 3O_2^* \leq P^* \end{cases} \tag{A.15}$$

where

$$B_1 = e^{d(O-3P^*)}[\frac{1}{a+d}(\frac{1}{d} + \frac{2}{a+d} + 3P^*) + \frac{1+2P^*}{2}] \tag{A.16}$$

$$\begin{aligned} B_2 = e^{d(O-3P^*)}[(\frac{1}{d} + P^* + \frac{1}{a+d})((\frac{1}{a+d} + 2P^* - O)e^{(a+d)(P^*-O)} + O - 2P^*) \\ + \frac{(1-e^{2aP^*})(e^{-(a+d)P^*}-1)+1}{d(a+d)} + \frac{P^*}{2} + \frac{2P^*}{a+d} + \frac{2}{(a+d)^2}] \end{aligned} \tag{A.17}$$

$$\begin{aligned} B_3 = e^{d(O-3P^*)}[e^{(a+d)(P^*-O)}(e^{(a+d)} + P^* + \frac{1}{d}) + \frac{1}{d(a+d)^2}(2d(2 + P^*(a+d)(2 + P^*(a+d)) \\ + \frac{a+d}{d}e^{-(a+d)P^*}) + (-3d + (O-3P^*)(a+c))e^{-(a+d)+2(a+c)P^*})] \end{aligned} \tag{A.18}$$

$$\begin{aligned} B_4 = \frac{1}{d(a+d)^2}(3de^{a(O-3P^*)} + e^{(2P^*-O)a-dP^*}(3aP^*(a+d) - d) - e^{(a-2d)P^*-aO}((1+ \\ 3P^*)(a+d) + d)) + \frac{1}{d(a+d)}(-a(O+P^*)e^{a(O-2P^*)-dP^*} + de^{-a(O-3P^*)}(2dP^{*2} - \\ \frac{3}{a+d} + (O-P^*)(\frac{5P^*-O}{2}d - 3 + \frac{3P^*-O}{2}a))) \end{aligned} \tag{A.19}$$

For $P^* < 0$, we obtain the following expression:

$$f_{O_3^*}(O_3^*) = P_2 \cdot f_{O_1^*}(O_3^*) + \left(\frac{ad}{a+d}\right)^3 \begin{cases} e^{aP^*+d(O-P^*)}\left(\frac{a+d}{ad} - \frac{e^{aP^*}}{a} + \frac{2-(a+d)P^*}{(a+d)^2}e^{aP^*}\right) \\ \qquad\qquad \text{for } O_3^* < P^* \\ e^{a(2P^*-O)}\left[e^{aP}((2P^*-O)(O-P^*) + \frac{2-P^*(a+d)}{(a+d)^2}) + \right. \\ \left.\left(\frac{1}{ad} - \frac{e^{aP^*}}{a(a+d)} + (O-P^*)\left(\frac{1}{d} + \frac{1-e^{aP^*}}{a}\right)\right)\right] \\ \qquad\qquad \text{for } O_3^* \geq P^* \end{cases} \tag{A.20}$$

and the final outflow distribution may be calculated as,

$$f_{O_3}(O_3) = \delta(O_3)\int_{-\infty}^{0} f_{O_3^*}(x)dx + H(O_3)f_{O_3^*}(O_3) \tag{A.21}$$

The integral in A.21, the probability of zero outflow from the third wetland in a cascade, can be calculated as,

$$P_3 = \int_{-\infty}^{0} f_{O_3^*}(x)dx = \left(\frac{ad}{a+d}\right)^3 \begin{cases} e^{-3dP^*}\left[\frac{3P^{*2}}{2d} + \frac{P^*(a^2+5a+4d)}{d(a+d)^2} + \frac{a+3d}{d^2(a+d)^2} + \frac{1}{d^2}\right. \\ \left.\left(P^* + \frac{a+2d}{d(a+d)}\right)\right] \\ \qquad\qquad \text{for } P^* > 0 \\ \left(e^{aP^*}+1\right)\left[\frac{e^{2aP^*}}{a}\left(\frac{2}{(a+d)^2} + (3P^{*2}+P^*) - \frac{3P^*}{a+d} + \right.\right. \\ \left.\left.\frac{2P^{*2}}{a+d}\left(\frac{1}{a+d} - \right.\right.\right. \\ \left.\left.\left.P^*\right)\right) + \frac{e^{aP^*}}{a^2d} + d(4ad(a+d)^2 - (a^2+d^2)^2)\right] \\ \qquad\qquad \text{for } P^* \leq 0 \end{cases} \tag{A.22}$$

The average outflow from the third wetland in a cascade may be found as,

$$\bar{O_3} = P_2\bar{O_2} + (\frac{ad}{a+d})^2 \begin{cases} \frac{3(a+d)^2}{(ad)^3}(d-a+adP^*) + \frac{e^{-cP^*}(a+d)}{ad^3} + \frac{e^{-2cP^*}}{(a+d)d^3}(a+2d+ \\ d(a+d)P^*) + \frac{ae^{-3dP^*}}{(a+d)^3}[\frac{(a+2d)^2+d^2}{d^3} + \frac{P^*}{2d^2}(3dP^*((a+d)^2-ad)+ \\ 4a^2+14ad+18d^2)] & \text{for } P^* > 0 \\ \\ (\frac{1}{d} + \frac{1-e^{ap^*}}{a})^2 + \frac{e^{aP^*}}{d(a+d)} + e^{2aP^*}[\frac{1}{a^2(a+d)}(1-(1+\frac{1}{a})(e^{-aP^*}-1))+ \\ \frac{e^{2aP^*}}{a^2(a+d)}(3+\frac{2d}{a} - P^*(a+d) - \frac{3P^*de^{aP^*}}{2}(1-aP^* + d\frac{4d+13a+\frac{d^2}{a}}{(a+d)^2})) \\ & \text{for } P^* \leq 0 \end{cases} \tag{A.23}$$

Note that the average outflow of Equation A.23 should be multiplied by the correction factor of $\frac{1}{3(\beta+1)}$, to be normalized by the catchment area.

A.4 Outflow distribution of cascade depth of four

Here the outflow distribution of cascades with four wetlands is calculated considering,

$$O_4^* = \beta_4 R + P' - D_4 + O_1 + O_2 + O_3 \tag{A.24}$$

We will introduce a new term $\gamma_4 = \beta_4 R + P' - D_4$. We have already calculated the resultant distribution of this for single wetland cascades (where $\gamma_1 = O_1^*$). Then, for cascade depth of four, distribution of potential outflow can be found from solving the integral in Equation 3.6 where $n = 4$ as (for $P^* > 0$),

$$f_{O_4^*}(O_4^*) = P_3 \cdot f_{O_1^*}(O_4^*) + (\frac{ad}{a+d})^4 \begin{cases} C_1 & \text{for } O_4^* < P^* \\ C_2 & \text{for } O_4^* \leq P^* \leq 2O_4^* \\ C_3 & \text{for } 2O_4^* \leq P^* \leq 3O_4^* \\ C_4 & \text{for } 3O_4^* \leq P^* \leq 4O_4^* \\ C_5 & \text{for } 4O_4^* \leq P^* \end{cases} \tag{A.25}$$

$$C_1 = \frac{e^{d(O-4P^*)}}{6(a+d)^3}[16P^{*3}(a+d)^3 + 3P^{*2}(a+d)^2(\frac{5a}{d} + 21d) + 6P^*(\frac{a^3}{d^2} + \frac{8a^2}{d} + 23a + 16d) + \frac{6((a+3d)^2 - ad)}{d^2}] \tag{A.26}$$

$$C_2 = \frac{-e^{-aO-4dP^*}}{2(a+d)^3d^2}[3e^{P^*(a+d)}(2a^2 + 10d^2 + 8ad + 2dP^*(2a^2 + 7ad + 5d^2) + d^2P^{*2}(a+d)^2) + e^{P^*(a+d)}(-2(2a^2 + 9ad + 14d^2) + 2O(a^3 + 5a^2d + 9ad^2 + 5d^3) + 2P^*(2a^3 + 15a^2d + 39ad^2 - 26d^3) + dP^{*2}(\frac{25}{3}P^*(a+d)^3d + 9a^3 + 52a^2d + 77ad^2 - 34d^3) + OP^*d(a+d)^2 (4a + 10c + 3dP^*(a+c)))] \tag{A.27}$$

$$C_3 = \frac{e^{-aO-4dP^*}}{6(a+d)^3}[-3e^{P^*(a+d)}(3P^*(a+d)^2 + 4P^*\frac{a^2}{d} + 14P^*a + 10P^*d + \frac{2a^2}{d^2} + \frac{8a}{d} + 10)$$
$$+\frac{6e^{2P^*(a+d)}}{d^2}((a+2d+dP^*(a+d))(2a-d+(Oa-2P^*)(a+d))) + e^{O(a+d)}((a+d)^3$$
$$(3O^2P^* - 21OP^{*2} + 37P^*) + (a+d)^2(-6OP^*(\frac{3a}{d}+10) + 3P^{*2}(9\frac{a}{d}+46)) + (a+d)$$
$$(-6O(\frac{3a}{d}+7) + 6P^*(\frac{9a}{d}+31)) + \frac{3}{d}O^2a((a+2d)^2 + d^2 + 2d^3) + \frac{12(3a+4d)}{d})] \tag{A.28}$$

$$C_4 = \frac{-e^{-aO-4dP^*}}{d^2(a+d)^3}[-e^{2(a+d)P^*}(a+2d+dP^*(a+d))(2a-d+a(a+d)(O-2P^*))-$$
$$de^{3(a+d)P^*}(6a-4d+3(O+P^*)a^2 - d^2O + 3P^*(a+d)^2 + 2adO - \frac{a}{2}(3P^*-O)^2(a+d)^2)$$
$$-10d^2e^{O(a+d)}((4P^*-O)(a+d)+2) + e^{P^*(a+d)}(P^*d(a+d)(2a+5d) + (a+d)^2 + d^2 +$$
$$(a+d)^2P^{*2}c^2/3) - d^2(a+d)^2e^{O(a+d)}(4P^*-O)^2((4P^*-O)\frac{a+d}{6}+2)] \tag{A.29}$$

$$C_5 = \frac{-e^{-aO-3P^*d}}{(a+d)^3}[e^{aP^*}((a/d+2)^2 + 1 + P^*(a+d)(2a/d+5+3/2P^*(a+d))) + e^{P^*(2a+d)}$$
$$(\frac{2P^{*2}}{d}(a+d)^2 - \frac{2a+3d}{d^2} - 2 + (a+d)(\frac{Oa(a+2)}{d^2} - P^* + \frac{aP^*}{d^2}(a+d)(Od-2)))$$
$$-e^{P^*(3a+2d)}(\frac{aO^2}{2d}(a+d)^2 - \frac{O(a+d)}{d}(d+3a(a+d)P^*-1) + \frac{3aP^*}{2d}(3P^*(a+d)^2+4a)$$
$$+\frac{3P^(a+d)^2}{c} + \frac{6a}{d} - 4) - e^{4a+3d}(10(O-4P^*)(a+d) + 2 + (a+d)^2(O-4P^*)^2((O$$
$$-4P^*)(a+d)+12))] \tag{A.30}$$

For $P^* < 0$, we obtain the following expression:

$$f_{O_4^*}(O_4^*) = P_3 \cdot f_{O_1^*}(O_4^*) + \left(\frac{ad}{a+d}\right)^4 \begin{cases} \frac{e^{aP^*+d(O-P^*)}}{(a+d)^3}[\frac{(a+d)^4}{(ad)^2} + \frac{d^4e^{2aP^*}}{2a}(3P^{*2}a(a+d)^2 - 6P^*a^2 \\ -2P^*ad + 4P^*d^2 + 4a - 6d) - \frac{e^{aP^*}(a+d)^2}{a^2d}(d - a + \\ P^*(a+d))] & \text{for } O_4^* < P^* \\ \\ \frac{e^{a(2P^*-O)}}{2(a+d)^2}[2(a+d)^3\frac{(a+d)(O-P^*)+1}{(ad)^2} + \frac{e^{2aP^*}}{a}(OP^*(d-a \\ -2(a+d)(5a-3d) + a(a+d)^2(8O-3P^*)) + (a+ \\ d)(O^2(2a-d) + P^{*2}(11a-5d)) + \frac{2(2a-3d)(1+O(a+d))}{a+d} \\ +\frac{a(a+d)^2}{3}(O^3 - 16P^{*3})) + \frac{e^{aP^*}(a+d)}{a^2d}(a(a+d)^2 + 2((a \\ -d) + O(a^2-d^2) - P^*(a+d)(2a-d))] \\ & \text{for } O_4^* \geq P^* \end{cases} \tag{A.31}$$

and the final outflow distribution may be calculated as,

$$f_{O_4}(O_4) = \delta(O_4)\int_{-\infty}^{0} f_{O_4^*}(x)dx + H(O_4)f_{O_4^*}(O_4) \tag{A.32}$$

The integral in A.32, the probability of zero outflow from the fourth wetland in a cascade, can be calculated as,

$$P_4 = \int_{-\infty}^{0} f_{O_4^*}(x)dx = (\frac{ad}{a+d})^4 \begin{cases} \frac{e^{-4cP^*}}{3(a+d)^3}[\frac{4P^*(a+d)^2}{c}(2P^*(a+d) + \frac{3(a+3d)}{c}) + \frac{3P^*}{c^3}(3a^3 + \\ 17a^2c + 35a^2c + 21c^3) + \frac{3}{c^4}((a+2d)^2 + \\ 2d^2(a+3d))] & \text{for } P^* > 0 \\ \\ \frac{1}{a(a+d)^2}[\frac{(a+d)^6}{a^3d^4} - \frac{e^{aP^*}(a+d)^5}{(ad)^3} + \frac{e^{2aP^*}(a+d)^3}{(ad)^2}(P^*(a+d)-1) \\ +e^{4aP^*}(P^* + \frac{8}{3}P^{*2}(a+d)(P^*(a+d)-3) - \frac{5}{a+d}) - \\ \frac{(a+d)e^{3aP^*}}{ad}(2 + 1.5P^*(a+d)((a+d)P^* - 2))] \\ & \text{for } P^* \leq 0 \end{cases} \tag{A.33}$$

The average outflow from second wetland in a cascade may be found as,

$$\bar{O}_4 = P_3\bar{O}_3 + \begin{cases} \frac{e^{-4dP^*}}{6ad(a+d)^7}[6a^5(a^3+6a^2d+14ad^2+14d^3)+6a^4e^{dP^*}(a+d)^2((a+2d)^2+ \\ d^2)+6a^2e^{3dP^*}(a+d)^6+6P^*a^5d(a+d)(4P^*a^2d+3a^2+16P^*ad^2+ \\ 14ad+12P^*c^3+21d^2)+16P^{*3}a^5d^3(a+d)^3+3P^*a^4de^{dP^*}(a+d)^3(4a+ \\ 10d+3P^*d^2+3P^*ad)+24e^{4P^*d}(a+d)^7(d-a+P^*ad)+6a^3e^{2P^*d} \\ (a+d)^4(a+2d+P^*d^2+P^*ad) & \text{for } P^*>0 \\ \\ \frac{de^{aP^*}}{a(a+d)^7}[(a+d)^6+de^{aP^*}(a+d)^4(2a+d-aP^*(a+d))+d^2e^{2aP^*}(a+d)^2 \\ ((2a+d)^2+a^2-aP^*(a+d)(5a+2d)-1.5P^{*2}a^2(a+d)^2)+d^3e^{3aP^*} \\ (4a^2P^{*2}(a+d)^2(3a+d)-\frac{16}{6}P^{*3}a^3((a+d)^3-2d^3)-aP^*(21a^3+ \\ 35a^2d+17ad^2+3d^3)+14a^2(a+d)+d^2(6a+d))] & \text{for } P^*\leq 0 \end{cases} \tag{A.34}$$

Note that the average outflow of Equation A.34 should be multiplied by the correction factor of $\frac{1}{4(\beta+1)}$, to be normalized by the catchment area.

Appendix B

Hydrographs of QRB Subbasins

B.1 Supporting Information for Chapter 3

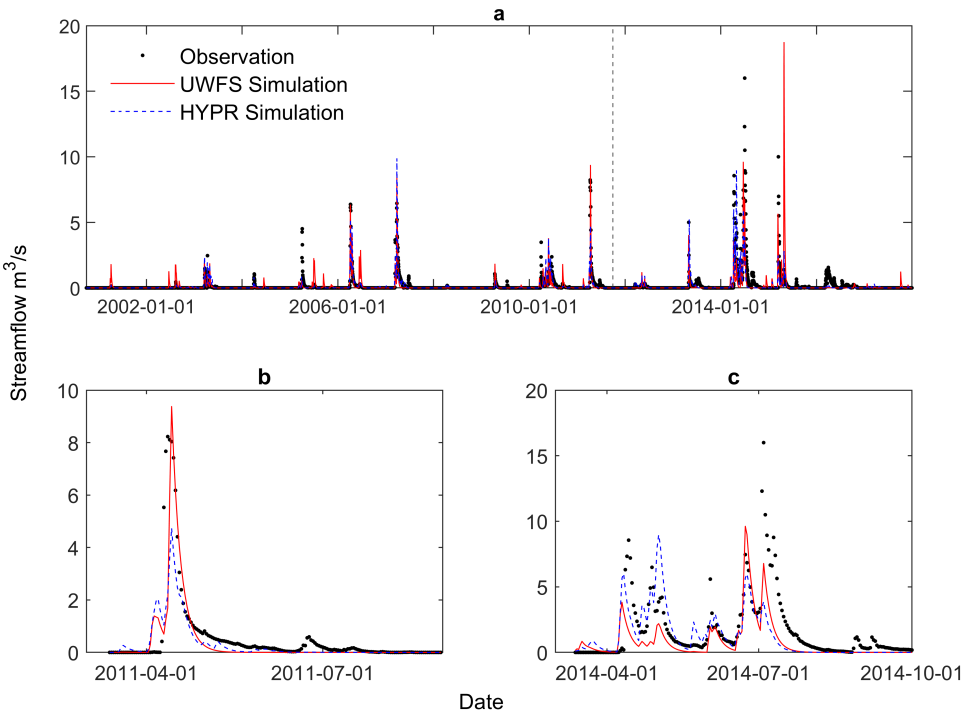

Figure B.1: Simulated and observed hydrograph by UWFS and HYPR models in Raven for Lewis watershed inside QRB basin, located in Saskatchewan, Canada for a) the total duration of the study period from 2000 to 2017, b) for an event in the Calibration period, c) for an event in the validation period. The vertical dashed line separates calibration and validation period.

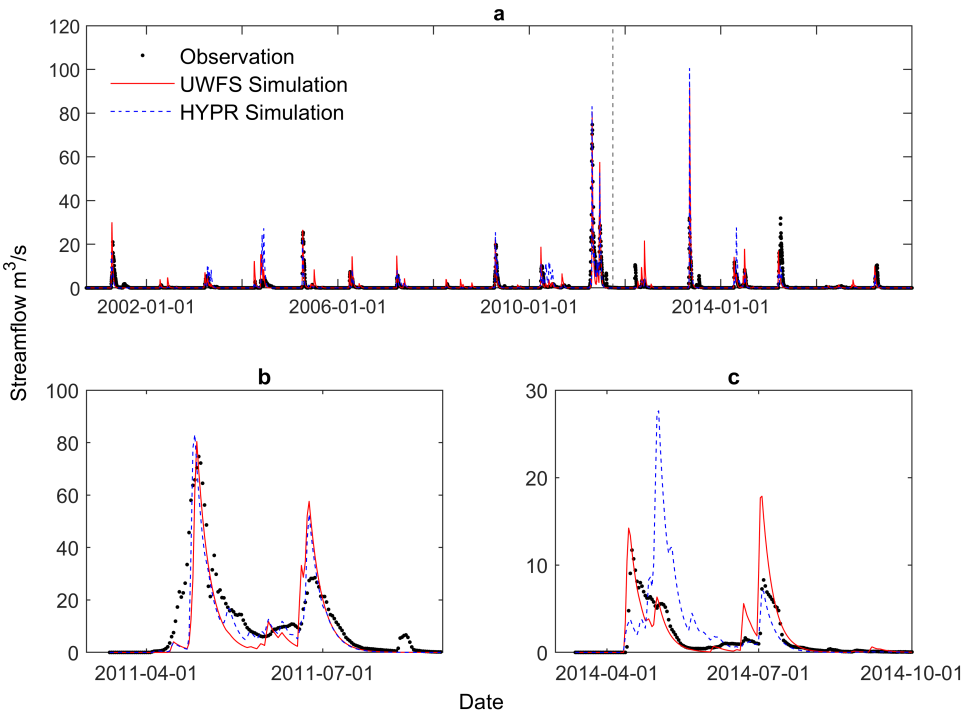

Figure B.2: Simulated and observed hydrograph by UWFS and HYPR models in Raven for Kronau Marsh watershed inside QRB basin, located in Saskatchewan, Canada for a) the total duration of the study period from 2000 to 2017, b) for an event in the Calibration period, c) for an event in the validation period. The vertical dashed line separates calibration and validation period.

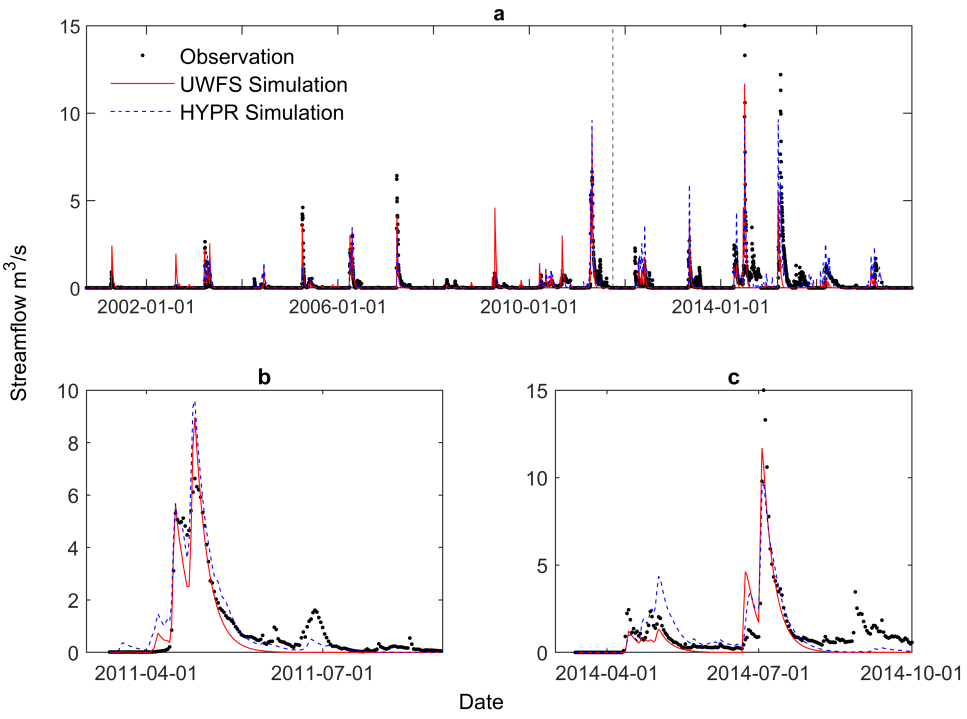

Figure B.3: Simulated and observed hydrograph by UWFS and HYPR models in Raven for Jumping Deer watershed inside QRB basin, located in Saskatchewan, Canada for a) the total duration of the study period from 2000 to 2017, b) for an event in the Calibration period, c) for an event in the validation period. The vertical dashed line separates calibration and validation period.

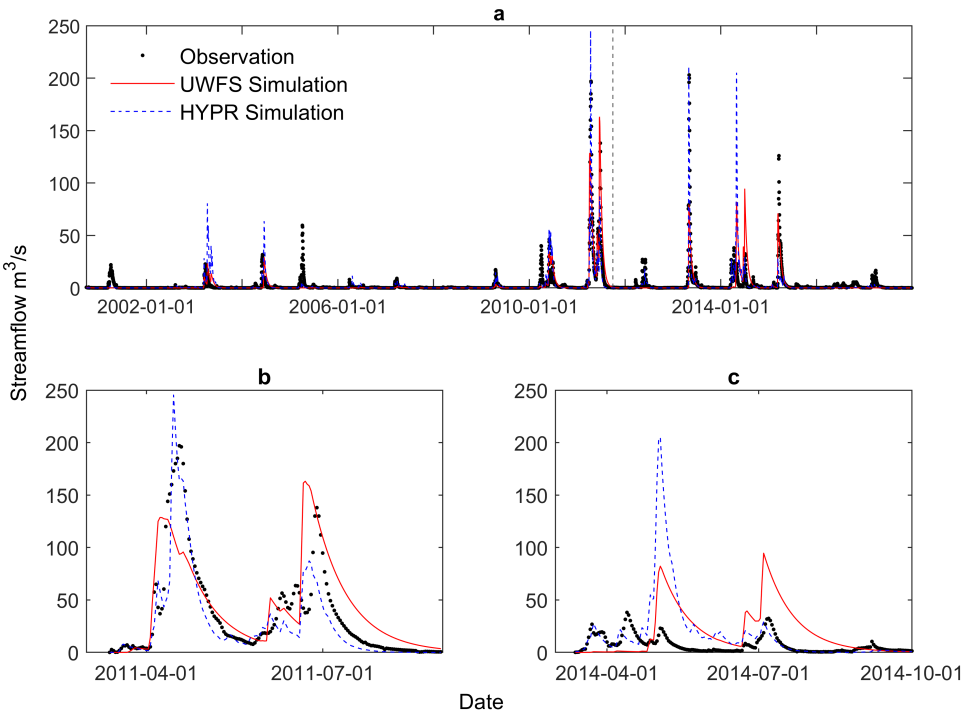

Figure B.4: Simulated and observed hydrograph by UWFS and HYPR models in Raven for Moose Jaw watershed inside QRB basin, located in Saskatchewan, Canada for a) the total duration of the study period from 2000 to 2017, b) for an event in the Calibration period, c) for an event in the validation period. The vertical dashed line separates calibration and validation period.

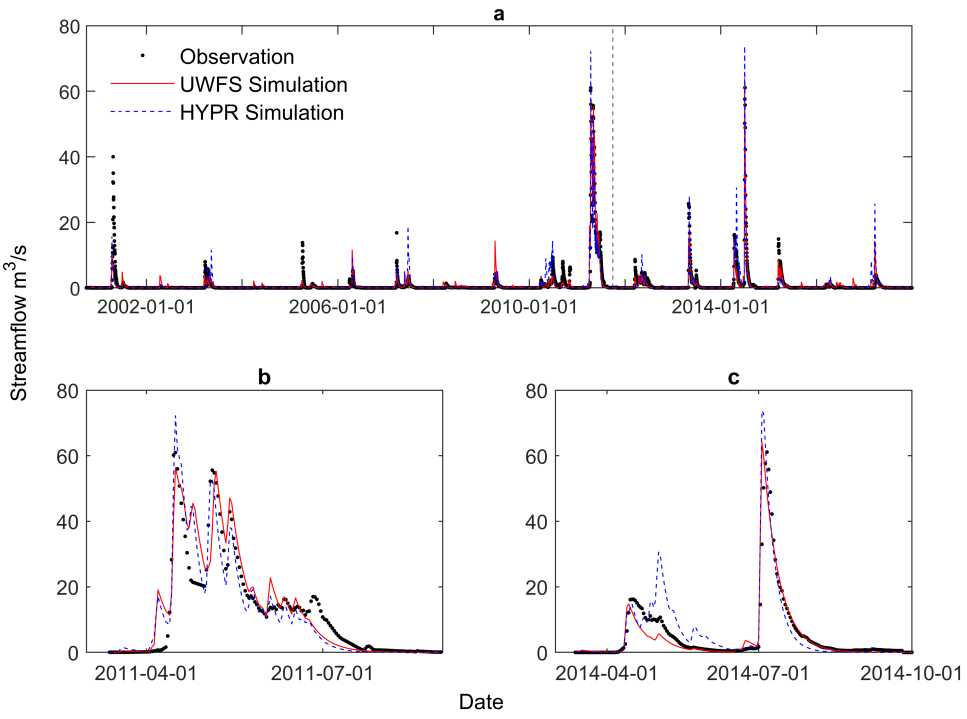

Figure B.5: Simulated and observed hydrograph by UWFS and HYPR models in Raven for Ekapo watershed inside QRB basin, located in Saskatchewan, Canada for a) the total duration of the study period from 2000 to 2017, b) for an event in the Calibration period, c) for an event in the validation period. The vertical dashed line separates calibration and validation period.

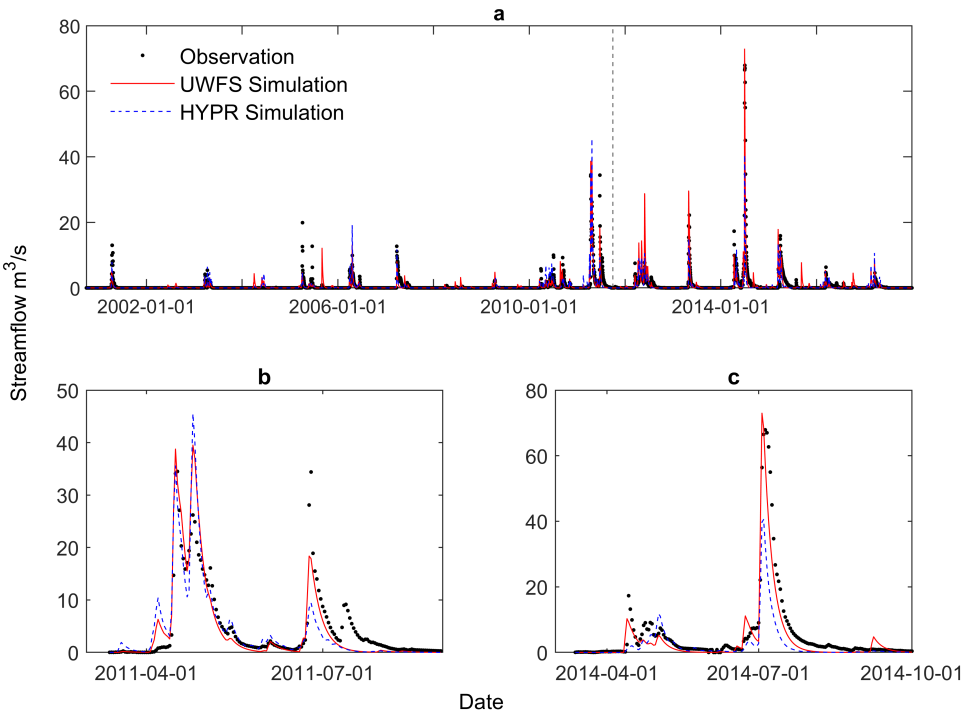

Figure B.6: Simulated and observed hydrograph by UWFS and HYPR models in Raven for Pheasant watershed inside QRB basin, located in Saskatchewan, Canada for a) the total duration of the study period from 2000 to 2017, b) for an event in the Calibration period, c) for an event in the validation period. The vertical dashed line separates calibration and validation period.

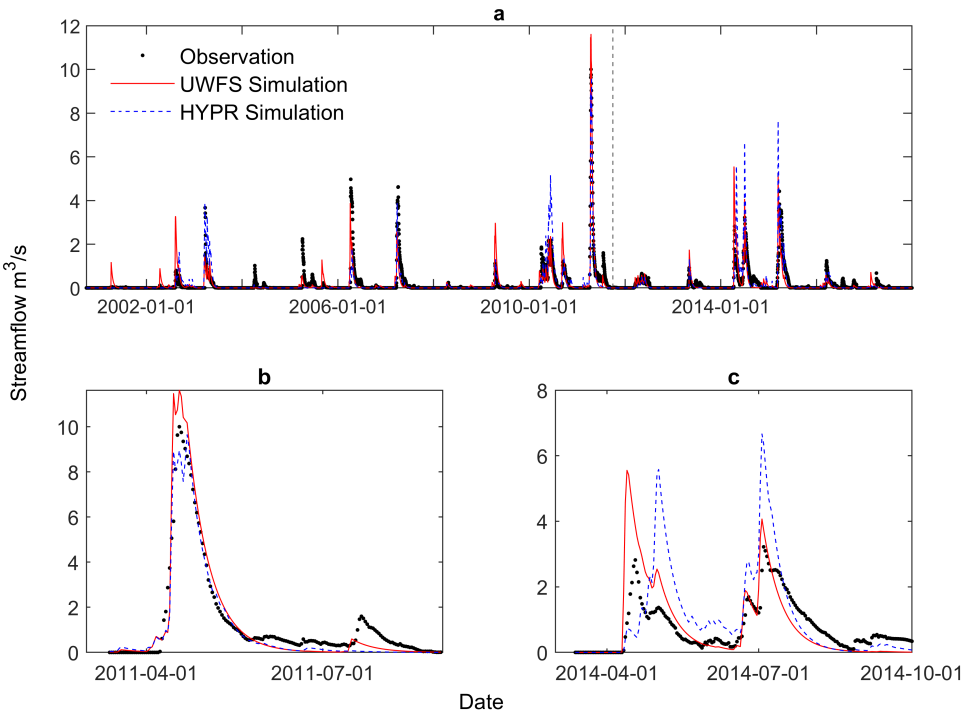

Figure B.7: Simulated and observed hydrograph by UWFS and HYPR models in Raven for Saline watershed inside QRB basin, located in Saskatchewan, Canada for a) the total duration of the study period from 2000 to 2017, b) for an event in the Calibration period, c) for an event in the validation period. The vertical dashed line separates calibration and validation period.

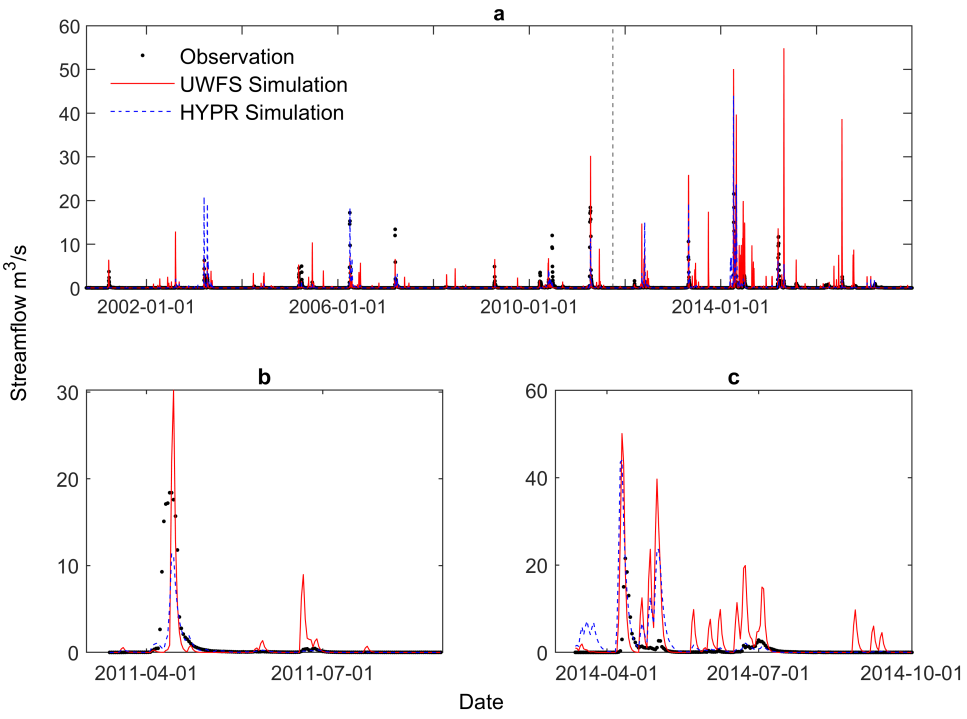

Figure B.8: Simulated and observed hydrograph by UWFS and HYPR models in Raven for Ridge watershed inside QRB basin, located in Saskatchewan, Canada for a) the total duration of the study period from 2000 to 2017, b) for an event in the Calibration period, c) for an event in the validation period. The vertical dashed line separates calibration and validation period.

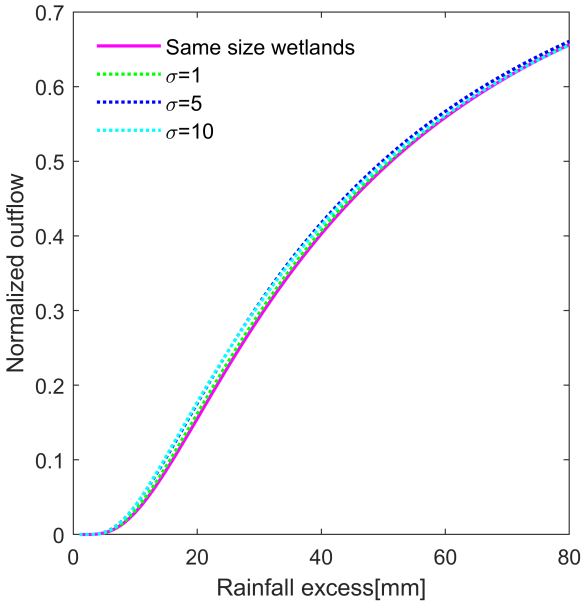

Figure B.9: Comparison of normalized runoff generated from wetlands cascade depth of two with uniform and nonuniform sizes based on three different lognormal distributions of wetland area ratio with mean of one and standard deviations of 1, 5, and 10 using the Monte Carlo approach

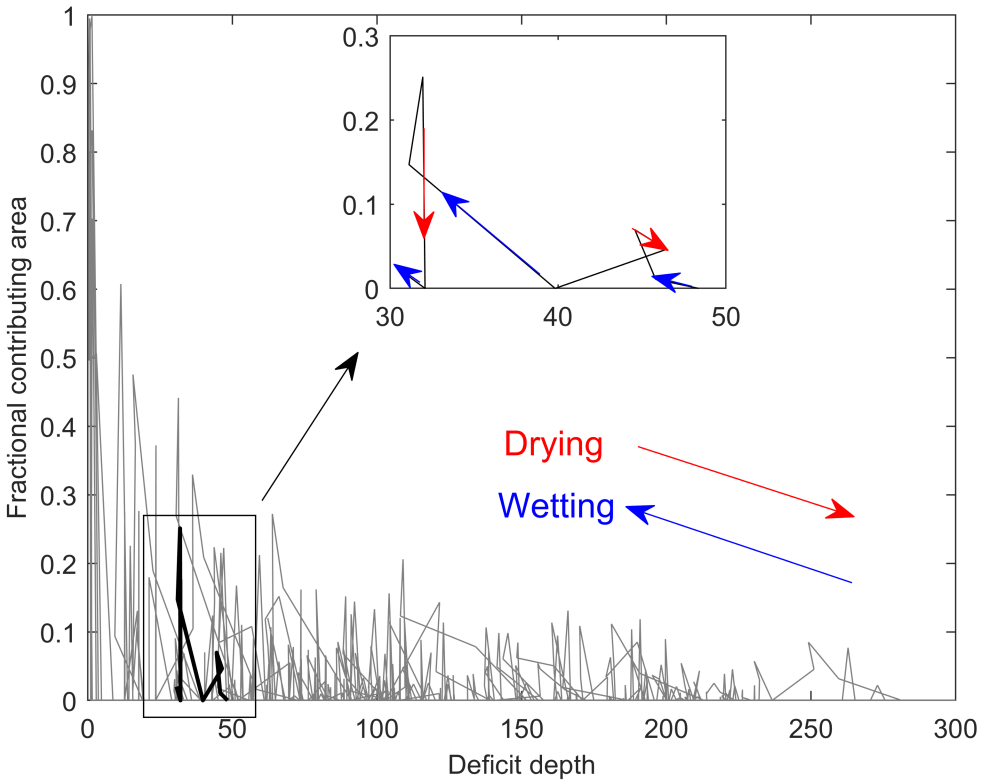

Figure B.10: Hysteresis relationship between fractional contributing area and average deficit depth simulated using UWFS